Topology Synthesis of Compliant Systems with Embedded Actuators and Sensors

by

Brian Patrick Trease

A dissertation submitted in partial fulfillment
of the requirements for the degree of
Doctor of Philosophy
(Mechanical Engineering)
in The University of Michigan
2008

Doctoral Committee:

Professor Sridhar Kota, Chair
Professor Carlos E. Cesnik
Professor Richard Brent Gillespie
Professor Kazu Saitou

will I be able to do it?

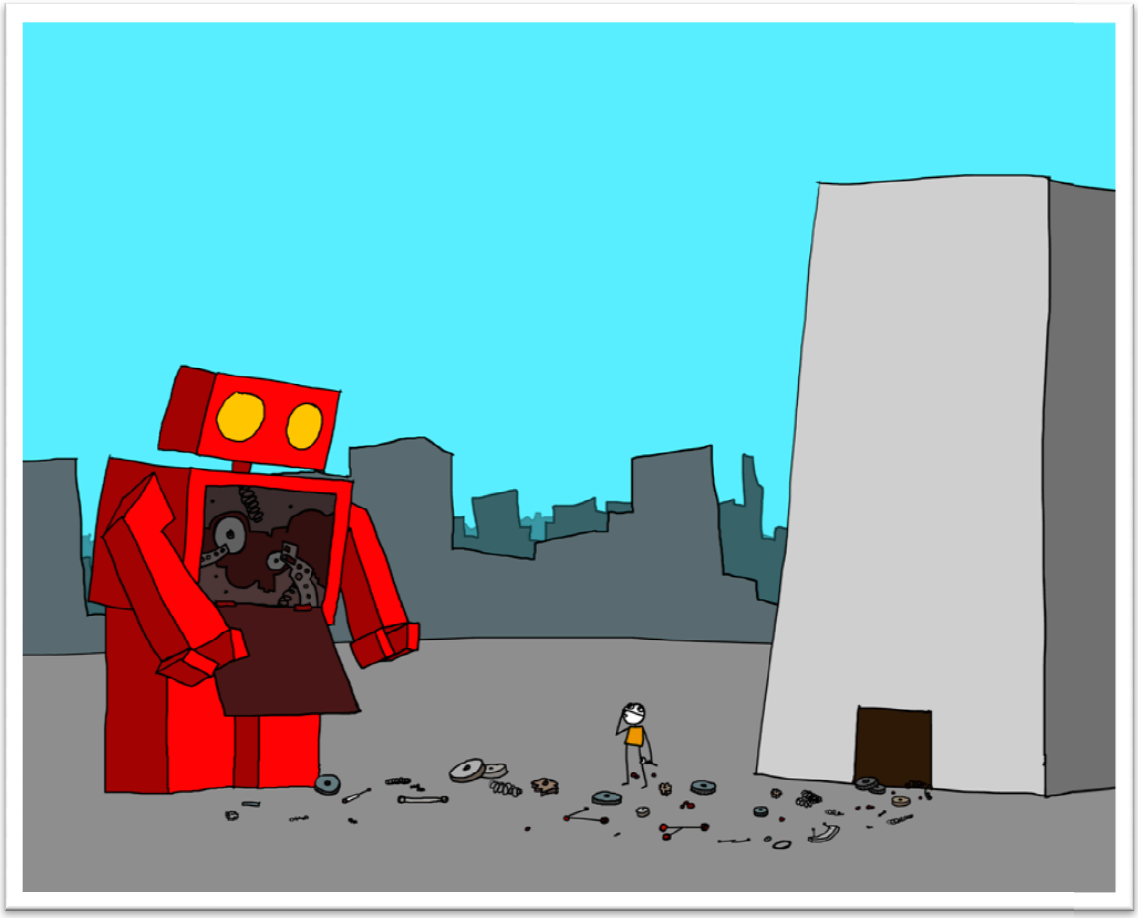

To Mimi, who makes me better at everything and makes everything better.

Acknowledgments

There are too many to thank that made it possible for the production of this dissertation. I am deeply indebted to my colleagues, friends, coworkers, and professors who guided me along, providing support when I need it most. In particular, I am grateful to have worked for and along the side of my advisor, Sridhar Kota, who teaches by example the power of the relentless pursuit of creativity. His broad support and confidence allowed me to develop my own confidence through many tangential projects, both at the university and at off-site internships. Through him I've learned essential lessons of engineering far beyond those found in the typical textbook – lessons about the value of people, communication, passion, and commitment. Yet my growth during graduate school was more than just as an engineer. My personal understanding of the world, myself, and my role in society has also undergone dramatic change. For these, my friends and family have played the instrumental role. My mother, father, sister, and brother continually offered new perspectives on the world I am trying to understand. And it is together with my wife, Mimi, that we keep exploring, learning, and asking more questions that keep my fire burning with a passion for engineering.

Over seven years ago I began postgraduate studies as a child and now confidently move on to an engineering career as an adult. That transitional is critical, and it is all those I knew, worked, and loved along the way that convinced me of the importance of my

chosen trade. I'm not exactly sure *when* "engineer" became my identity, but it is the intense pride I have in that title which leaves no question that I've found my calling.

In addition to my committee, I acknowledge several professors who made my UM education exciting and challenging:

> Diann Brei, John Shaw, Deba Dutta, Paul Webb, and Brent Gillespie. Brent gets mentioned here again for teaching the most exciting, difficult, time-consuming, and inspiring course I've taken, ME552: Electromechanical Design.

Thanks you to everyone in my family for their unconditional support and cheer:

> Mom, Dad, Nicole, Tony, Brad, Linda, Tom, Kathy, Jessica, Kelly, and many more.

Thank you to my wonderful labmates in the Compliant Systems Design Lab:

> Charles Kim, Kerr-Jia Lu, Tony Tantanawat, Dave Lax, Audrey Plinta, Zak Kreiner, Mike Cherry, Christine Vehar Jutte, Froukje Euwe, Youngseok Oh, Yong-Mo Moon, Zhe Li, Girish Krishnan, and Dragan `Maric.

Thank you to all of my UM colleagues that have affected my life in so many ways:

> Bart Peintner, Greg Sawicki, Sarah Calve, Felix Huang, Paul Griffiths, Ercan Dede, Steve Collins, Jarod Kelly, Anupam Pathak, John Redmond, Jiro Doke, Shawn O'Conner, Peter Adamzyck, Becca Stoloff, Rob White, Mari Hou, James Allison, Erin MacDonald, Ross Morrow, Brian Jensen, Jay Michalek, Lalit Patil, Mike Resciniti, and Glenn Watkins.

Part of my development was learning to seek as much support as possible from whomever claimed they might offer it. Some of these sources include:

> ME Department Administrative Staff
> ME Department Computer Support Staff
> UM Career Center
> Rackham Graduate School
> Flexsys, Inc.

Finally, I have been fortunate to benefit from many sources of funding, including the following:

Department of Mechanical Engineering
Naval Research Lab
DARPA Revolutionizing Prosthetics Program
National Science Foundation Graduate Research Fellowship Program
National Science Foundation Engineering Research Center for Reconfigurable Manufacturing Systems
Air Force Research Lab and Wright-Patterson Air Force Base
Sandia National Labs
Rackham Graduate School Travel Funding

Table of Contents

List of Figures

List of Tables

Abstract

The basic premise of a *compliant system* is the integration of motion/force transmission via elastic deformation with embedded actuation and sensing. Current electromechanical systems are generally fashioned in the rigid-and-discrete paradigm where one first designs a rigid structure with mechanical joints and then adds actuators and sensors, with the design of controls only following as an afterthought. The objective of this research is a *systems* approach to synthesis of mechanism, structure, actuation, and sensing, thereby advancing from traditional mechanical design to *automated* compliant system design. In previous studies of compliant mechanisms and their synthesis, single-actuator mechanisms have primarily been considered, with the determination of the actuator's type, orientation, size, and location occurring *outside* of the automated design synthesis, at the designer's option. A new algorithmic framework is presented, in which structural topology and actuator/sensor placement are *simultaneously* synthesized for maximum energy efficiency and adaptive performance. Significantly, this is not a traditional ad hoc method; sensor and actuator placement affect structural topology and vice versa.

The methods used include genetic algorithms, graph searches for connectivity, and multiple load cases implemented with linear finite element analysis. Fundamental

metrics for the inclusion of embedded components in a multifunctional compliant system are developed and investigated. Actuators, modeled as both force generators and structural compliant elements, are included as topology variables in the optimization. The essential framework for the integration of controls with compliant mechanisms is established. Specifically, the concepts of controllability and observability, as redefined for compliant systems, are proven as a successful starting point for the design of multifunctional, adaptive systems. These concepts refer to the unique system response for each component (actuator or sensor) it contains. Results are presented for several problems, focusing on the application of shape-morphing aircraft structures. Through examples and design studies, the metrics and the methodology demonstrate that multiple, optimally-placed components indeed offer performance benefits for mechanical systems, both in terms of efficiency and multifunctional execution. Finally, the extension of controllability to address the problem of single-point manipulation is performed to show the generalized use of the new methodology in benefitting the design of compliant systems.

Chapter 1

Introduction

1.1 Introduction

Rapid advances are being made in novel actuation, materials, and fabrication technologies. The combination of these fields enables a new breed of complex, multifunctional devices that offer many advantages over predecessor technologies. Some benefits include autonomy, adaptability, self-repair, and self-replication. However, as all these technologies are coming online, we engineers do not yet know how take advantage of their synthesis beyond the patterns in our collective mind that remain from yesterday's designs.

One such multifunctional device considered in this dissertation is a *compliant system*. The basic premise of a compliant system is the integration of motion/force transmission via elastic deformation with embedded actuation and sensing. These systems hold the potential to lead to tightly integrated, highly functional, multi-purpose, adaptive systems. Yet the lack of rigid elements and the integration of components breaks the assumptions designers typically hold for granted and a great deal is yet to be learned.

Of the new possibilities and synergies, the design for and around smart actuators is of particular interest. While typical force generators are very stiff, these smart materials

can be as compliant as their transmission structures and the external environment they act against. When both actuator and structure are compliant, many of the old design tools need to be reinvented.

One way to approach this problem and work towards adaptability and autonomy is to focus on designing a system where each internal component has as unique effect on the external environment as possible. Achieving this quality in a multifunctional structure is inherently difficult, since every component can be intrinsically coupled by the other tasks required of the structure. This is part of the definition of a multifunctional device. For example, imagine a weight-bearing variable-stiffness structure driven by several compliant actuators of varying load magnitude. The goal may be for resolution of control by using the actuators independently, but they remain coupled in their design and operation in that they are all part of the gravity load path and one's operation affects all the others. Such tradeoffs and the beneficial results are formulated and explored in this dissertation.

Compliant systems take their cue from the field of compliant mechanisms, which is the foundation of this research. Compliant mechanism design is the formal field of study that addresses the elastic transmission part of the proposed problem. It has been recognized as a research topic in mechanical engineering for fifteen years, and has recently begun to be recognized, requested, and applied by the commercial market. The trajectory from traditional mechanism to compliant mechanism to adaptive

compliant system is shown in Figure 1. There are many advantages of using compliant, monolithic devices for applications in manufacturing, biomedical, aerospace, and robotic applications. A particular benefit that motivates this current endeavor is that the combination of compliant actuators and structures provides force feedback much more similar to that observed in biological structures (i.e. humans) than do stiff actuators and rigid mechanisms. However, while there are apparent advantages from co-design of structure and actuator, the field of compliant mechanisms has for the most part considered traditional and stiff actuators. Further, the actuator properties have been left out of both analysis and the development of design algorithms. Many novel actuators are better modeled as load-displacement curves than as a fixed force or displacement generator; in this dissertation, the interaction of the actuator and the system during analysis determines the actual output performance.

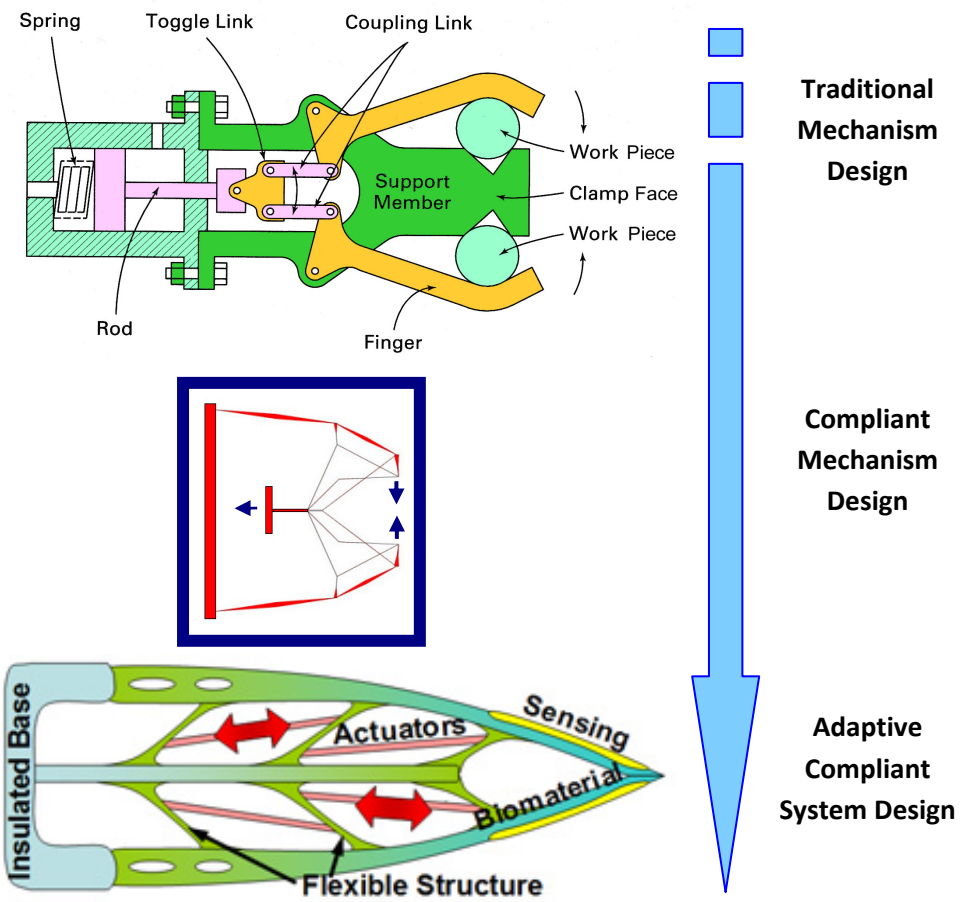

Figure 1: Transition from "Traditional Mechanical Design" to "Adaptive Design with Distributed and Embedded Compliant Systems". Current State-of-the-Art is "Compliant Mechanism Design".

A driving application of compliant systems is shape-morphing structures (patents: Kota, 1999; Kota, 2002). In demand more than ever by aerospace and energy generation industries, shape-morphing structures have provided a challenge for both conventional and compliant mechanisms for many years. They have typically been designed with a priori notions of the desired shape change (Saggere and Kota, 1999). However, there are many situations where the desired shape change might not be known ahead of time and could be a function of the environment. There is also the possible need to achieve multiple shape states. For such applications, the best solution should have a controllable response with exceptional manipulability. This dissertation recasts the

shape-morphing problem as the challenge of how to design a *set* of actuators capable of creating *any* desired shape, rather than just one specific shape change.

Techniques in design optimization have been the standard approach used in most compliant mechanism design work, and are also the path chosen for addressing the current task. Problem parameters are defined and the empty physical design space is parameterized so that a computer-coded algorithm can determine the best structure and topology. Figure 2 shows an example of the problem definition for actuator/sensor placement and a conceptual solution to be generated algorithmically based on the synthesis framework. Many optimization methods have been used in the past, which can be split into two different groups: continuous and discrete. The discrete presence of components in this problem, along with the many possible separate solutions, motivates use of the discrete optimization methods. These methods include the field of evolutionary optimization, of which I apply genetic algorithms in particular.

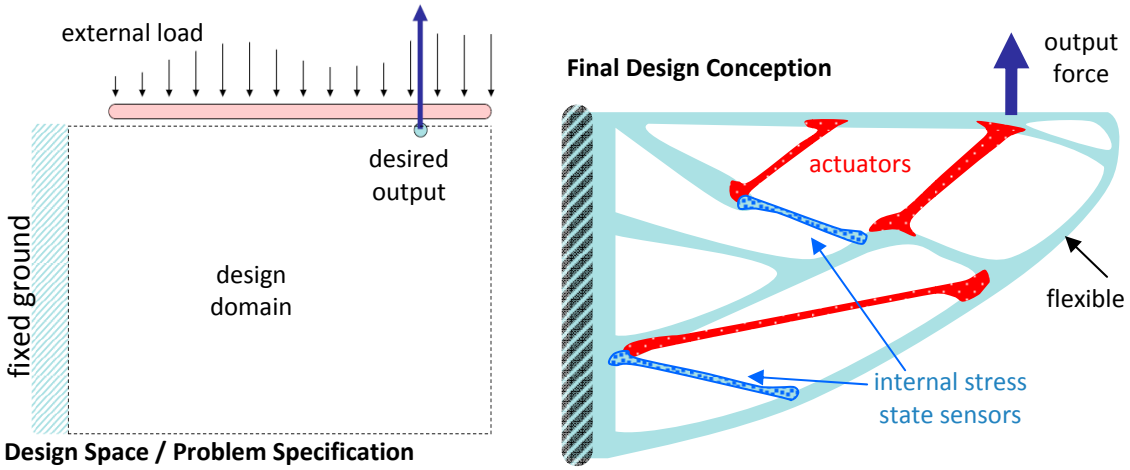

Figure 2: Vision of an adaptive compliant system. Beginning with a specified design space, external loading conditions, and desired mechanical task, I seek to synthesize a fully-compliant system with embedded and distributed actuators and sensors.

Using the tools described above, this dissertation presents an objective and a methodology to encourage a high quality of component independence in multifunctional systems. Central to this method is the concept of *structural orthogonality*, another term for the described goal of a unique system response for every actuator. I demonstrate the usefulness of the new metrics in many applications, including adaptive shape-controllable systems, compliant end-effector manipulability, and optimal internal sensor layout for monitoring external loads. In all these cases, the components do more than simply allow changes/measurements between one state and another, but allow for *linear combinations* of each other to reach across a broad space of control and measurement.

For instance, objective functions are added to ensure "orthogonal deformation modes" for the actuators and "orthogonal sensing modes" for the sensors, where orthogonal refers to the algebraically unique interaction each set of internal components has with the external surface. While there is much to be gained from this goal, performance can be gained from multiple actuators before even considering the linear combination problem. The initial examples compare efficiencies of multiple actuator systems, since that problem needs to be addressed first, after which the concepts of controllability and observability are introduced.

1.2 Motivation

The motion-and-force-transmission part of the compliant system problem has been researched for nearly fifteen years in the field of compliant mechanisms (Frecker et al.,

1997; Hetrick and Kota, 1999; Saxena and Ananthasuresh, 2001; Yin and Ananthasuresh, 2003). As mentioned, these jointless, monolithic devices use flexures and deformation to transmit motion and force, rather than rigid bodies with conventional mechanical joints, providing several well-known benefits such as elimination of wear, clearance, and backlash from mechanical joints. This design paradigm is inspired by nature, where strength and *compliance* are observed in its designs, as opposed to the goal of strength and *stiffness* employed in traditional engineering. In fact, I refer to such systems in terms of both mechanism *and* structure; in this research both conceptions are used. The interchangeability of these terms highlights the significance of the multiple roles played by this technology and blurs the distinction between a (flexible) structure and a (jointless) mechanism.

This research extends the biological analogy to the creation of truly monolithic *systems* – autonomous, adaptive, efficient, self-contained devices. The design methods and the applications of compliant mechanisms already apply to many domains in micro-, meso-, and macro-scales. The past success in the field motivates a new level of sophistication in synthesis of compliant systems including controls and adaptive structures. Frecker (2003) illustrates the gaps in knowledge amongst these synergies. Her survey of the fields shows that work has been done in (1) actuator placement on non-compliant predetermined structures, (2) the actuator material distribution problem (see §2.6 Actuator Architecture below) , and (3) the coupling structure for a prescribed actuator (i.e. actuators are fixed, not variables), which are incremental steps in the progression of

adaptive structure technology. However, the topic of systems-level *concurrent* synthesis of actuator component placement and topology design, a fundamentally different approach to the design of smart mechatronic systems, is yet to be addressed. By combining these fields, a new paradigm emerges for comprehensive designs that offer a basis for autonomy via the improved energy efficiency and adaptability that their inherent compliance provides.

The concepts of controllability and observability (degree to which the external environment can be sensed) arise from the consideration of control – a natural question after the leap from single to multiple actuator structures. These concepts represent the structural adaptability of the system. The use of a compliant mechanism/structure enables increased sensitivity and output function with fewer actuators/sensors. In other words, with structural compliance a reduced number of *internal* sensors and actuators can affect and sense a large range of *externalities* over a large physical region. This is further motivated by the increasing availability of novel materials and fabrication methods for multifunctional devices. Design of such devices is not yet intuitive and requires maintaining *component independence* in inherently *coupled* multifunctional systems.

1.2.1 Biological Inspiration

Through this synthesis, we continue to be inspired by nature, and become more intimate with the question of the relationship between nature and engineering design.

If compelled to take inspiration from biology, we engineers need to better understand nature itself to know how and when to appropriately apply biomimetics.

The idea of *internal, remote, and* ***local*** components performing *external and* ***global*** sensing and actuation is biologically inspired. In human and animal biology/psychology, *distal attribution* is the experience of thinking one is sensing phenomena directly where they occur, whereas we actually sense them in structures internal to the body (Loomis, 1992). While we speak informally of "the five senses" that connect us with the external world, most of our senses are in fact monitoring internal conditions. This dissertation is motivated by the question of machines benefiting from such introspection as well.

1.2.2 Applications

The use of multifunctional elements as both structural members and actuators, the integration of multiple materials, and the freedom from dependency on external drivers are specifically attractive to many fields. Many biomedical applications require these qualities, including surgical tools and grippers, active-assist joints, and active valves. At a larger scale, we can create sense-and-control response within compliant shape-morphing structures for aircraft wings and lumbar support devices.

There are other applications suggested by biology that can take advantage of distributed actuator sets. In facial expression, there is the task of using a minimal, discrete set of a muscles/actuators to create a diverse set of expressions (shape changes), further complicated by the coupling of the compliant actuators and the compliant skin. Thus,

the proposed methodology can help generate devices to aid expression in humanoid robotics. The design of the human voice-box and vocal tract is a similar problem, where only a few muscles are capable of producing a wide variety of shape change which we modulate to create speech. Again, this principle of component independence can be used to create analogous acoustic technology. Additional applications specific to shape and point manipulation are described in Chapter 6 and 7.

1.3 Scope

The focus of this research lies at the intersection of four system components: structure, actuation, sensing, and control (see Figure 3). While the ultimate goal is achieved by simultaneously integrating all of these in the design synthesis process (**A**+**B**+**C**+**D**), I have broken these down and focused on the interaction of the individual components.

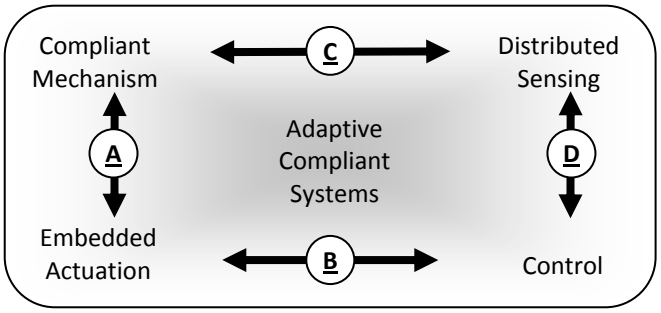

Figure 3: Topics comprising the Synthesis of Adaptive Compliant Systems (A, B, C, and D refer to *interactions*)

I have investigated these basic research issues: *(1)* optimal layout of the compliant structure and actuators (**A**), *(2)* the framework for the event of embedded controls in adaptive compliant systems (**A**+**B**), and *(3)* the logical extension of the embedded *actuator* framework to create a parallel method for a distributed *sensor* network (**C**+**D**).

In all of these, I seek a generalized synthesis scheme in which the design requirements are captured in a mathematical form to transform an initial grid of elements into an optimal layout of elastic beams, sensors, and actuators. This dissertation presents a specific methodology for the first two issues, **A** and **A+B**, along with numerical results and discussion. The extension to **C+D** is then demonstrated. The final example of this dissertation combines all four areas together (**A**+**B**+**C**+**D**) to achieve optimized compliant systems with both actuators and sensors, but without explicitly addressing *controller* design.

1.4 Organization of Dissertation

This first chapter has indentified the simultaneous synthesis of compliant systems and embedded components as a compelling research endeavor. Chapter 2 first explores the foundational work in compliant mechanisms that is the basis on which I build. Chapter 2 also reviews the literature for similar work regarding actuator and sensor placement, as well as the manufacturing technologies that are now making multifunctional systems possible and accessible. In Chapter 3 the specific tasks of this dissertation are defined and formulated. Particular attention is given to how actuators and sensors will be represented within a compliant mechanism framework. The actual implementation of these ideas for optimization in a genetic algorithm is covered in Chapter 4. The objective functions to be optimized are formulated in Chapters 5 and 6. First is energy efficiency, which is studied for increasing numbers of actuators in the results section of Chapter 5. Chapter 6 introduces additional objective functions pertaining to the concepts of controllability and observability as structural properties. Many studies are

performed to assess the robustness and nonlinearity of these properties. This chapter concludes with examples of controllable devices, observable devices, and finally devices that have both properties. Chapter 7 demonstrates the generalizable power of the same metrics, applying them to the task of single-point manipulation with a compliant system. Finally, Chapter 8 reviews the key findings and contributions of the dissertation, with comments on the issues of nonlinearity, controls, and dynamics.

Chapter 2

Related Work

The foundation and inspiration for the development of compliant systems comes from the field of compliant mechanisms. The relevant history and contributions of this field will first be discussed. A short review of research outside of the field in regards to the new tasks of control and sensing is also in order.

2.1 Background

A brief history of compliant mechanism design begins with the work of Ananthasuresh in 1994 (Anathasuresh, 1994; Anathasuresh and Kota, 1995), who first proposed using a structural optimization approach for mechanism design. Many followed, implementing the ground structure approach, energy efficiency formulation, refined size/shape optimization, and inclusion of nonlinear deformation effects. Refer to the dissertations of Lu (2004) and Saggere (1997) for a detailed history.

Compliant mechanisms can be designed for any desired input-output force-displacement characteristics while also meeting specified volume/weight, stiffness, and natural frequency constraints. As flexure is permitted in these mechanisms, they can be readily integrated with unconventional actuation schemes including artificial muscle,

thermal, electrostatic, piezoelectric, and shape-memory-alloy actuators. The synthesis of these mechanisms has been well studied (Yin and Ananthasuresh, 2003), and their advantages have been well documented, including: energy storage, ease of manufacture, and absence of wear, backlash, and friction.

Figure 4: (a) Comparison of a multi-part conventional office-stapler with a no-assembly compliant stapler, (b) Adaptive Compliant Wing – embedded compliant mechanism provides leading edge camber change on demand (c) A MEMS electrostatic actuator integrated with a compliant motion amplifier running at 27KHz. (U.S. Patents: Kota, 1999 and 2002)

2.2 Distributed Compliance

Figure 5 illustrates the idea of distributed compliance, showing a MEMS actuator with an integrated compliant motion amplifier.

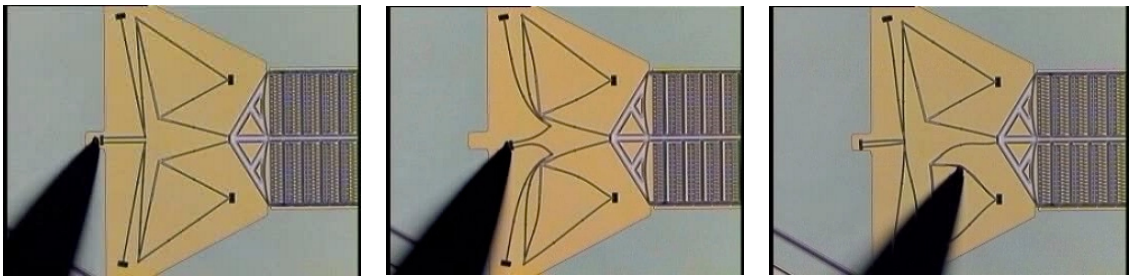

Figure 5: A MEMS actuator integrated with a 20X motion amplification compliant mechanism is being mechanically probed. Figures illustrate distributed compliance where beams and the mechanism deform as a whole without any stress-prone flexural joints. The device was fabricated at Sandia National Labs using Sandia's SUMMiT-5 process. (U.S. Patent: Kota et al., 2001)

A significant difference exists between conventional flexures and the compliant mechanisms discussed in this dissertation. Conventional flexures have relatively rigid

sections connected by very thin flexural joints. These flexures localize the deformation and are prone to high stresses and reduced fatigue life. Such flexures have been known for a long time (Paros and Weisbord, 1965) and have been successfully employed in less-demanding applications (e.g. shampoo bottle lids). The mechanisms discussed here have distributed compliance, i.e. they deform as a whole and do not have any joints, flexural or conventional. The property of distributed compliance (Yin and Ananthasuresh, 2003) has enabled the study of compliant mechanisms for use in shape-morphing (Saggere and Kota, 1999; Kota, 2002; Lu and Kota, 2003; Lu, 2004; Trease and Kota, 2007) that are predecessors of this current work.

2.3 Synthesis Methodology

Synthesis involves two stages: (I) generation of the mechanism topology and (II) determination of optimum size, geometry, and shape of various constituent elements of the mechanism. A pictorial summary of one such design method is shown in Figure 6, illustrating how a compliant gripper is created algorithmically. Starting with functional requirements of desired forces and displacement, a conceptual design is automatically created in Stage I topology synthesis. Based on material constraints (e.g. permissible stress, strain), fabrication constraints (e.g. minimum feature size), external loads, and desired mechanical advantage, the exact size, shape, and geometry of each of the beam elements is optimized in Stage II.

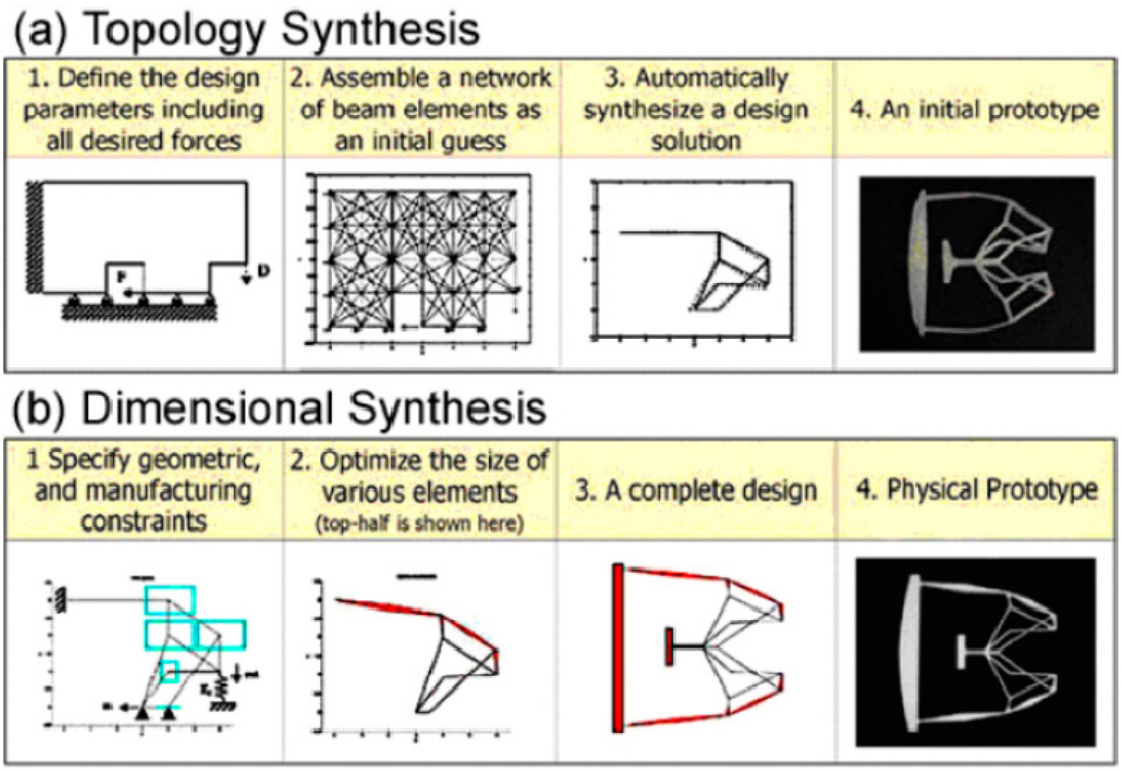

Figure 6: An illustration of the typical two-stage approach for compliant mechanism synthesis: (a) Stage I: topology synthesis, and (b) Stage II: dimensional synthesis. Image from Lu, 2004.

2.3.1 Parameterization

An important task for any topology synthesis problem is the parameterization of the design space. The physical design space must be broken down so as to be represented by a set of variables that an optimizer can act on. The earliest methods for topology synthesis use a technique known as homogenization (Bendsoe and Kikuchi, 1988), where a grid is placed over the design space, with each cell containing a hole of variable size and orientation. While this is still in use, a more common technique also based on a cellular grid representation is the Solid Isotropic Material with Penalization (SIMP) method (Bendsoe, 1989). Here, every cell element is filled with material and the design variables determine the stiffness properties as a fraction of the material modulus, from

zero to one. Both of these methods often have issues leading to *lumped* compliance (hinges) in their final designs.

Since *distributed* compliance is favored for compliant mechanisms, this has motivated other techniques such as the Grounded Structure Approach (GSA), which is used in this dissertation. Here the design space is covered by a grid of nodes. The nodes are connected by beam or truss elements; the design variable is typically the thickness of each element. The designer has the option of specifying the degree of nodal connectivity. That is, every node can be connected by an element to every other node in the grid, or only to nearby neighbors. The former is a more complete representation, but more computational costly, as the number of elements scales quite dramatically as the number of nodes increase. The latter has been proven successful by many in the field. To offer some additional design freedom while still limiting the number of elements, some have parameterized the node locations as well, allowing them to wander within a proximal range determined by the designer (Hetrick, 1999).

The extreme form of the wandering nodes method is to have only a few nodes and let them wander the entire design space. Several have done this, connecting the nodes with straight line elements (i.e. the Load Path Method by Lu, 2003 and 2004). Others have used the wandering nodes as the control points for curving splines that pass through them (Jutte and Kota, 2007).

Another quite novel parameterization is the Level Set Method. Here the topology is implicitly defined by a point-wise defined function the covers the entire design space. The function thus represents a surface that when sliced horizontally divides the design space into two regions: those above the surface and those below it. These two regions are then considered as the empty void and the material-filled solid region.

Finally, because of issues inherent to any parameterization, some have tried a building block approach to designing compliant mechanisms (Kim et al., 2006). Here, elements of known shape and function are combined in series and parallel. The methods focus on theories and understanding of how the individual elements will interact as a whole. These methods also have the benefit of being more intuitive to the engineer that is able to see how the function is broken down part by part. However, in this dissertation, the multi-objective tasks that are targeted are beyond the scope of building blocks, as each component interacts with each other in different ways for each objective; the final configuration and performance is non-intuitive and emergent.

2.3.2 Optimization Methods

Because of the broad design space and number of elements, most topology synthesis problems are designed with optimization methods. Many approaches have used continuous optimization with gradient-based search. These work well when the entire objective function can easily be calculated repeatedly for the entire design space. It is often possible to even calculate the closed-form analytic derivative of the objective function, which can speed up solutions dramatically.

However, there are many aspects that make continuous optimization unfavorable. First, the design space is quite often noisy and nonconvex, which leads gradient-based methods only to locally optimal solutions. Further, when the parameterization is discrete (i.e. elements are either on or off), or when there is a discrete number of components (actuators) to be optimized, then gradients often have little meaning and ability to drive the optimization. In these cases, another set of algorithms is often favored. These are evolutionary algorithms which perform global search over a design space, of which the most commonly used in topology synthesis are genetic algorithms. These have been used by many in the field for a variety of parameterizations (see Parsons and Canfield, 2002, for a history). Genetic algorithms are also readily transformed to explore entire Pareto fronts of multi-objective problems. That is, they can explore all possible combinations of the relative weightings of the terms in the objective function. This enables much deeper insight as to the fundamental tradeoffs and limitations of design, as has been demonstrated by several works by Canfield et al. (2006).

2.4 Controllability and Observability

A collection of related literature regarding the optimal placement of actuators and sensors for acoustics and vibration control is summarized by Padula and Kincaid (1999). While many of these studies use genetic algorithms, they focus on structural rather than mechanism (motion transmission) problems. For them, mechanical tasks are typically defined externally to the system, while the structural properties are typically internal. Several researchers have investigated the placement of actuators on vibrating plates

(Hać and Liu, 1993; Sadri et al., 1999) and at least one (Bruant et al., 2001) considers actuator and sensor placement on simple, fixed structures (1 to 3 beams), also for vibration suppression. Most authors examined only fixed topologies, except for Begg and Liu, who investigated simultaneous topology optimization and actuation placement for cantilevers (Liu et al., 1997) and trusses (Begg and Liu, 2000). The objectives of vibration suppression problems are fundamentally different than my own. It remains to be seen whether the same metrics used for controllability and observability of smart structures for vibration suppression can be applied to compliant systems, which do not suppress vibration but perform prescribed mechanical tasks.

2.5 Shape-Morphing Mechanisms

The task of shape change has been addressed by several others studying compliant mechanisms (Saggere and Kota, 1999; Kota, 1999 and 2002; Lu and Kota, 2003). Shape-change objectives can be implemented via least squares formulations, by calculating the deviations of points on a deflected structure from corresponding points on a target curve. These works considered the one-degree-of-freedom shape-change problem, where the final target shape is determined ahead of time and specified by the designer when formulating an objective function. With the introduction of multiple, optimally-placed actuators, my work does not seek a specific target shape, but rather the ability to achieve any shape required of the device.

Saggere and Kota (1999) had recognized some of the issues that are now quite relevant again. They confirm the benefits of reduced actuator number, stating: "Other

challenges in applying this technology are the numerousness of the actuators required, the associated complexity of their control and nonavailability of robust distributed parameter control strategies." They goes on to affirm the concept of internal components acting externally:

> ***"Moreover, since the actuator in this approach can be located away from the structure, the actuators and the structure can be protected from undesirable effects such as exposure of smart actuators to unstructured environment and stress concentrations at the interface between the structure and the smart material. This is especially useful in the camber shaping of wing structures where it is desirable to enclose the actuation system completely within the contour of the airfoil leaving the external surface smooth for a drag-free performance."***

2.6 Actuator Architecture

There are a few literature references to the optimization of *actuator architecture*. Actuator architecture problems aim to lay out the material makeup of an actuator, but do not address how that actuator relates to the rest of a physical system. Most of these studies focus on the distribution of only the actuator material, without any supporting structural elements. (Nelli Silva et al, 2000: piezoelectric actuator material distribution; Anusonti-Inthra et al., 2003: actuator material layout in a flexible airfoil; and Langelaar & Van Keulen, 2004: shape-memory-alloy actuator material distribution.) Their results consist of only actuators; see Figure 7 and Figure 8. Such a structure may be suitable when considering the entire device as a single actuator component, but is impractical in describing implementation of discrete actuator components within a mechanical

system. Bharti and Frecker (2003) consider the passive and active material distribution problem. However, the choice of actuator or structure is not a variable but a post-processing decision, and again, the results are not yet applicable to practical component layout (Figure 10). Their results are better interpreted as the layout of passive and active material within a *single* actuator component. However, the need for discrete actuator *placement* is stated, but no method is yet provided for how a systematic and accurate interpretation is to be made. Such limitations in the related research further motivate my pursuit of this current research.

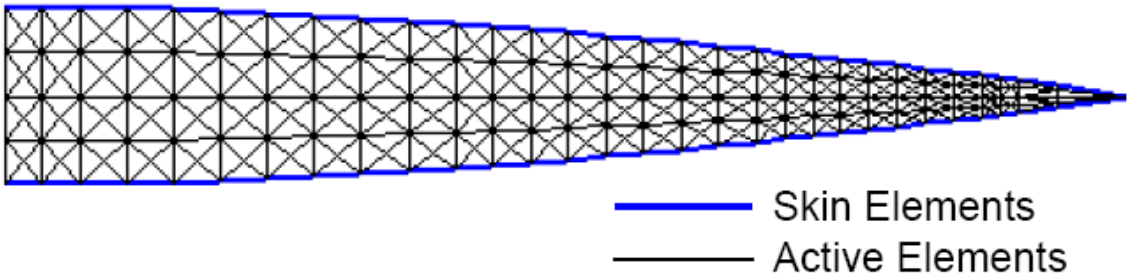

Figure 7: Design Domain Used for Actuation Distribution in a Flexible Airfoil. Results are shown in Figure 8. (Anusonti-Inthra et al., 2003).

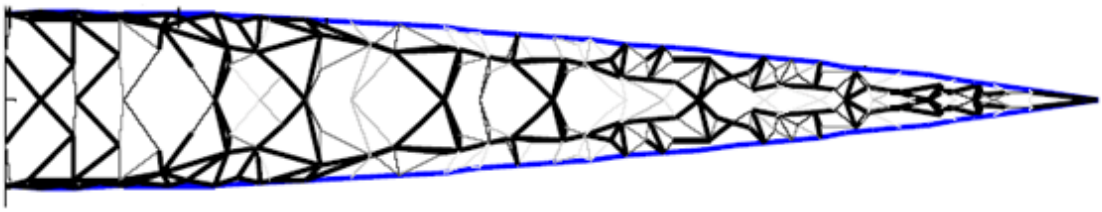

Figure 8: Actuator Distribution Optimization Results with a Volume Constraint of 50%. (Anusonti-Inthra et al., 2003).

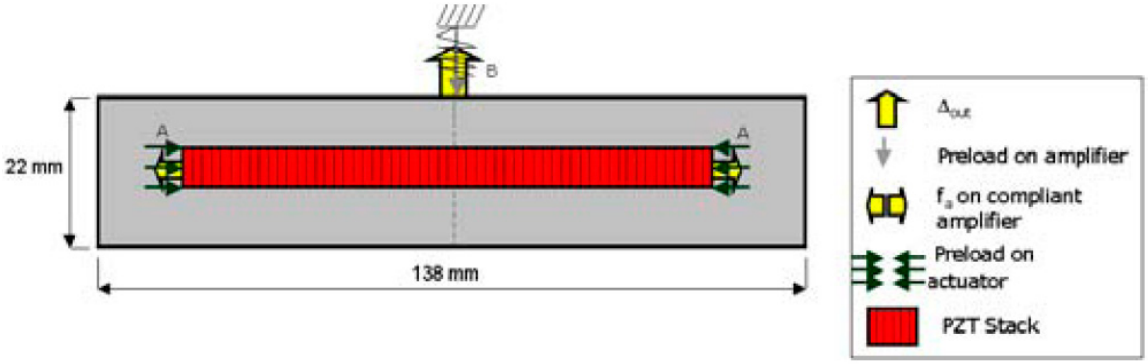

Figure 9: PZT Flextensional Actuator Problem, shown with internal, fixed actuator. Results are shown in Figure 10. (Bharti and Frecker, 2003)

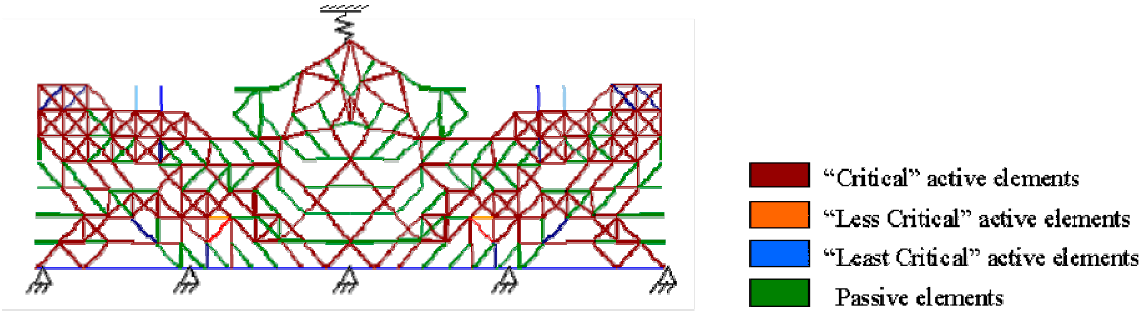

Figure 10: Results: Topology Optimization with all elements shown in different shades according to their relative importance in providing a maximized output deflection. (Bharti and Frecker, 2003)

The results in Figure 10 are undesirable for the same reasons as those in Figure 8. This is only a "material distribution" problem and not a means for integrating actuators within a structure.

2.7 Tensegrity Structures

Some readers may also be familiar with the concurrent role of actuators and structure within tensegrity systems (Skelton et al., 2001). However, such systems are fundamentally different from those in this dissertation, in material, methodology, and suitable applications. By their definition, tensegrity structures consist of axially-loaded cables and struts and are often used in self-deployment applications, while compliant

systems consist of compact structures performing mechanical tasks based on the controlled bending of beams.

2.8 Actuator Placement

Studies of the combined topology and multiple actuator problem remain very few and preliminary in nature. Bharti et al. (2005) employ different element types than presented in this dissertation for their structure (i.e. trusses and tensegrity structures instead of beams). Johnson and Frecker (2004) have also investigated optimal multiple actuator placement. They determine active (piezoelectric) and passive material distribution within a structure by using a genetic algorithm. In contrast to this work, they use truss elements, the actuator number is not explicitly controlled, but implicitly governed by an active volume ratio constraint, and there is no means of imposing or checking structural connectivity. Nonetheless, their preliminary results may offer a valuable comparison to my own, especially their studies of design parameters such as external spring stiffness.

Finally, Bernardoni et al. (2004) provide a study of a building-block approach to compliant mechanism design. Although sensors are not considered at all, some of their building blocks contain the actuators themselves, allowing for optimal actuator placement. While building blocks simplify the design process and are often intuitive, they do not offer the generality sought in this dissertation. Bernardoni's work is still quite relevant in the shared use of genetic algorithms and Pareto optimality. The topology is generated automatically using a multi-objective genetic algorithm such that

the force/motion ratio is maximized. The set of optimal solutions is explored by using the notion of Pareto optimality. An application of their design method is tested on an actuated compliant mechanism with two output degrees of freedom, using a manipulability metric from robotics to ensure independent control of the x and y degrees-of-freedom of an output point.

2.9 Sensors

The integration of *sensing* and compliant mechanisms has received much less attention than has actuation. However, it is well-known that using an elastic element in series with an actuator allows for force measurement, either by strain gauge or visual inspection. On the other hand, the task of precise measurement for feedback controllers is quite different with distributed compliant mechanisms. Compliant machines with distributed compliance, inertia, and sometimes damping or frictional elements, are more challenging to model or sense than lumped-parameter machines. Whereas traditional mechanisms use point-like sensors (e.g., the joint rotation sensor in a robot), compliant mechanisms do not concentrate their motion at a single point (c.f. a revolute joint). Traditional motion sensors, such as potentiometers, LVDTs, and optical encoders, are situated on the translational or rotational axes are matched to the discrete motions of traditional mechanisms. With relative motion no longer localized, there may be no obvious candidate location for optical encoders, either linear or rotary.

Fortunately, the distributed nature of compliant mechanism is amenable to other sensing schemes. The motion that must be sensed is distributed spatially across the

entire extent of a compliant member. This "distributed" character of motion in a compliant mechanism is well matched to "distributed sensing". For example, strain gauges can be placed anywhere on the structure and will map to the actuator displacements and external loadings. A more creative solution has also been developed for compliant mechanisms through collaboration of Kota and Peshkin (U.S. Patent: Peshkin, 2004). By proper design of Mutual Inductance Sensors (MIS), one can effectively integrate the motions of the compliant member being sensed over its spatial extent. The technology consists of embedded wires (or other conductive traces) in the compliant members. A pair of such traces – one may be thought of as a transmitter and the other as a receiver – communicate electromagnetically, coupled by their mutual inductance, which varies in response to deflection of the compliant member. Importantly, the signal from a distributed sensor is an integrated signal, which accumulates the deflection of the compliant member along its entire extent. Such sensors readily lend themselves to the compliant mechanism framework, as has already been physically demonstrated and depicted in Figures 11-13.

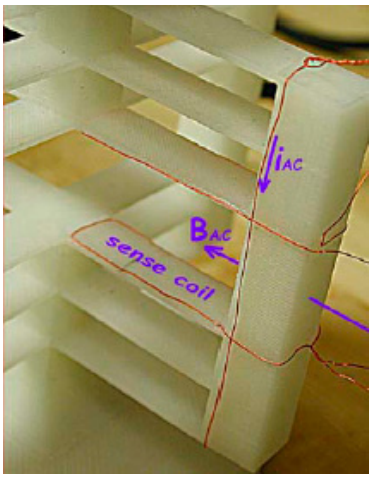

Figure 11: A compliant translational joint with MIS embedded sensing. Joint material is ABS plastic. Sensors consist of single-loop wire coils.

A key feature of the technology is that the transmitters and receivers may consist of single traces (multi-turn coils are not necessary.) The resulting signals are small but easily detected with modern electronics. Single traces can be fabricated inside or applied to the surface of compliant members. On traditional mechanisms, signals from distributed sensors would need wires to cross the gaps at other axes of motion, but on compliant mechanisms there need not be such gaps. In some uses, there may be many receivers for a single transmitter. An example of the use of distributed sensors on a compliant mechanism is measuring the deflection and shape of a compliant wing or fin in an autonomous aerial or underwater vehicle.

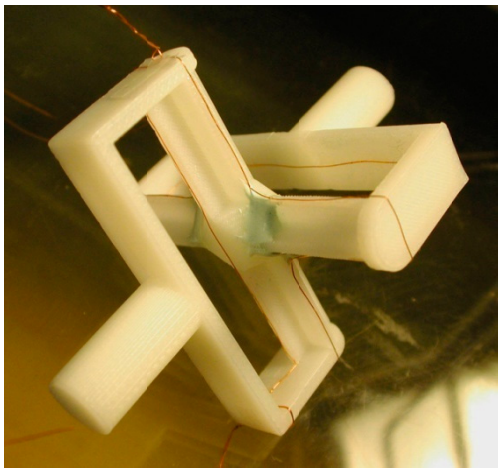

Figure 12: A compliant universal joint with MIS embedded sensing. Joint material is ABS plastic. Sensors consist of single-loop wire coils.

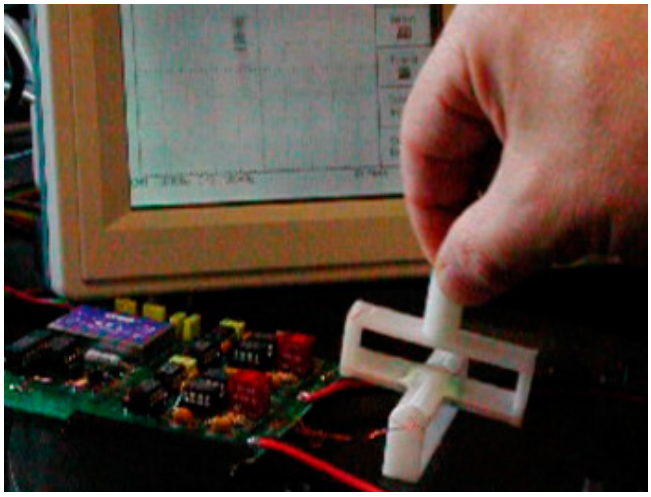

Figure 13: Tracking of a Compliant Universal Joint with embedded MIS sensing.

2.10 Manufacturing Techniques

Mentioned in the introduction are many new manufacturing techniques that are making multifunctional/multimaterial devices with embedded components more realizable. These include the wide variety of techniques that fall under rapid prototyping, such as stereolithography, fused-deposition modeling, and laser-sintering of metals. Further advances are being made in ink-jet based solid free-form modeling, which is now capable of layering a wide variety of materials within a single device. Examples even

include functioning fuel cells and batteries created without the interaction of human hands or machining tools (Lipson, 2005; Malone and Lipson, 2006).

The biomimetics laboratory at Stanford has been developing other processes capable of embedding components such as batteries, actuators, sensors, and fabric flexures within bodies of both soft and hard plastic. Their Shape Deposition Manufacturing (SDM) is a developing rapid prototyping technology in which mechanisms are simultaneously fabricated and assembled (Cham et al., 2002). As shown in Figure 14, the basic SDM cycle consists of alternate deposition and shaping (in this case, machining) of layers of part material and sacrificial support material. The resulting mechanisms can have almost arbitrary geometry, embedded actuators and sensors, and locally-varying stiffness properties, making them more robust and simpler to control.

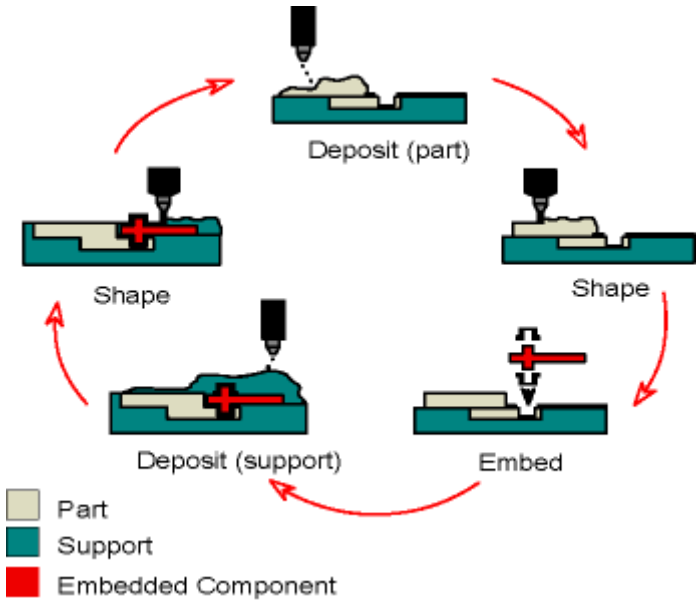

Figure 14: Shape Deposition Modeling. A new rapid prototyping technique that will enable fabrication of compliant systems. From http://www-cdr.stanford.edu/biomimetics/

2.11 Chapter Summary

Chapter 2 has placed the content of this dissertation within the context of the related literature. The field of compliant mechanisms is reviewed and is clearly the starting point for consideration of compliant systems. Several studies have looked at aspects of the research presented in this dissertation, but none in the generalized manner I present. The actuator, sensor, and manufacturing technologies that are fundamental to this dissertation are also covered. The next chapter looks at these components and formulates metrics for evaluating their performance within multifunctional compliant systems.

Chapter 3

Formulation

The following sections discuss the issues, tasks, and basic formulations that will bring us closer to the goal of highly efficient, multi-component, multifunctional engineered devices.

3.1 Basic Research Issues

The basic research issues of this dissertation are to identify and implement the appropriate objective functions for synthesis of embedded compliant systems. The choice of objective function may depend on whether actuator power, actuator number, and/or actuator effectiveness is to be optimized. In addition, I have studied potential actuators for use in such systems. A practical choice must be made when considering how an actuator's limitations constrain the design goals. Once chosen, the next task is to mathematically characterize actuators for inclusion in the optimization. Successful results require guaranteed structural connectivity, an important issue that is ensured using graph-based search methods. Another issue is setting the framework for "design for control" of embedded compliant systems. This is established by developing specific definitions for the input and output functions of the structure, followed by their mathematical implementation in the algorithms.

3.2 Task Definition

The first step is development of the optimization algorithms. Hypothetical actuators are chosen as the inputs to one of the following problems: Single-Input/Single-Output (SISO), Multiple-Input/Single-Output (MISO), or Multiple-Input/Multiple-Output (MIMO) mechanism design. These problems are traditional categories of mechanism design that can be applied to many situations. Work has already been done on the single-output problem with both single-actuator and multiple-actuator inputs (SISO and MISO). The next task would be the MIMO problem, which often is the same as the shape-change problem. Beyond those tasks, I also consider the multiple-load-case problem, which is the generalization of the adaptive-output problem. That is, with more than one actuator, more than one output can be achieved, and it is desirable to achieve as many *unique* outputs as possible with a small number of actuators.

Once the type of problem is chosen, all relevant quantities are parameterized for use in mechanical analysis and optimization. An output node is selected, for which a desired displacement or output force is prescribed. Multiple output nodes are chosen for shape control applications. Whether single or multi-node output, I also specify an external-load sensing region. The structure 'communicates' with its environment through this interface. The system must fit within a specified design space.

To properly constrain this research effort, several limitations have been imposed. Parameterization is limited to fixed-node ground structures, without any wandering nodes. Only frame elements are used, with one analysis element per topology element.

Finally, all the analyses are linear. These imposed limitations allow for very fast performance of the genetic algorithms, in that the stiffness matrices need only be calculated once. In the conclusions of this dissertation, I will go on to demonstrate how these simplifications not only improve speed but also effectiveness. The results that come from the fast, linear approximations are very good for the Stage I topology optimization, typically the more difficult and "creative" part of the design process (see §2.3). Should further refinement be required and performance verified, the resulting designs are excellent candidate for the Stage II size and shape optimization, a well-studied problem which is not covered in this dissertation.

3.2.1 Specific Tasks

Exploiting compliance or elasticity of the underlying structure has several benefits including elimination of mechanical joints, joint-wear, and joint-clearance. The inclusion of multiple actuators offers further possibilities: energy efficiency can be increased, reducing requirements of external energy sources. Increased actuator efficiency can be attained by seeking global optima at the system level. The proposed paradigm also embodies the notion of "continuous". Rather than placing discrete sensors throughout a rigid and discrete structure, distributed sensing can be achieved by embedding compliant sensors (simple wires coupled by mutual inductance) within a compliant structure (see §2.9). Such an arrangement may be practical for many applications ranging from haptic feedback on surgical manipulators to sense-and-control adaptive aircraft wings.

The vision of an adaptive, embedded compliant system is a synthesis of compliance, actuation, sensing, and control. It is a system that both senses and responds to the external environment via internal structures; a black box converting inputs to outputs. This trade from external to internal components offers several benefits, initially introduced in §1.2. First is efficiency by part reduction. A few well-placed actuators inside a structure may be capable of many complex deformations of the external structure. Likewise for sensing: rather than numerous, costly pressure sensors along the external boundaries of the system, a small number of internal sensors can determine the internal state of stress and map it to the external environment (see Figure 15 and Loomis, 1992). Such elements are safe from potentially harsh environments; they are even protected from the conditions they are sensing or generating. Furthermore, placing flow sensors or pressure sensors on the *surface* of an airfoil can adversely affect the flow characteristics.

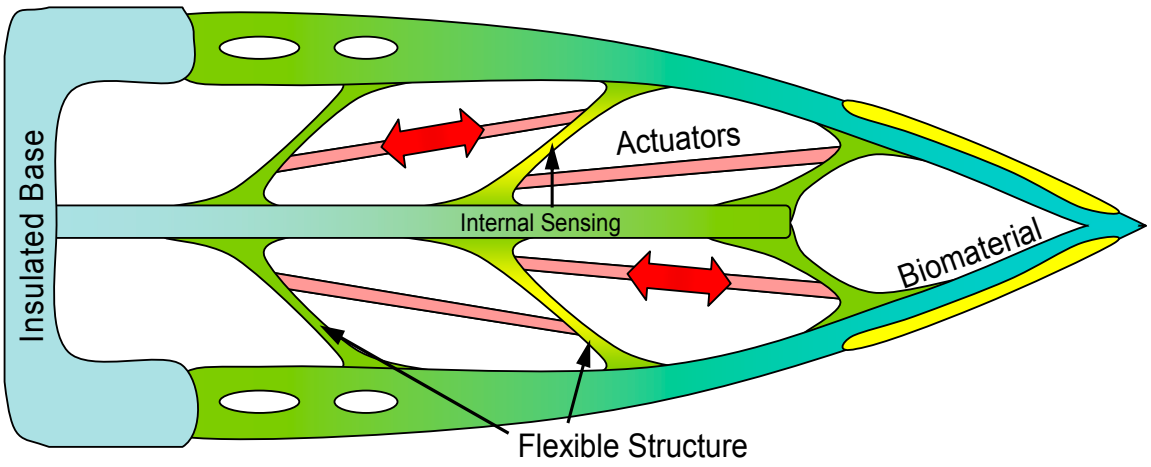

Figure 15. Artistic Vision of a fully Embedded and Distributed Compliant System

More specifically, I use the internal stress states as a means to map the external conditions. This is particularly useful, for instance, when the on-set of stagnation pressure on an airfoil must be sensed slightly in advance to signal an appropriate actuator to deform the trailing edge by a certain amount, thereby changing the angle of attack. Certain internal elements of the compliant system can be designed to deform predictably to maximize the sensitivity of a sensor embedded within these elements. Although force can be sensed directly at the point of interest with pressure sensors, the external pressure forces are interpolated from the internal stress state of structure. Utilization of such internal sensors has the potential to measure "modes" of pressure deflection. Summing various modes of deflection may be better than directly measuring along the surface of interest. This will further protect the sensors from the environment and fewer internal sensors may be needed. More importantly, the placement of internal sensors avoids the tradeoff of needing the output to be stiff against external loads yet compliant enough to create measurements.

Most importantly from a research viewpoint, essentials of the basic design conflict can be studied. A specific conflict to be examined is the need for components to be *decoupled* to actuation, yet *coupled* with respect to external loading. Further, the same elements that form the load-bearing paths are also used to leverage the displacement of the actuators. One seeks to find insight to these questions by exploring the results from a flexible and generalized methodology.

3.3 Embedded Actuation

By "embedding actuators" within a compliant mechanism, I refer to a topology design process that simultaneously determines the configuration of the actuators and the compliant structure. That is, certain beams in the initial set will transform into actuators during topology synthesis. The result is not simply an optimized mechanism, but an optimized system with the number, size, location, and orientation of all actuators matched to the simultaneously synthesized structure of the mechanism. Such a system will have better performance compared to one in which the actuator is "integrated" after the fact.

Most actuators can be characterized by four key design specifications: force, size, displacement, and frequency. Power consumption can be treated as a cost factor for further comparison. Typically, actuators with high displacement provide low force and vice versa. Even for a given actuator, the maximum force and maximum displacement are not achieved at the same time. The maximum force is the "blocking force" measured when there is zero displacement. The maximum displacement is the "free displacement" measured when there is no load in resistance. Therefore, each actuator is not represented by a point on this graph, but by its characteristic performance curve. It is therefore critical that actuator selection is based on the entire motion characteristics (force-displacement curves) rather than single-point designs. Huber, Fleck, and Ashby (1997) provide a systematic method of selecting actuators.

3.3.1 Actuation Selection and Evaluation

Actuators best matched to our needs will be those that exhibit capability as structural elements. Actuators of interest include Electrostrictive Polymer Artificial Muscles, Electrically-activated Polyacrylonitrile (PAN) muscles, Ionic Metal Composite muscles, and Shape-Memory-Alloy (SMA) actuators. Studies can evaluate which actuators are the most practical and how their limitations affect the research objective. For example, shape memory alloy wires on their own provide little structural stiffness except in tension. Piezoelectric benders may serve well as long as not loaded in tension. A possible solution is a smart actuator composite; a composite material embedded with shape memory alloy wires would be able to support bending and compressive loads as well as generate force.

3.3.2 Commercial Artificial Muscle Actuators

Of particular interest are commercial artificial muscle actuators. These are among the cutting edge of actuator technology, often supplying the greatest displacements and strains compared to others. Their biological-inspiration may indicate suitability for use in compliant systems. The actuators have bidirectional operation and are feasible as structural members as they possess both axial and bending stiffness. Examples fabricated by Artificial Muscle, Inc. are shown in Figure 16.

Figure 16: Commercial Artificial Muscle Actuators. Bending and linear types are shown. http://www.artificialmuscle.com/

3.3.3 Actuator Modeling

A powered actuator generates a force that corresponds to its unique load-displacement actuation curve and the stiffness of the system upon which it acts. Thus, one should capture this load-displacement curve within the structural analysis. The analysis will reveal the actual actuator output force and displacement.

I use a linear actuator model, depicted in Figure 17. In the model, neither force nor displacement is applied directly, which is often the case in previous literature. Rather, I apply constant *power*, which more realistically represents real actuator operation. The actuator's output will be a portion of the block force (F_b) and free displacement (d_F). The ratio of F_b/d_F is the actuator stiffness, k_{act}. The actual force (F_o) and displacement (d_o) are determined by the actuator's interaction with the rest of the compliant system (see the system stiffness line in the figure). This results in a coupling of actuator properties to compliant mechanism design that allows for more accurate system synthesis. In the analyses for the algorithm, this is implemented by using a beam element of the correct actuator stiffness, with axial forces equal to the block force applied at the ends of the beam (i.e. $F_{in1} = F_{in2} = F_b$ in Figure 20-a).

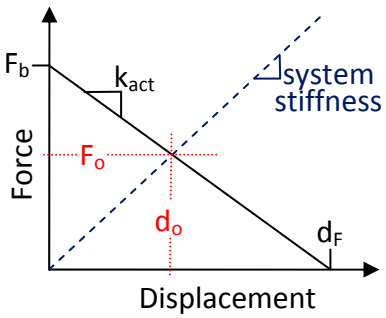

Figure 17: Actuator model parameters. Only the stiffness curve (k_{act}) is provided. Interaction with the system determines the actual output force (F_o) and displacement (d_O).

Using the above actuator formulation in an optimization process that maximizes system efficiency should result in structures that are stiffness matched to the actuators. This tendency is left as a hypothesis and not explicitly imposed in my formulation. The results in Chapter 5 (§5.4) are used to validate whether stiffness-matched structures actually result. It is noted that the stiffness of the structure also includes the stiffness of the actuator. Thus, I predict that both the actuator stiffness and output stiffness will determine the final structural stiffness through the goal of maximum system efficiency.

3.4 Embedded Sensing

As described in §2.9, compliant systems are *not* lumped-parameter devices. Aspects of the dynamics that are unmodeled or unsensed often limit the performance of traditional (lumped-parameter) machines under closed-loop control. For instance, in a robot arm, one may have a rotational encoder at a joint, but without means to monitor the flexing of a link. Robot links are built to be relatively stiff, so that modeling them as perfectly stiff is a good approximation, at least up to some frequency. Stiffness adds weight of course, motivating the development of alternative solutions. One such solution is provided by compliant systems with embedded sensing.

Of the two embedded sensing methods described in Chapter 2, the strain gauge method is applied in this dissertation. Strain is chosen to be measured at the *center* of a beam on its surface. While this restriction does not affect the quality of the results generated in this work, other possibilities are discussed in the results section for optimal sensor placement, §6.2.3.

The equation for strain at the midpoint along the beam is:

$$\varepsilon\left(\frac{l}{2}\right) = \frac{(x_2 - x_1)}{l} \pm \frac{h}{2l}(\theta_2 - \theta_1) \tag{1}$$

where ε is strain, l is the beam length, h is the in-plane beam thickness, x_i is the axial nodal displacement, and θ_i is the nodal rotation. The fact that each beam has two different possible strain readings corresponding to its center is important and is reflected later in Chapter 6 when determining which set of sensors has the most independent response.

3.5 Efficiency & Orthogonality

The specific metrics to be developed to evaluate and design compliant systems are energy efficiency and component orthogonality. Energy efficiency is a standard metric for the design of compliant and is further considered for multi-actuator systems in Chapter 5. Two other concepts at the core of this dissertation derive from the desire for component independence (orthogonality) in multifunctional systems. For actuators, I call this property *controllability* while for sensors it is *observability*. These concepts

were first described in the Motivation section of Chapter 1, are now defined, and will be formulated and demonstrated in Chapter 6.

I borrow the terms controllability and observability from the field of control theory. A task of this research is to create specific, mathematical definitions of these terms as they apply to spatial inputs and outputs of compliant structures. While it may result that my definitions are only analogous to those from controls, it may turn out that the specific parts of the controls definition apply directly to my problem. From Ogata's Modern Control Engineering textbook (1990), these terms are defined:

> ***Controllability: A system is said to be controllable if it is possible by means of an unconstrained control vector to transfer the system from any initial state to any other state in a finite interval of time.***
>
> ***Observability: A system is said to be completely observable if every state can be determined from the observation of y(t) [sensed output vector] over a finite time interval. The system is, therefore, completely observable if every transition of the state eventually affects every element of the output vector. This is useful in reconstructing unmeasurable states from measurable ones.***

While the above definitions include the concepts of *state* and *time*, these are disregarded in the quasi-static concerns of this dissertation. Thus, these terms are not entirely correct with regard to controller design, but serve to remind the designer of the structural tasks being pursued. When incorporating controller design in future

extensions of this research, one should take care to use the qualifier "structural" before these terms.

3.6 Structural Analysis

The basis for calculating all of the compliant system metrics in this dissertation stems from linear finite element analysis (FEA). The results from the FEA are used to calculate efficiency, stress, controllability, and observability as needed. The element of choice for all the analyses is the beam (frame) element, which captures the desired planar bending and deflections required of compliant systems. The shape functions for the beam element are cubic hermite polynomials, which result in linear stress and strain along a beam's length. A beam has six degrees of freedom (x, y, and θ at each end), for which the stiffness matrix, k, is given in Eq. (2). The stiffness has units such that it converts the displacement vector (x_1, y_1, θ_1, x_2, y_2, θ_2) to the force vector (F_{x1}, F_{y1}, M_1, F_{x2}, F_{y2}, M_2).

$$k = Eb\begin{bmatrix} \frac{h}{l} & 0 & 0 & -\frac{h}{l} & 0 & 0 \\ 0 & \frac{h^3}{l^3} & \frac{h^3}{2l^2} & 0 & -\frac{h^3}{l^3} & \frac{h^3}{2l^2} \\ 0 & \frac{h^3}{2l^2} & \frac{h^3}{3l} & 0 & -\frac{h^3}{2l^2} & \frac{h^3}{6l} \\ -\frac{h}{l} & 0 & 0 & \frac{h}{l} & 0 & 0 \\ 0 & -\frac{h^3}{l^3} & -\frac{h^3}{2l^2} & 0 & \frac{h^3}{l^3} & -\frac{h^3}{2l^2} \\ 0 & \frac{h^3}{2l^2} & \frac{h^3}{6l} & 0 & -\frac{h^3}{2l^2} & \frac{h^3}{3l} \end{bmatrix} \quad (2)$$

3.7 Chapter Summary

This chapter began with the practical steps and tasks required to achieve the goals of multifunctional compliant systems described in Chapter 1. Mathematical models were created to address the performance of actuators and sensors within a compliant system. The key objectives of energy efficiency and structure/component orthogonality were also introduced; these will be further formulated in their own respective chapters, Chapter 5 and 6. First, though, Chapter 4 will cover how these concepts are implemented within a genetic algorithm to enable computer-aided design.

Chapter 4

Methodology

With the goals of compliant system design that were formulated in the previous chapter, a methodology for implementing and optimizing those characteristics is now developed.

4.1 Overview of Methodology

The basic outline of the research is shown in a flowchart in Figure 18 and a pictorial example in Figure 19. First, the design specifications are identified, from which the problem type is determined (Figure 19-a). The available solutions to the problem potentially contain compliant mechanism, actuator, and sensor components. The design space must be properly parameterized in terms of these components (Figure 19-b), which is critical for the success of the optimization.

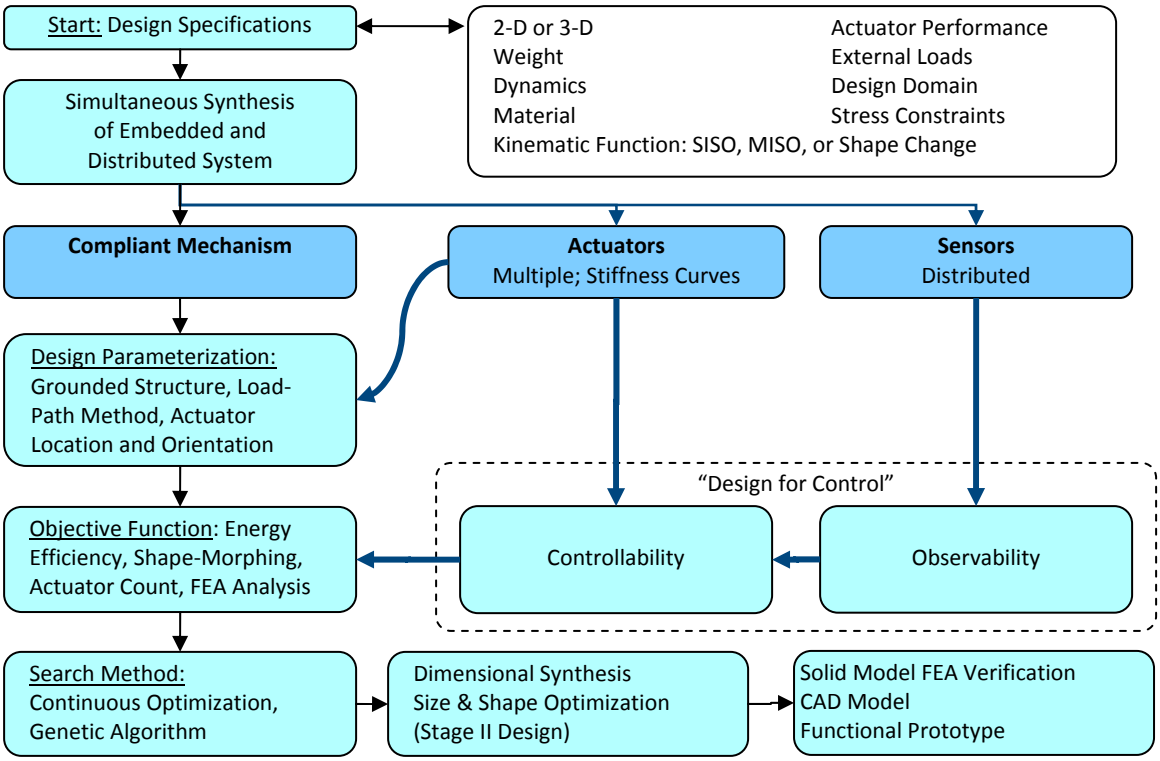

Figure 18: Overview of the Synthesis Method

The high-level goals of optimization in the embedded actuator problem are to minimize actuator number and size, to maximize energy efficiency, and to meet other constraints on factors such as size, weight, displacement, and stress. Application of a search method finds the optimal system (Figure 19-c). Results are further refined in size and shape optimization (Figure 19-d). Finally, there will be verification of the design and methodology via solid model finite element analysis and testing of functional prototypes (Figure 19-e,f).

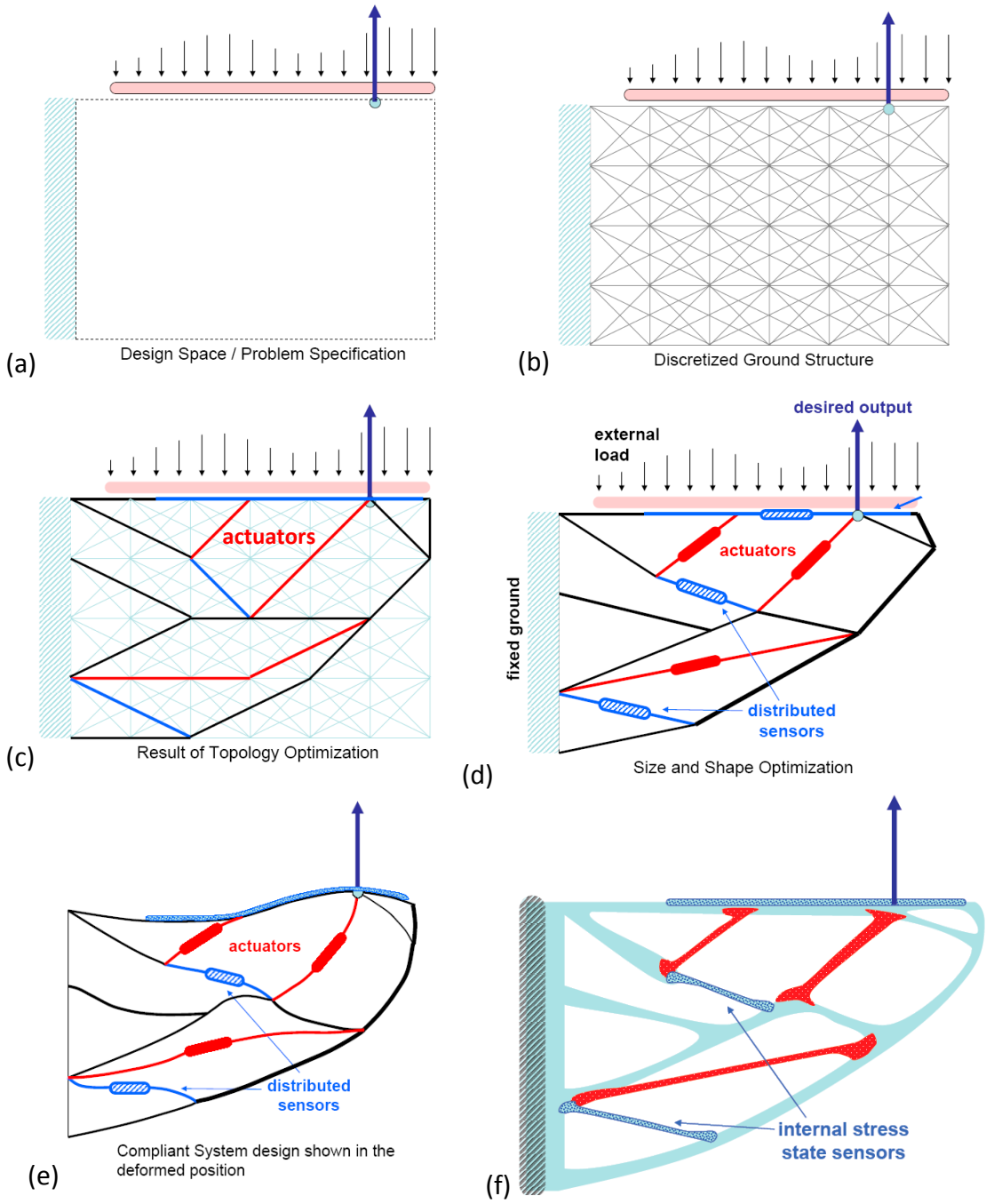

Figure 19: Various steps in the synthesis scheme. (a) design specifications. (b) initial array of beam elements as a ground structure. (c) optimized topology of beams, actuators, and sensors. (d) size optimization. (e) deformed position verified with solid model FEA. (f) physical interpretation, fabricated for experimental verification.

I begin with the given problem specifications and design space, depicted in Figure 19-a.

The workspace constrains the maximum allowed size of the system. Portions of the

workspace deemed to be fixed (connected to either ground or another structure) are indicated. The specific output points (blue circle) and desired output direction (blue arrow) are shown. Many synthesis problems also include reaction forces at the output point; either a reaction load or an external spring. Here, the external load is applied along a loading region depicted in pink. The external load in the case is an uneven pressure along a line, shown by the black arrows. Note that no input ports are specified; it is only required that the actuators fall within the physical workspace.

Step (b) shows the workspace discretized using the ground structure approach, described in §2.3.1. Resolution depends on the number of nodes used and the adjacency of connected nodes. In the figure, no elements span more than two square units. Each element is represented by a discrete variable that will determine its presence in the optimal structure. The structural and actuator materials are specified, allowing each element to contribute to the overall structural stiffness.

Step (c) is the result of the topology synthesis optimization achieved with a genetic algorithm. The result reflects the specified objective function subject to the given constraints. Actuators are indicated in red and elements with embedded sensing in blue. Mechanical work terms are found by analyzing the structure with the finite element method. Actuators are represented by more than point forces or displacements; they are designated as structural elements with load-deflection output curves, as discussed in §3.3.3.

After the topology is determined and fixed in step (c), the individual elements are resized and reshaped in step (d), the Size and Shape Optimization (Stage II, §2.3). All of the external loading conditions are still applied, but the objective function may be changed to fine tune the structure's function, such as optimal geometric advantage. Buckling constraints may be included at this stage to check and prevent element failure. Note how the elements adjust in length and thickness, yet the original topology is maintained.

Step (e) shows the synthesized structure in its deformed state. As stated earlier, the distributed internal sensors are preferred to external sensors because they can determine external loads with fewer elements, while not exposed to the environment. It is intended that the internal and embedded nature of the sensors provides for simplified control of the embedded actuators. Finally, step (f) shows a physical interpretation of the synthesized structure. The figure conveys the vision of a monolithic compliant skeleton with embedded sensors and actuators acting as a cohesive whole.

I report several examples of the methodology in use. The first is the traditional task of displacement amplification, now accomplished with multiple actuators. The second task is a controllable and observable shape-adaptive wing, possible *only* within the new multiple actuator formulation. The final examples look at extending the methodology from shape control to *point* control. All problems use the same genetic algorithm (GA)

for optimization and grounded structure approach (GSA) (Frecker et al., 1997; Hetrick and Kota, 1999) for parameterization. The remainder of this chapter describes the general methodology common to all problems, with the specifics of the objective functions described in their own chapters, 5 and 6.

4.2 Parameterization by the discrete Grounded Structure Approach

The design domain (workspace) is broken down into a grid of nodes, which are interconnected by beam elements (Figure 20-b). A design variable exists for every element and determines whether the element is present. A value of zero deactivates the element, removing it from the structure; other values represent thickness values. In the current algorithm, the thickness can be one of three predetermined discrete values. In addition, there is a variable for every actuator to be used in the structure. This variable has a value between 1 and the total number of elements. Its value marks the element selected to be the actuator in a given structure. This approach guarantees a specified number of actuators for each problem and will prevent results like the cluttered ones found in related Actuator Architecture literature (§2.6). However, when using the GSA with a genetic algorithm, a number of connectivity problems can occur (Lu and Kota, 2003); a variety of graph-checking constraints are added to resolve the issue.

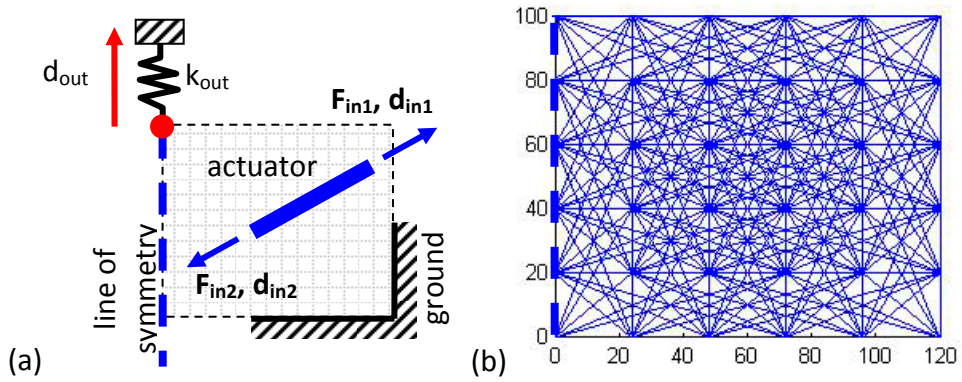

Figure 20: (a) Design Domain for an symmetric actuator amplifier. An output spring is used as a basis for calculation of energy efficiency. (b) Discretization: 6x6 grid, 250 elements

Connectivity, mutation, and cross-over are all governed by graph searches. Graph connectivity is stored in a data structure that indicates how every node is connected to every other. The data structure is a lookup table that indicates the distance between any two of the nodes. While the data structure is complete (every connection is accounted for), not every connection is in the allowed pool of available elements. That is, the ground structure is not "fully connected". Instead, the data structure is easily filtered to include only elements less than a specified length and discard any overlapping elements. This partially connected structure results in many fewer design variables and greatly reduced computation time, while still effectively representing the design domain.

The variables that represent actuators and sensors are even more restricted. A maximum and minimum length for each is specified by the designer, which is used to further filter the element set. This helps in preventing scaling effects in the formulation; i.e. a fine resolution network of short elements is possible, while the available set of actuators can be restricted to much longer elements.

4.2.1 On the Selection of Grid Resolution

It is up to the designer to determine how many nodes and elements should be in the ground structure. Solutions times grow as these numbers increase. Therefore, as few elements as possible that are capable of generating feasible designs should be used. In this dissertation several grid sizes are employed: 5x5, 6x6, 8x4, and 8x7. Reasonable results are found with even with the smaller numbers of nodes and elements. This is one of the benefits of the grounded structure approach; the elements are already in the form of what is considered the likely solution: long beams. Thus, increasing the resolution does not necessarily lead to the discovery of better designs.

An additional rule of thumb for the controllability and observability problems is that the ground structure should contain enough mobility along its shape-morphing boundary to achieve the different necessary shape modes. The number of edges along this boundary should be at least twice the number of actuators to be used in the structure. This is further discussed in §6.1.6.

4.3 Objective functions

An objective function is used to drive the optimizer toward a desired goal. Primary objective functions in the compliant mechanism literature often address energy efficiency and stored strain energy. I consider energy efficiency as well as secondary objective functions that minimize actuator power consumption, minimize the total number of actuators used, or minimize total length of all elements present (much like a

volume constraint). Controllability and observability are additional primary objective function terms to maximize responsiveness and adaptability, which are explored in §6.

All objective function terms are calculated from the results of linear finite element analysis (FEA), with only one beam element placed between each of the nodes in the topology being analyzed. Actuator segments serve as *both* force generators and structural elements. Refer to §3.6 for details of the FEA.

4.4 Constraints

Of particular importance are constraints that guarantee the ground, input, and output are all connected to the same structure, and that there are no other floating structures. I have used connectivity constraints, implemented as graph searches, as a *filter* rather than an objective function term, by simply discarding and replacing the designs with connectivity violations. Other possible constraints include weight, power consumption, and displacement requirements, all of which have been addressed.

Finally, a total element length (L_t) constraint is used. L_t is the sum of the lengths of *all* the elements in a given design. Whereas volume constraints are often used in the literature, my primary intention is to reduce complexity, not necessarily weight. Volume constraints tend toward slimmer beams, while a length constraint creates no such bias. A penalty is applied to the absolute value of the difference between the length and a user specified target length. The general form of the complete objective function is now given in Eq. (3), where η is the primary system metric being optimized (e.g. efficiency).

w_i are the relative weights of each additional term. L_{target} is desired total element length.

$$maximize\left[\eta + w_i \times (n\ various\ constraints) + w_{n+1} \times \left|L_t - L_{target}\right|\right] \quad (3)$$

4.4.1 Stress Constraints

Stress constraints are imposed to ensure the structures do not fail. Stress is calculated from the results of the linear finite element analysis. The bending stress is linear along the length of the element, and thus a maximum magnitude at one of the ends. Combining the bending and axial stress yields Eq. (4).

$$\sigma(z) = E\frac{(x_2 - x_1)}{l} \pm Eh\left[y_1\frac{12z - 6l}{l^3} - y_2\frac{12z - 6l}{l^3} - \theta_1\frac{12z - 6l}{l^2} - \theta_2\frac{12z - 6l}{l^2}\right] \quad (4)$$

Where z is the distance along the element, from zero to l, and $(x, y, \theta)_i$ are the nodal displacements. For each element, the stress is calculated at both ends $(z=0, z=l)$ and for both cases of the ± operator, with the maximum of these four stresses being recorded. Cases where the calculated stress is greater than the yield stress are penalized, which can be achieved several ways in the objective function. A discrete method is to count the number of overstressed beams in a given structure, and then apply the penalty weight to that count number. Alternatively, one could sum the stress-yield differences for all the elements that are overstressed, and apply the penalty to this quantity. In this dissertation, the single maximum stress in the entire structure is found,

from which the yield stress is subtracted and a penalty is applied. In all versions of the stress constraint, the penalty is applied only when the constraint is violated.

While I am using stress as a penalty, it is important to note that there are other ways to handle overstressed elements. If the stress results from actuator loads and not external loads, then rather than directly penalize overstressed designs, one could dial back the actuator force causing the overstress. This reflects the notion that the actuators do not need to run at full power all the time just because they can. Reducing the actuator force will not affect the controllability objectives, but will affect the desired displacement objectives. That is, the overstress will result in less output displacement (to avoid the stress), which is accounted for in the displacement penalty in the objective function. This indirect effect on the objective function requires no explicit stress term, and may possibly open the design space to broader search. The two case studies in §6.7 implement this alternative stress constraint.

4.5 Discrete Nonlinear Topology Optimization and Synthesis

Given a model of the design space, the variables can be optimized via a **Genetic Algorithm** (GA) to yield a system topology. As discussed in §2.3.2, genetic algorithms are a form of nonlinear evolutionary optimization that seeks global optima as opposed to local optima and are especially suited for discrete, nonlinear problems. (See Eiben and Smith, 2003 and Goldberg, 1989 for more information.) Genetic algorithms convert the design variables into a sequence of *genes* that can be propagated from generation

to generation with the effects of cross-over and mutation. Every design is evaluated with FEA which is used to calculate the terms of the fitness function.

The genetic algorithm starts with a population of randomly generated designs. The selection scheme in a genetic algorithm is based on the "survival of the fittest." Members are sorted and ranked according to their objective (fitness) functions. Their ranking determines the likelihood of being chosen as a parent for the next generation in a roulette selection. I also implement "genetic engineering", i.e. the trimming of elements before the fitness evaluation and "Lamarckian modification", i.e. the trimming of inconsequential elements after the fitness evaluation. Inconsequential elements are those that can be removed without changing the fitness evaluation, and can be found by searching for nodes with zero displacement or beams with zero stress. The highest scoring members (top 10%) of the *combined* parent and offspring population become the parent population for the next generation (i.e. elitism), guaranteeing that good designs are not lost.

Note that the actuator parameterization does not have any inherent meaning in the physical representation (i.e. there is a random map from genotype to phenotype). Therefore, the cross-over and mutation operators are modified to impose physical meaning, captured in graph tables (see §4.2) that indicate proximity and connectivity of elements. For example, during mutation, actuators are only allowed to mutate to a limited set of elements: those to which they are directly connected.

4.6 Dense Structures

A particular challenge has been controlling the results of initial random population generation. Given purely random chance, most initial structures will be highly dense and highly connected, with almost every node connected to the structure, resulting in a nearly rigid-body structure, as depicted in the first frame of Figure 21. To control this problem in the initial population, the likelihood of an element existing is given an uneven bias toward zero (*zero bias*). The greater the bias, the sparser, and usually the more desirable, are the initial structures (Figure 21). Zero bias is represented as a fraction, 1/N (used in (Trease and Kota, 2006)), or as a percent, 100/N% (used in Figure 21). A value of 1/5 (20%), means that any given element only has a 20% chance of being used, meaning a structural density of approximately 20%. This comes at a cost, however: many of the sparse initial structures are not valid because they do not have enough elements to provide connectivity. This conflict is handled by simply rejecting these initial members and trying again with another random structure (*infanticide*). The best initial structures tend to result when choosing a bias that rejects about 90-95% of the initial attempts. For example, when attempting to populate the first generation with 200 members, between 2,000 and 7,000 members are checked before 200 good candidates (connected structures) are attained. While this may seem overabundant and computationally costly, it far outweighs the inefficiency of running an algorithm where 90% of the members cannot even participate in the objective function.

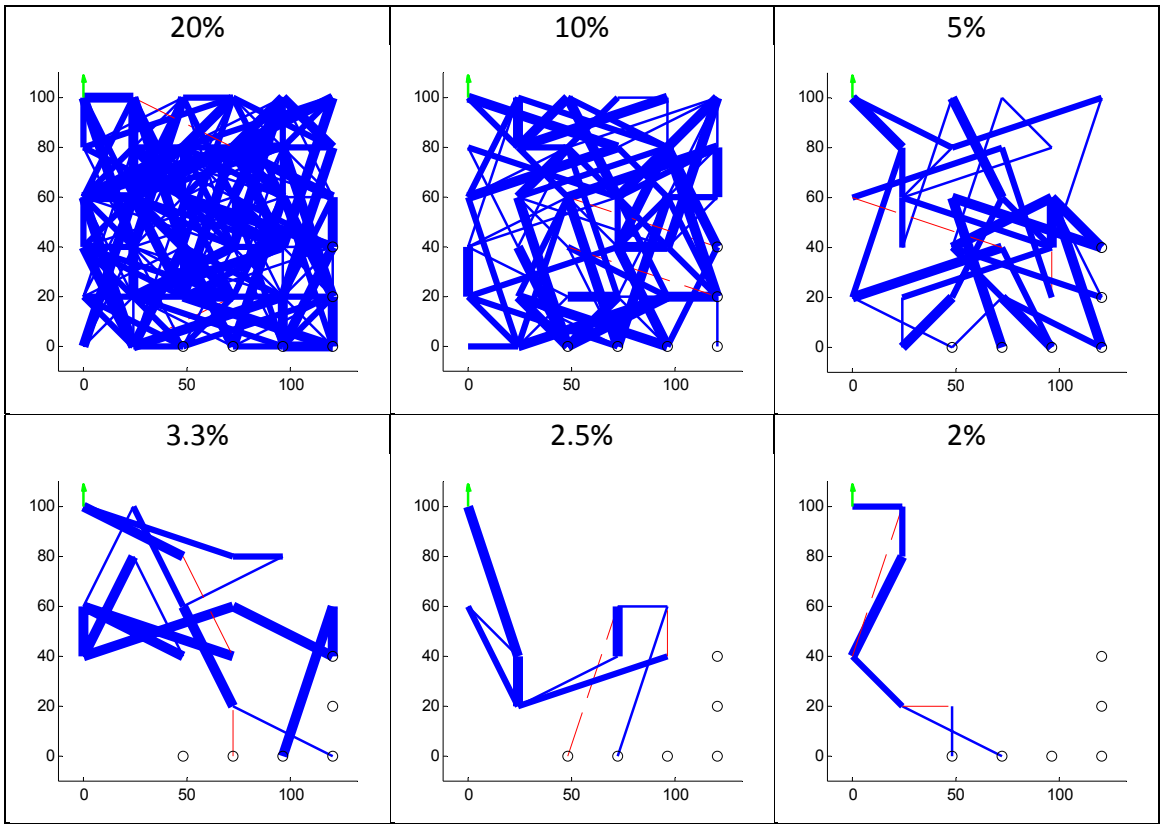

Figure 21: Effect of Zero-Bias on Structural Density of Initial Population Members
In each structure, every element has an X% chance of being included.

4.7 Genetic Algorithm Modifications

Graph searches are implemented to ensure connectivity of the actuators, output port, and at least one ground point all within the same graph. Disconnected structures that do not meet minimal requirements for analysis, such as that pictured in Figure 22, will be rejected (*infanticide*) and replaced with a new member. A brief overview of this process is shown in Figure 23 and described in further detail in the Modified Genetic Reproduction section.

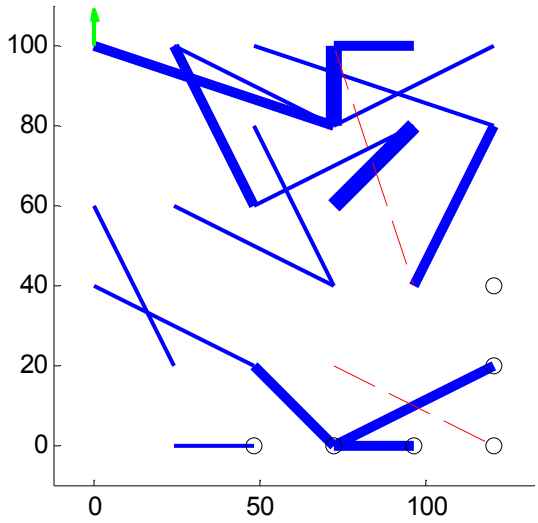

Figure 22: Example of a Disconnected Structure that would be rejected from the population before the assessment of the fitness function. (white circles are ground, green arrow is output node, dashed red lines are actuators)

Also of major importance has been the implementation of genetic modification. This is referred to as Lamarckian evolution or genetic engineering. Before the structures are even analyzed, all excess subgraphs are removed (*genetic engineering*). Further, elements that are discovered not to be contributing to the objective function after analysis are removed and not passed on (*Lamarck*).

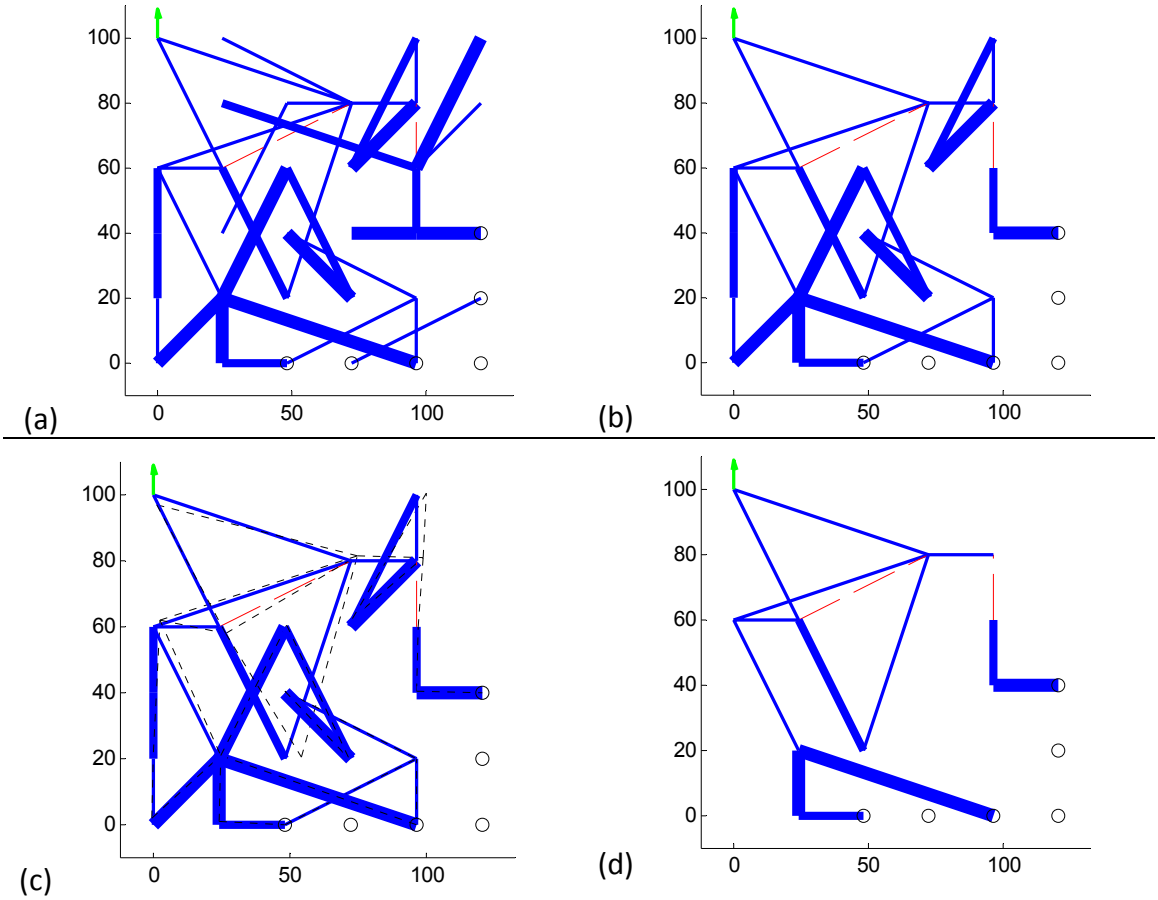

Figure 23: Brief Overview of Reproduction. (a) initial random design; (b) trimming of disconnected elements (*genetic engineering*); (c) analysis for fitness function with the deformed structure depicted in dotted black lines; (d) elimination of non-participating elements (*Lamarck*) (white circles are ground, green arrow is output node, dashed red lines are actuators)

4.8 Cross-over Strategies

It is desirable to have a meaningful cross-over strategy that corresponds to the actual problem when devising genetic algorithms. That is, the exchange of genes should correspond to the exchange of subsystems in the phenotype. However, in my parameterization, genotype sequencing does not map to phenotype expression. In the current practice, results of cross-over are always checked to ensure that no duplicate actuators result in a given structure. In the case of duplication, cross-over is simply repeated until acceptable designs result.

4.9 Mutation Operators

As with cross-over, it is desirable to have as much physical meaning as possible reflected in how the elements are mutated. While the numbering of the elements is somewhat arbitrary with regards to their physical layout, their graph connectivity is already captured in a data structure. When an element is chosen for mutation, it mutates to a different thickness or a value of zero. When an actuator is chosen for mutation, it mutates to other nearby elements to which it is directly connected. The set of neighbor elements is filtered to include only elements between the desired minimum and maximum actuator lengths. Again, checks are made for actuator duplicity in a given structure, and may result in the mutation being run again.

4.10 Note on Size and Shape Optimization

I have focused only on topology optimization, considered the more difficult of the two design stages described in §2.3. Further dimensional (size and shape) synthesis can be implemented with standard continuous optimization methods to address many other practical constraints and performance requirements. These include materials (permissible stresses and strains), desired fatigue life, prevention of localized buckling, natural frequency, manufacturability constraints on geometry, etc. During this process, the nodes or interconnection points are allowed to wander within a certain window thereby modifying the geometry without altering the topology. In size and shape optimization the topology is fixed and only the node locations and beam width and thickness change.

4.11 Statistical Results

Because genetic algorithms rely on stochastic probabilities for selection, cross-over, and mutation, their results are statistical and nondeterministic. Algorithm performance cannot be judged on the results of one run. In this research, every unique optimization problem is run 10 to 20 times to provide values for average performance and standard deviations. Every change in parameters requires a unique optimization run.

To aid the algorithms in converging, the length constraints are used to hold the designs to a certain number of elements, rather than simply minimize or optimize the number of elements. Otherwise, the design space appears to be too broad and certain regions of solutions are skipped altogether. Thus, in Pareto-front style, for each optimization problem four values of target length are imposed, with statistical results gathered for *each* of these.

4.12 Practical Note on Genetic Algorithms

Genetic algorithms are criticized at times for their use in engineering design because of their perceived nature as a black-box operator. However, it is noted here that this need not be the case; there are many ways to "open the box" and observe the process. Myriads of information can be gathered during the process and much of it can be observed even during run-time to inform the designer of the algorithm's progress. See Eiben and Smith (2003), Chapter 14, for an introduction to genetic algorithm performance metrics. One of these run-time metrics includes diversity of the population, measured as the standard deviation of the objective function. Real-time

histograms of the objective function can illustrate the main designs in the population, which can be tracked as their peaks move, diverge, and unite. Further, this can be done for each individual *component* of the objective function, allowing the designer to see which terms are driving the optimization in each stage of the evolutionary process. It is also useful to track many of these metrics for both the parent and child population of a current generation, to observe what direction the mutation and cross-over operators are pushing the population. I have also employed other metrics to track algorithm performance, such as the percentage of child designs that are rejected by the filters that check for graph connectivity. Algorithm stagnation can also be detected in several ways, such as a zero standard deviation of the population's objective functions. However, even with variation in the objective function, stagnation might be present in that all designs might consist of only the same three actuators. A metric counting the number of unique actuator combinations in the population is used to monitor this condition. This long list of possibilities demonstrates two points: there are many forms of feedback to improve algorithm performance and that the feedback itself offers insight into the dynamics of the solution, potentially highlighting to how the components of the objective function relate to each other and are balanced in optimal solutions.

4.13 Chapter Summary

This chapter began by establishing a practical design parameterization capable of representing structural elements, actuators, and sensors. The appropriate constraints to guide the optimization and ensure quality results were also introduced. A genetic

algorithm is used to coordinate the optimization and the relevant issues regarding cross-over, mutation, and structural connectivity were addressed. Finally, a statistical framework for assessing the performance of the algorithms is motivated, to be demonstrated in the examples of the next three chapters. Chapter 5 will focus only on the first metric, energy efficiency, providing a benchmark example common for compliant mechanisms and then exploring the benefits of multiple, optimally-placed actuators.

Chapter 5

Results for Multiple Actuator Placement

While there is great potential in the ideas of independent response to be explored in Chapters 6 and 7, the problem of using multiple actuators for combined performance and efficiency must be addressed first, thereby demonstrating a practical means for working with them. In fact, even when used all at once, there are performance benefits of multiple actuators to be gained when compared to single actuators in traditional compliant mechanism problems. This is the case even when the total power consumption and cost of having multiple actuators is considered. The methodology of the previous chapter is now used to perform studies of these potential benefits.

In these studies, the number of actuators is held constant during optimization, rather than minimized. The same problem is repeated for one, two, and three (or more) actuators, to create a Pareto front from which trends and optimal values can be observed. Not only does this simplify the complexity of the actuator variable set, but it helps the optimizer explore a broader space, and makes observation of trends related to the number of actuators possible. This is also acceptable because the end goal is to have a design with a reasonable number of discrete actuators in it; the fewer the better

as long as the objectives are met. Alternative approaches to actuator placement allow for a large and arbitrary number of actuators in the final designs.

5.1 Constant Power Consumption

There are many ways to evaluate power consumption so as to fairly compare designs of varying numbers of actuators. One possibility is to have all actuators driven by the same voltage, then measure the power consumption and efficiency for the resulting structures. Another practical method is to ***normalize*** the force-capabilities of the actuators so that all structures consume the same amount of power. Then, the achievable displacement and energy efficiency provide a means of comparison. This second method is employed in this dissertation.

Even with the second method of constant power consumption, there are still many ways to vary actuator command to achieve constant power. One reasonable method is to assume that either voltage or current input will be the same for *each* actuator, then to calculate the *single* value of the input that results in the structure having the target power consumption level. The examples in this dissertation are based on normalization via voltage input. For this normalization, the total power consumption is a function of both the number of actuators and their lengths. All of the designs are normalized to consume the same amount of power as does a single reference actuator of a characteristic length. The characteristic length is chosen to be the shortest diagonal element in the design domain. A derivation of the normalization follows:

Power *(P)* consumed per actuator is proportional to voltage *(V)* squared:

$$P = \frac{V^2}{R} \tag{5}$$

where R is the electrical resistance of the actuator. The summed power (P_T) of all the actuators (R_i) is:

$$P_T = \sum \frac{V^2}{R_i} \tag{6}$$

However, we want to apply only one voltage (V_a) to all the actuators, giving us:

$$P_T = V_a^2 \sum \frac{1}{R_i} \tag{7}$$

$$V_a^2 = P_T \left(\sum {R_i}^{-1} \right)^{-1} \tag{8}$$

For actuators, R is proportional to (length/cross-section-area) and V is proportional to the blocking force, F_b. Holding the cross section area constant, we can specify our reference power (P^*) as that consumed by an actuator of characteristic length L_o and blocking force, ${F_b}^*$:

$$P^* = \frac{V^{*2}}{R_0} \propto \frac{F_b^{*2}}{L_0} \tag{9}$$

Where V^* and R_0 refer to the reference actuator. We specify the normalizing value V_a as a fraction (a) of V^*, $V_a = aV^*$. Substituting these and $P_T = P^*$ into Equation (8) results in:

$$a^2 V^{*2} = \frac{V^{*2}}{R_0}\left(\sum {R_i}^{-1}\right)^{-1} \tag{10}$$

$$a^2 F_a^2 = \frac{F_a^2}{L_0}\left(\sum {L_i}^{-1}\right)^{-1} \tag{11}$$

Finally, we find the blocking force coefficient (a) to be applied to all actuators in a given design in Eq. (12). The normalize blocking force is now $F_b = aF_b^*$, which will give the structure the targeted power consumption.

$$a = \frac{1}{\sqrt{L_0 \sum \frac{1}{L_i}}} \tag{12}$$

A similar derivation leads to a different result when the same *current* is used for all actuators, instead of voltage. The final result of that derivation is Eq. (13), but is not implemented in this dissertation. Here, each actuator has its own a_i coefficienct.

$$a_i = \frac{L_i}{\sqrt{L_0 \sum L_i}} \tag{13}$$

The choice to normalize all actuators to one electrical input (either voltage or current) simplifies the manufacture and operation of the resulting system. The constant output of a single power source is sufficient. However, it is noted that this was one of many choices; there are multitudes of ways to achieve designs of equal power consumption when the electrical input can be different for each actuator. These extra degrees of freedom could be exploited by the optimization to find even more candidate designs.

5.2 Objective Function

In the first example, the objective function is to maximize total system *energy efficiency*, expressed in terms of a spring-based efficiency, η_{tot}. That is, while the actuators act against the structure at the input ports, springs (k_{out}) are placed at the output ports to simulate the reaction loads (See Figure 20). Hetrick and Kota (1999) derived the spring-energy efficiency as the calculation of work output (W_{out}) divided by work input (W_{in}) in Eq. (14), where all forces and displacements are measured parallel to the intended direction of motion.

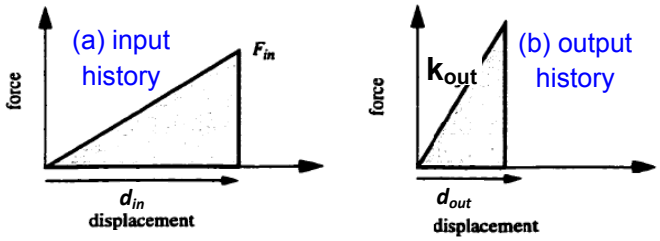

Figure 24: (Top) Basis for calculation of Energy Efficiency. (Bottom) The Input and Output Work History (Spring Formulation) (Hetrick, 1999)

$$\eta_{tot} = \frac{W_{out}}{W_{in}} = \frac{W_{out}}{\sum W_{in}} = \frac{k_{out} d_{out}^2}{\sum F_{in} d_{in}} \leq 100\% \tag{14}$$

It is also possible the break this total efficiency down into *actuator* efficiency and *structural* efficiency. The actuator efficiency is readily found by calculating the work of the input displacement relative to only the actuator stiffness. Since the input work is the total work possible for the system, W_{in} is written as W_{tot} for clarity:

$$\eta_{tot} = \frac{W_{out}}{W_{tot}} = \frac{W_{trans}}{W_{tot}} \frac{W_{out}}{W_{trans}} \tag{15}$$

where W_{trans} is the amount of work delivered through the transmission (compliant mechanism) to the output. Eq. (15) is equivalent to Eq. (16), where system efficiency is the product of actuator efficiency (η_{act}) and structural efficiency (η_{struct}).

$$\eta_{tot} = \eta_{act}\, \eta_{struct} \tag{16}$$

The individual mechanical work terms are calculated from the displacements, d_i, retrieved from the FEA.

$$W_{tot} = \frac{1}{2} \sum F_{in} d_{in} \tag{17}$$

$$W_{out} = \frac{1}{2} k_{out} d_{out}^2 \tag{18}$$

$$W_{act} = \frac{1}{2} k_{act} d_{in}^2 \tag{19}$$

Finally, the derivation for the actuator efficiency, η_{act}, is given in the next three equations.

$$W_{tot} = W_{trans} + W_{act} \tag{20}$$

$$W_{trans} = W_{tot} - W_{act} \tag{21}$$

$$\eta_{act} = \frac{W_{trans}}{W_{tot}} = 1 - \frac{W_{act}}{W_{tot}} \tag{22}$$

Now we have two new metrics in addition to η_{tot}. η_{act} refers to the percent of work that the actuator is able to produce. This is necessarily small because the actuator spends considerable work overcoming its own stiffness. Of the work the actuator transmits, the portion that makes it to the output node is η_{struct}. This is less than one because some energy is stored in the elastic members of the structure. Being able to observe all three metrics helps in understanding the function and stiffness matching of the final design.

5.2.1 Constraints

The structure is required to meet a minimum displacement at the output node while deflecting against the external spring.

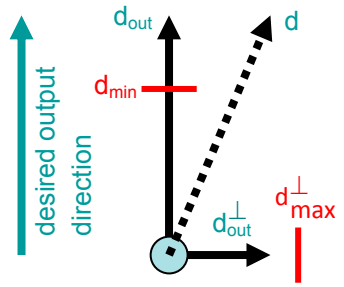

Figure 25: Values used to constrain minimum output displacement and maximum lateral displacement

Two constraint penalties are added to the objective function to monitor deflection (Figure 25). The first is a constraint that requires the output deflection in the desired direction to be greater than a minimum value, d_{min}. The second requires the output deflection perpendicular to the desired direction be less than a maximum value, $d_{max}^{\perp}$. To provide a fair comparison between multiple actuator designs, the forces are adjusted so that whether 1, 2, or 3 actuators are used, power consumption remains the same. The final form of the objective function is shown in Eq. (23), where η_{tot} is from Eq. (14) and w_1, w_2, and w_3 are relative weighting constants. In the formulation, the penalties are applied only when $d_{out} < d_{min}$ or $d_{out}^{\perp} > d_{max}^{\perp}$.

$$maximize \begin{bmatrix} \eta_{tot} + w_1 \times (d_{out} - d_{min}) + w_2 \times (d_{max}^{\perp} - d_{out}^{\perp}) \cdots \\ \cdots + w_3 \times |L_t - L_{target}| \end{bmatrix} \quad (23)$$

Care must be taken in imposing sensible constraints, at least when interpreting the final designs. That is, it is trivial for the lateral constraint to always be satisfied if the structures are producing very little deflection at all and not satisfying the desired deflection constraint. In other words, for some problems, the constraints may not always be conflicting.

5.3 Benchmark Study

The operational parameters of the genetic algorithm depend on the size of the chosen grounded structure. For a workspace grid of 5x5 nodes, there are 168 elements; for a 6x6 grid, there are 250 elements; every element is a design variable. As a general rule, the size of the population should be greater than the number of design variables. Populations of sizes from 150 to 250 members have been tried for both grid sizes. In the benchmark cases, the algorithms have been allowed to run for 1000 generations. The zero-bias for initial populations has been set to values from 1/30 to 1/60 (i.e. a 1/N chance of existing). There are two types of mutation that occur, and their likelihoods are as follows: normal element mutation (8-10%) and mutation of actuator element choice (10-15%).

A displacement amplifier has been studied. This problem is considered a benchmark problems for compliant mechanism design (refer to Lu, 2004). The design domain and specifications are shown in Figure 26. Lu's results for these problems with a single-output and a single-input are also shown in Figure 26.

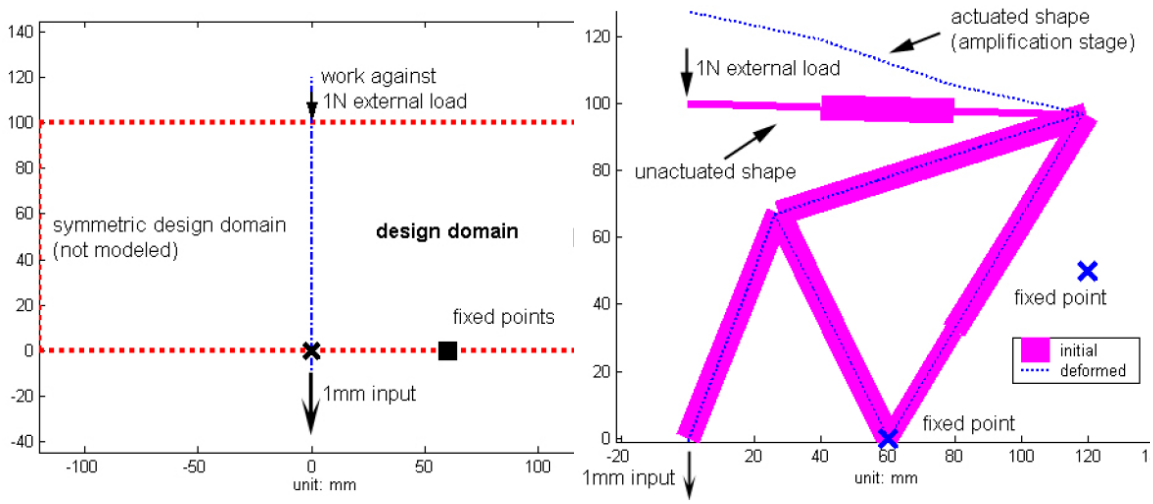

Figure 26: Design Domains and Results from Lu (2004) for Benchmark Amplifier Problem

Many different amplifier designs have been created in previous research (Joo, Kota, and Kikuchi, 2001; Kota et al., 2001 (patent); Hetrick and Kota, 2003 (patent)). This compliant mechanism serves as a transmission so that the input displacement is amplified at the output port. The overall design domain is 240mm by 100mm (9.45inch by 3.94inch). To ensure linear motion at the output port, the design is chosen to be symmetric about the y-axis. Thus, only the right half of the design domain is considered in the synthesis process.

Figure 27: Various Results from Benchmark Studies of the Symmetric Compliant Amplifier Problem. Design on left from Luo, Tong, and Wang (2007). Design on right has a U.S. Patent by Kota et al., 2001

Again, the goal is to amplify an input displacement into an output displacement along the device's line of symmetry (Figure 28). Such devices have played an important role in the design of MEMS actuators (Kota et al., 2001). The design specifications used now are actuator block force: 90N, element modulus: 2,480MPa, actuator modulus: 2,000MPa, output stiffness: 0.05N/mm, and minimum output deflection: 20mm. The parameters are summarized in Table 1.

Design Parameters	
actuator block force	90N
element modulus	2,480MPa
actuator modulus	2,000MPa
output stiffness	0.05N/mm
element out-of-plane thickness	1.5mm
minimum output deflection	20mm
domain footprint	240mm x 100mm
grid size	5 x 5
Algorithm Parameters	
element mutation rate	8-10%
actuator mutation rate	10-15%
cross-over rate	97%

Table 1: Design and Algorithm Parameters for the Benchmark Problem

Number	Variable	Type	Possible Values
1	Beam Thickness	discrete	0, 0.5, 1, 1.5mm
…	…	…	…
168	Beam Thickness	discrete	0, 0.5, 1, 1.5mm
169	Actuator 1	discrete	1-168
170	Actuator 2	discrete	1-168
171	Actuator 3	discrete	1-168

Table 2: Optimization Variables. There are 168 beam variables that determine whether the beam is absent or present with one of three discrete thickness values. The actuator variables specify which of the 168 elements in the network will be the actuators.

The complete objective function for the benchmark problem is shown below. Note the for this problem, the total element length, L_t, was simply minimized (i.e., L_{target} = 0). As the problem is symmetric, the lateral motion constraint ($d_{max}^{\perp}$) is not necessary.

$$maximize\ [\ \eta_{tot} + w_1 \times (d_{out} - d_{min}) - w_2 L_t\ ] \tag{24}$$

Figure 28 shows results for the best of a population of 150, with only one actuator variable. (Final result attained after 330 generations.) Note that even though the actuators are grounded on one end, they are still *embedded* in that they are part of the design domain and serve a structural role. Observe the similarities to Lu's result in Figure 26; though the nodes are in different positions, the topologies are the same.

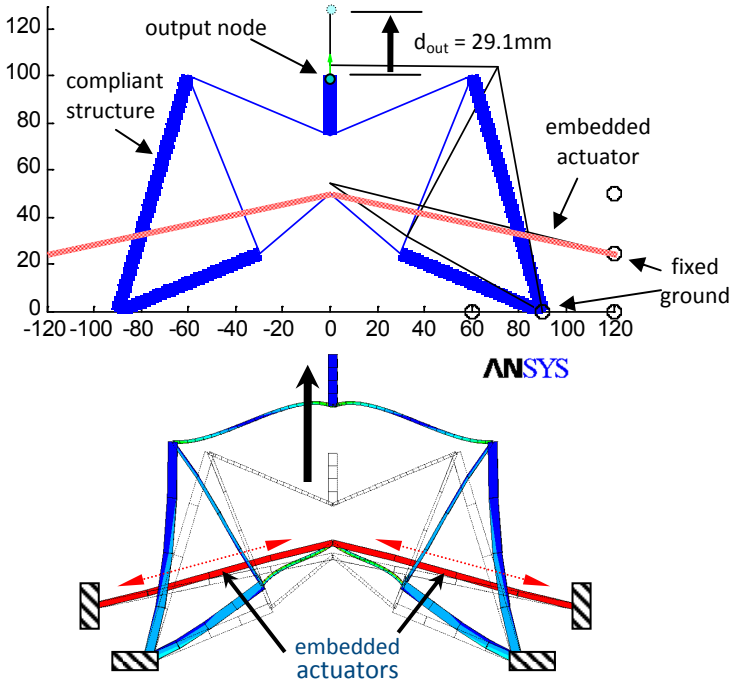

Figure 28: Symmetric Motion Amplifier. d_{out} = 29.1mm. d_{in} = ~0.5mm / actuator. Dashed lines represent deformed structure. System Efficiency = 51%. *Top*: Matlab optimization results. *Bottom*: ANSYS nonlinear finite element analysis.

5.4 Study of Stiffness Matching

As mentioned in §3.3.3 , actuators are modeled as compliant force-generators. The next study is a simplified version of the previous symmetric motion amplifier problem. The actuator number and location is now held fixed to allow observation of the typical resulting transmission structures. The theory is that systems of optimal efficiency should have matched actuator and structural stiffness. In this problem the structural stiffness is composed of the compliant mechanism stiffness and the output spring stiffness. This is the combined stiffness of everything which resists the actuator and is denoted k_{resist}. Note that the relation between k_{resist} and k_{out} is not simple, as the output spring is partially combined in series and parallel with the compliant system.

$$maximize\ [\eta_{tot} + w_1 \times (d_{out} - d_{min}) - w_2 \times (\eta_{stress}) - w_3 \times |L_t - L_{target}|] \quad (25)$$

The design parameters and variables are summarized in Table 3 and Table 4. Designs with overstressed elements are also penalized, proportionally to the degree they are overstressed ($\eta_{stress} = \sigma_{max}/\sigma_{yield} - 1$). Equation (25) is the complete objective function. For these studies, four different target lengths were tried, with 15 optimization runs for each. The target length is chosen as a multiple of the diagonal dimension of the design domain, l_{diag}, i.e. 2x, 3x, 4x, and 5x.

Design Parameters	
actuator block force	80N
element modulus	2,480MPa
actuator modulus	6,800MPa
element yield stress	37.7MPa
output stiffness	0.05, 5, and 50 N/mm
element out-of-plane thickness	1.5mm
minimum output deflection	5mm
domain footprint	240mm x 100mm
grid size	5 x 5
Algorithm Parameters	
element mutation rate	8%
actuator mutation rate	0%
cross-over rate	97%

Table 3: Design and Algorithm Parameters for the Stiffness Matching Problem

Number	Variable	Type	Possible Values
1	Beam Thickness	discrete	0, 0.5, 1, 1.5mm
…	…	…	…
168	Beam Thickness	discrete	0, 0.5, 1, 1.5mm

Table 4: Optimization Variables. There are 168 beam variables the determine whether the beam is absent or present with one of three discrete thickness values.

The goal is to achieve high system efficiency while attaining a minimum desired displacement of 5mm. Resulting structures for three different output spring magnitudes are shown in Figure 29. For statistical significance, 60 designs (15 for each of 4 length constraints) were synthesized for each output spring, with the results shown in Table 5. The resulting geometric advantage is also reported.

Given Parameters*		Efficiency				Matching	
k_{out}	k_{act}	η_{tot}	η_{act}	η_{struct}	k_{resist}	k_{resist} / k_{act}	G.A. (out/in)
0.05	408	1.6%	3.6%	46%	15.6	0.038	9
5	408	3.3%	7.5%	44%	33.1	0.081	1.7
50	408	5.8%	9.5%	62%	42.8	0.105	0.7

Table 5: Summary of Results for the Stiffness Matching Study. *Stiffness is reported in N/mm. Average values for 60 design runs are reported.

In the majority of the cases, the stiffness ratio (k_{resist} / k_{act}) is much less than one, indicating that the algorithm did not achieve stiffness matching with the given design parameters and variables. This is likely because the output spring and available structural material were simply not stiff enough to match the actuator stiffness, for any compliant system design. This is supported by the trend of increasing values for η_{tot} . As the output stiffness increases from 0.05 to 50N/mm, the algorithm creates structures

that are increasingly more matched in stiffness. Thus, given an adequately large output spring and stiffer structural elements, the algorithm should be capable of producing more efficient designs that are stiffness matched.

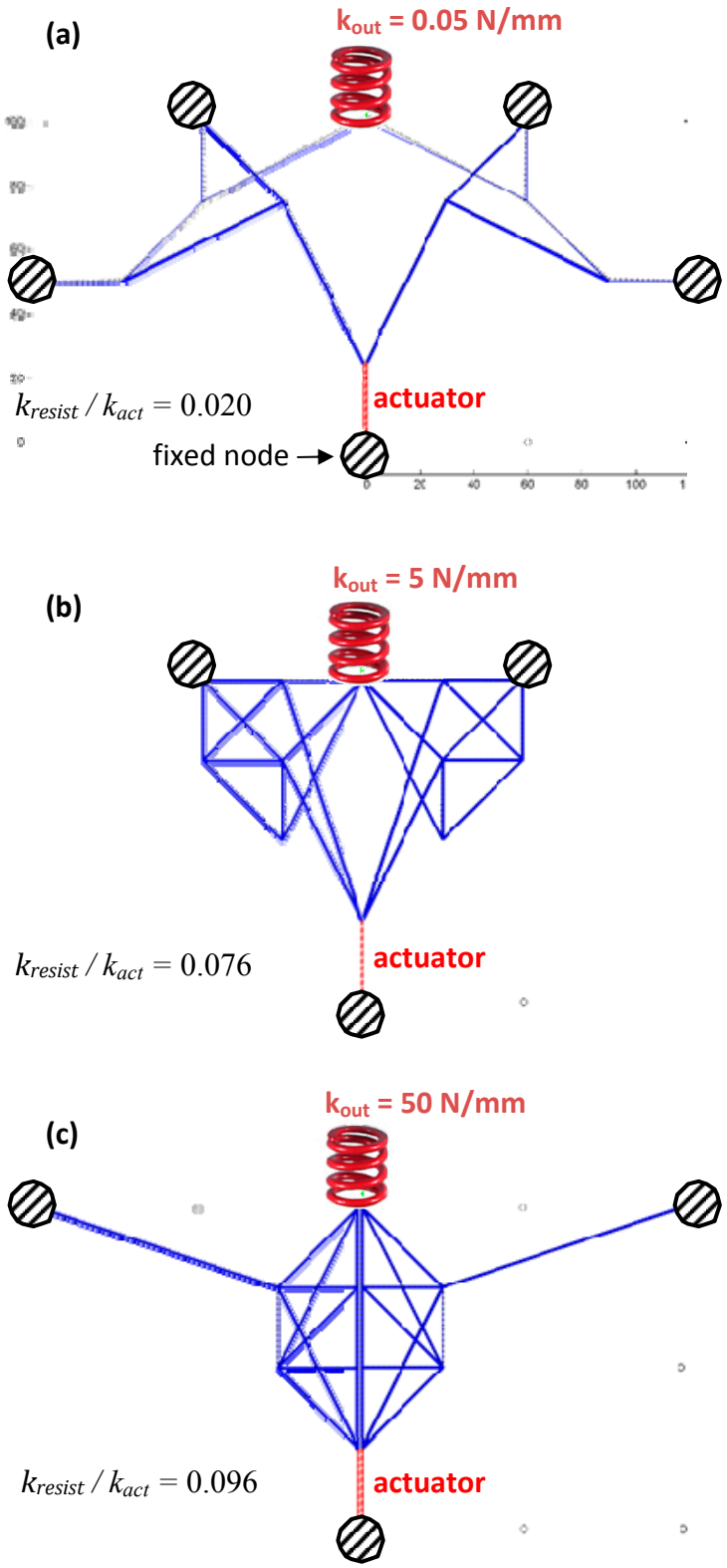

Figure 29: Sample of typical results for the Stiffness Matching investigation. As the output spring stiffness increases from (a) to (c), the compliant structure is also seen to become stiffer.

5.5 Asymmetric Multiplier Results

To better demonstrate the potential benefits of optimal placement of multiple actuators, an asymmetric multiplier problem is now considered. Here, the system must not only efficiently attain a desired displacement, but must also limit the undesired lateral displacement. The design space (Figure 30), is very similar to that from the previous symmetric problem. The design and algorithm parameters are listed in Table 6, followed by the optimization variables in Table 7.

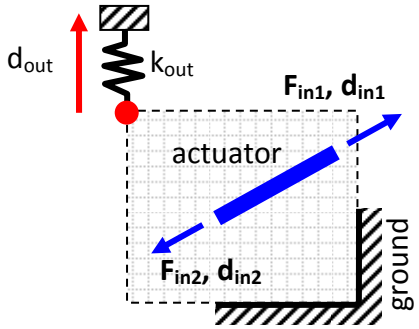

Figure 30: Design Domain for an asymmetric actuator amplifier. An output spring is used as a basis for calculation of energy efficiency.

Design Parameters	
actuator block force	90N
element modulus	2,480MPa
actuator modulus	6,800MPa
output stiffness	0.05, 5, and 50 N/mm
element out-of-plane thickness	1.5mm
minimum output deflection	3mm
domain footprint	120mm x 100mm
grid size	5 x 5
Algorithm Parameters	
element mutation rate	8%
actuator mutation rate	10%
cross-over rate	97%

Table 6: Design and Algorithm Parameters for the Asymmetric Multiplier Problem

Number	Variable	Type	Possible Values
1	Beam Thickness	discrete	0, 0.5, 1, 1.5mm
…	…	…	…
168	Beam Thickness	discrete	0, 0.5, 1, 1.5mm
169	Actuator 1	discrete	1-168
170	Actuator 2	discrete	1-168
171	Actuator 3	discrete	1-168

Table 7: Optimization Variables. There are 168 beam variables that determine whether the beam is absent or present with one of three discrete thickness values.

Again, the asymmetric problem is chosen to demonstrate the capabilities of multiple actuators with respect to both efficiency and constraint satisfaction. The task is to create y-displacement with a limit on the lateral x-displacement ($d_{max}^{\perp}$). See Figure 25 for a depiction of the two motion constraints. The complete objective also contains the total element length constraint, and is given in Eq. (26).

$$maximize \begin{bmatrix} \eta_{tot} + w_1 \times (d_{out} - d_{min}) + w_2 \times (d_{max}^{\perp} - d_{out}^{\perp}) \cdots \\ \cdots - w_3 \times \left| L_t - L_{target} \right| \end{bmatrix} \quad (26)$$

To provide fair evaluation as the number of actuators increase, each candidate design absorbs the same amount of power as does a single actuator of length 40mm, using the normalization method described in §5.1. Cases of 1, 2, and 3 actuators were investigated, across length ratio constraints of 2, 3, 4, and 5. (Length ratio, η_L, is defined as the total element length divided by the diagonal length (l_{diag}) of the physical design space.) More than 10 genetic algorithms were run for each combination of actuator number and length ratio. All studies were also conducted at several values of output

stiffness; results for k_{out} = 0.05 N/mm and 0.5 N/mm are given. The results for this study are shown in Figs. 31-34.

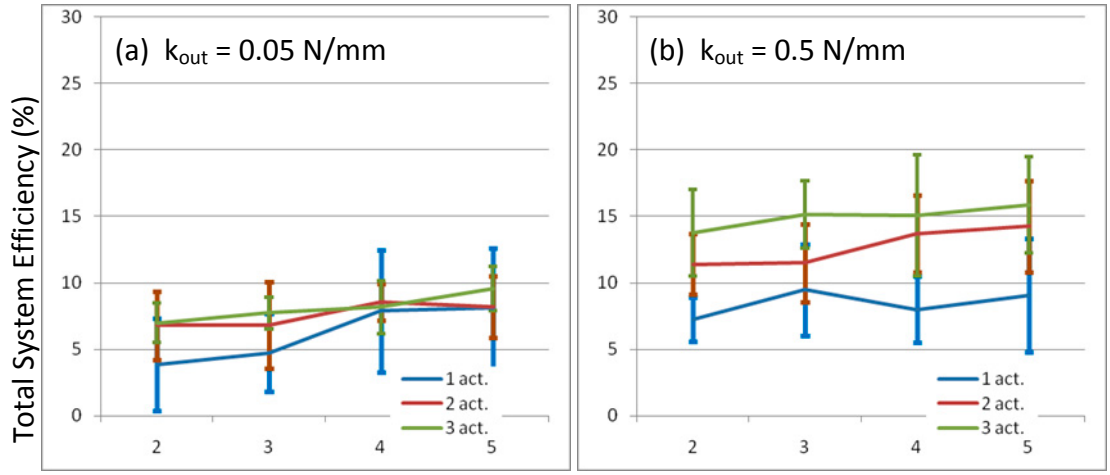

Figure 31: System Efficiency (%) as a function of Total Element Length and Number of Actuators. Standard deviation of genetic algorithm performance is indicated. The x-axis indicates the total element length (L_{tot}) in terms of the length ratio, η_L . $L_{tot} = \eta_L l_{diag}$.

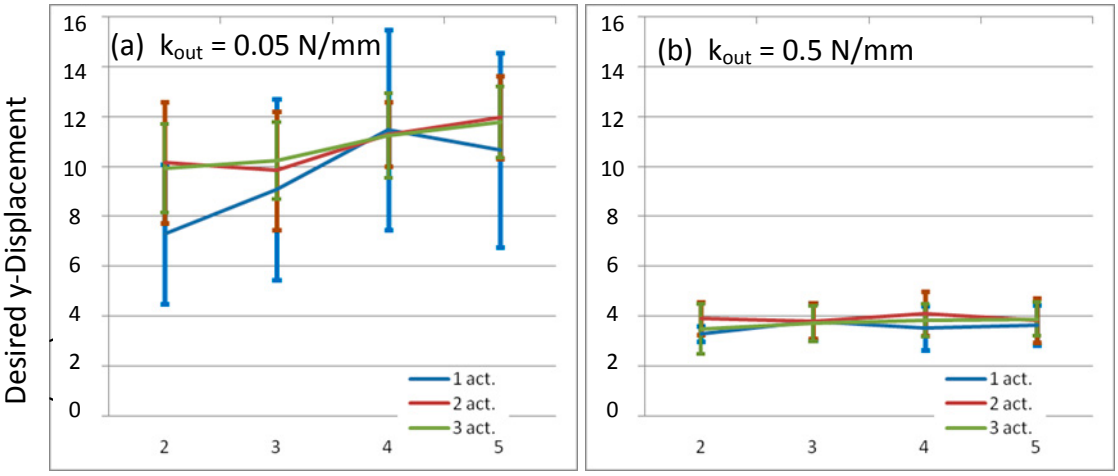

Figure 32: Desired displacement (mm) as a function of Total Element Length and Number of Actuators. Standard deviation of genetic algorithm performance is indicated. x-axis is the length ratio, η_L .

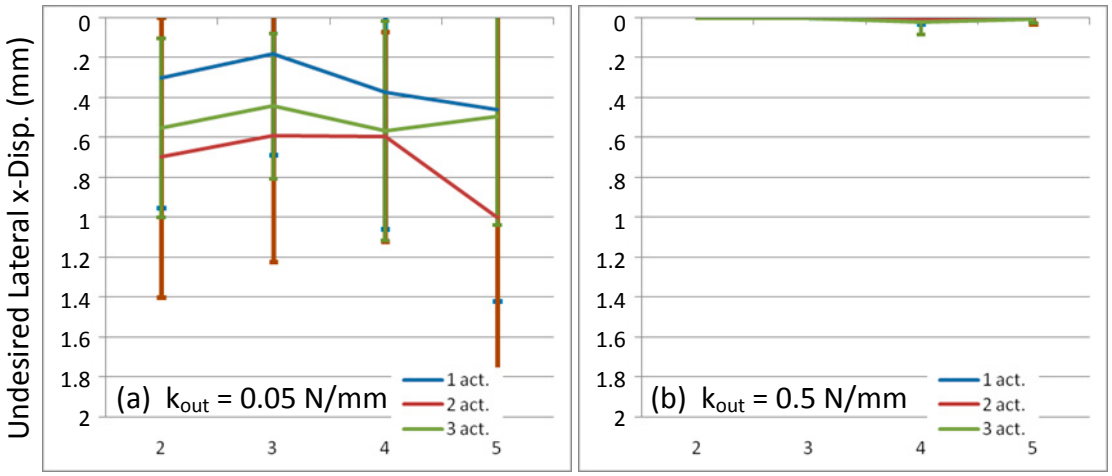

Figure 33: Undesired lateral displacement (mm) as a function of Total Element Length and Number of Actuators. Standard deviation of genetic algorithm performance is indicated. x-axis is the length ratio, η_L .

The above figures indicate that efficiency increases with the number of actuators (Figure 31), which supports the findings of Johnson and Frecker (2004) where "a number of medium active elements" are preferred to "a few large active elements." Efficiency also increases when greater total length is allowed, but these increases are not as significant. System efficiency also increases with a larger output spring that more closely matches the stiffness of the actuators (Figure 31-b). These trends are directly evident in Figure 35 below, which summarizes the data in Figure 31 as a function of the number of actuators. Regarding desired output deflection, the stiffer output spring results in stiffer structures, and the displacement is limited (Figure 32-b). However for the softer output spring, more displacement is possible, which is further achievable with more actuators (Figure 32-a). Finally, observing the lateral displacement, which is to be minimized, we see again that the stiffer spring naturally limits the displacement. Again, the softer spring results in a more compliant structure, which has more difficulty in constraining lateral motion. In Figure 33-a, we see that a single actuator best constrains the motion,

but that two actuators perform poorly, while three actuators are able to meet the constraints again. My interpretation is that one actuator does not accomplish much of *any* displacement on its own, so the threat of lateral motion is already low. Two actuators are more capable of creating the large desired displacement, but with an accompanying lateral component that the two actuators alone cannot manage. As the number of actuators further increases, they are able to both efficiently meet the desired displacement requirements while coordinating together to constrain the lateral motion. Figure 34 illustrates some typical designs for one, two, and three actuators from these studies.

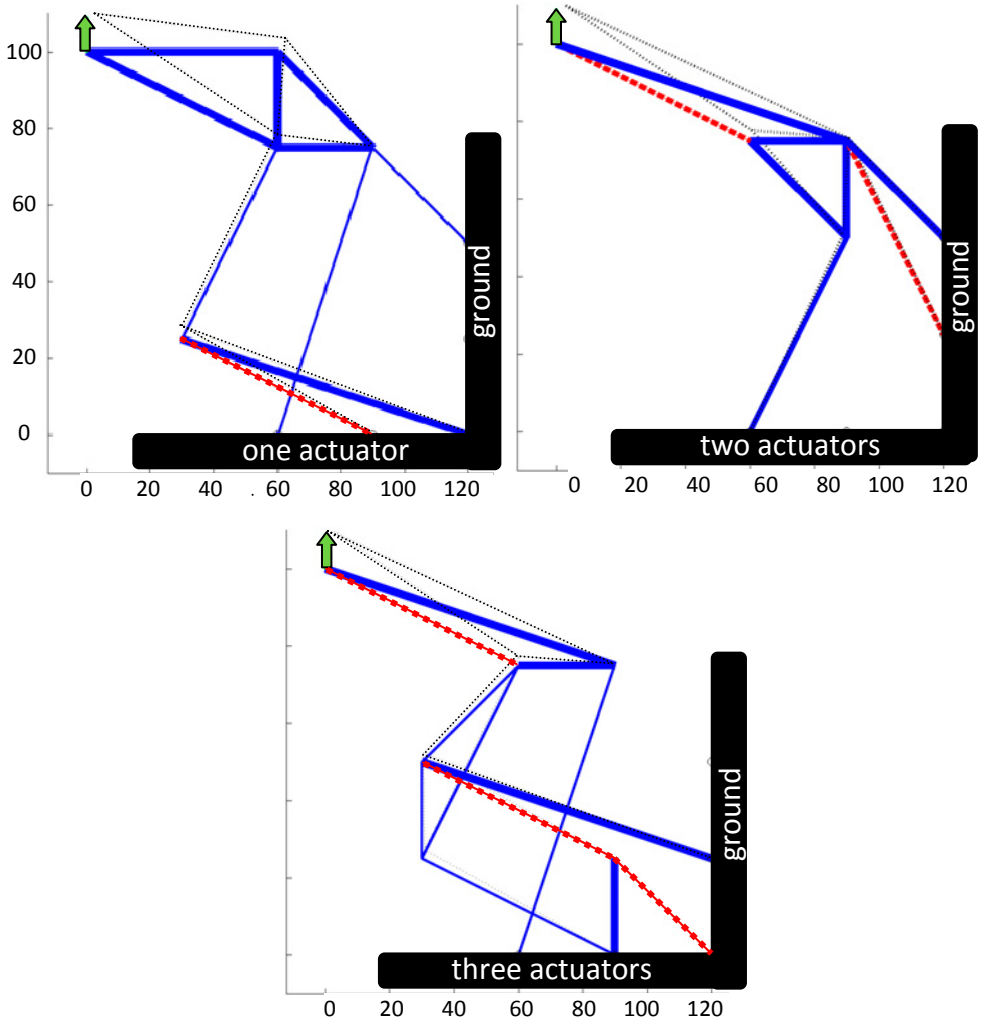

Figure 34: Asymmetric Problem Results, indicating Effect of Increasing Number of Actuators. Power input equal for all cases. Both efficiency and constraint satisfaction tend to increase with the number of actuators used. Multiple actuators cooperate to constrain lateral motion.
k_{out}: 0.05N/mm, Population size: 200, Mutation: 8-10%, Cross-over: 97%

To further understand the results in Figure 35, the corresponding *actuator* efficiency (η_{act}) and *transmission* efficiency (η_{struct}) are provided in Figure 36. These vary primarily as a function of the number of actuators, but not length ratio. Recall that system efficiency is the product of these two efficiencies: $\eta_{tot} = \eta_{struct} \times \eta_{act}$.

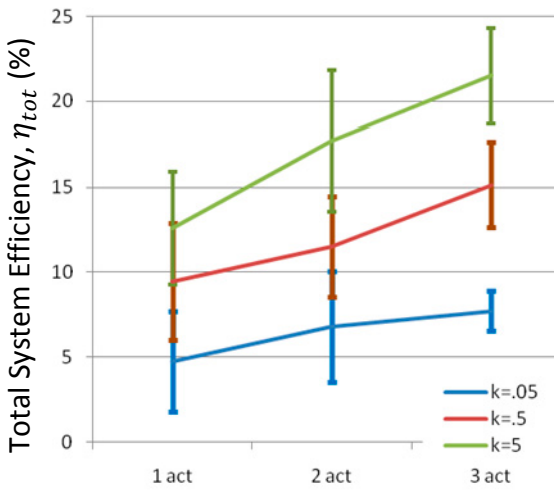

Figure 35: Summary of Actuator Studies. Increasing System Efficiency, η_{tot}, (%) as a function of number of actuators and output spring stiffness. Each curve represents results for a different output spring, with stiffness indicated in N/mm.
Length ratio = 2.

Figure 36 indicates that η_{struct} remains nearly constant for various output spring stiffness and length constraints. The actuator efficiency changes for both of these, however, which drives the trends observed for η_{tot} in Figure 35.

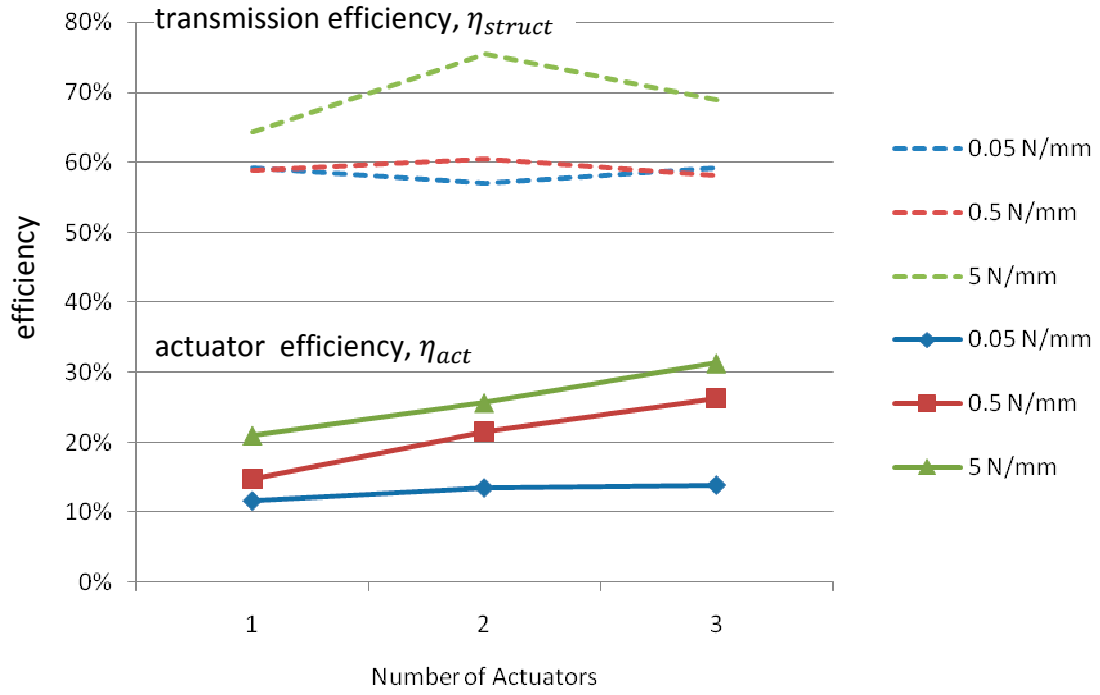

Figure 36: Breakdown of the energy efficiencies reported in Figure 36. Here, each point is the average for designs of all length constraints. $\eta_{tot} = \eta_{struct} \times \eta_{act}$.

5.6 Discussion

Encouraging results (Figure 28) show that the algorithm attains the goal of distributed actuation and demonstrate the desired attribute of distributed compliance. The new result for the benchmark problem above is similar in topology to the more successful of previously reported high-gain results, such as MEMS amplifiers (Kota et al., 2001), tailored actuator transmissions (Kota et al., 1999), and results using a load-path method (Lu and Kota, 2003). Note that I have focused only on topology optimization (Stage I), considered the more fundamental and difficult of the two design stages. Further dimensional (size and shape) synthesis (Stage II) can be implemented with standard continuous optimization methods to address many other practical constraints and performance requirements.

I also comment on the presence of tandem actuators, i.e. actuators that are connected end to end, essentially forming one larger actuator. The design algorithms do not explicitly prevent this case from happening. Rather, free reign is given to the optimizer to see whether such structures are preferred. If it is possible that two actuators function better placed together than when apart, then this is exactly the kind of information one needs to validate the benefit of multiple actuators.

5.7 Chapter Summary

This chapter sought to explore the benefits of using multiple, optimally-placed actuators in tasks previously attempted only with single, user-placed forces or displacements. To adequately account for the cost of additional actuators, a means was developed to hold power consumption constant for all cases considered, thus letting designs be evaluated on only their mechanical performance. A benchmark from the literature was used to demonstrate the validity of the design algorithm and that it can create designs with distributed compliance. The remaining studies looked at the statistical results of the algorithm in terms of performance efficiency and constraint satisfaction, with the trends indicating benefits gained from the use of multiple actuators. The remaining chapters will now go beyond the basic problems handled by compliant mechanisms to those *only* achievable with multiple embedded components.

Chapter 6

Shape Control and Sensing

With a methodology for simultaneous synthesis of compliant mechanisms and actuator placement now available, this chapter takes on the more novel and previously indefinable tasks of component independence in a coupled, multifunctional workspace.

6.1 Design for Controllability

A compelling task is the merger of compliant mechanisms and "design for control" within the synthesis methodology for compliant systems. The initial approach to integrate control with compliant mechanisms is not to optimize the controller, but to optimize the controllability characteristics of the system, defined as measures of how thoroughly a given set of internal actuators/sensors can achieve/sense a full range of output states on the external environment.

Controllability and observability of the structure will be calculated in terms of the linear independence of the actuators and sensors, which will be incorporated into the optimization. The work on controllability also provides the method for optimizing observability. I hypothesize that if the actuators independently affect the output displacement, then they can compensate for a variety of unknown loading conditions. A

key part of the design conflict is that not only are we attempting to achieve orthogonality while supporting external loads, but that we specifically want the structures to take advantage of internal compliant mechanism leverage to increase the amount of displacement under actuation.

6.1.1 Problem Formulation

The task of a compliant system is to serve as a mechanism with a specified functionality while also maintaining a structural stiffness to support external loads. I now add adaptability to that definition, so that compliant systems can detect and appropriately respond to unknown and arbitrary loading. Consider an example problem with an output region defined by two output points, P_1 and P_2. Imagine a simple airfoil that is to remain in a particular configuration despite changing pressure loads, as depicted in Figure 37. These points will be subject to unknown loading in the vertical direction, f(x). Each point represents a degree of freedom of the system, and thus two actuators (A, B) are required (at a minimum) to fully control the output points.

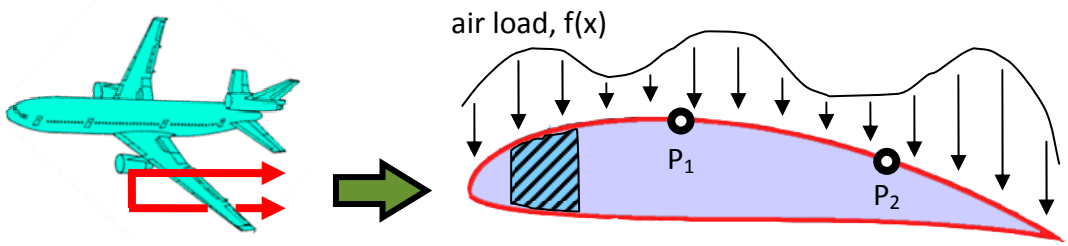

Figure 37: Aircraft wing cross-section subject to unknown and arbitrary air load, f(x). Points P_1 and P_2 are to be controlled by internal actuators and monitored by internal sensors.

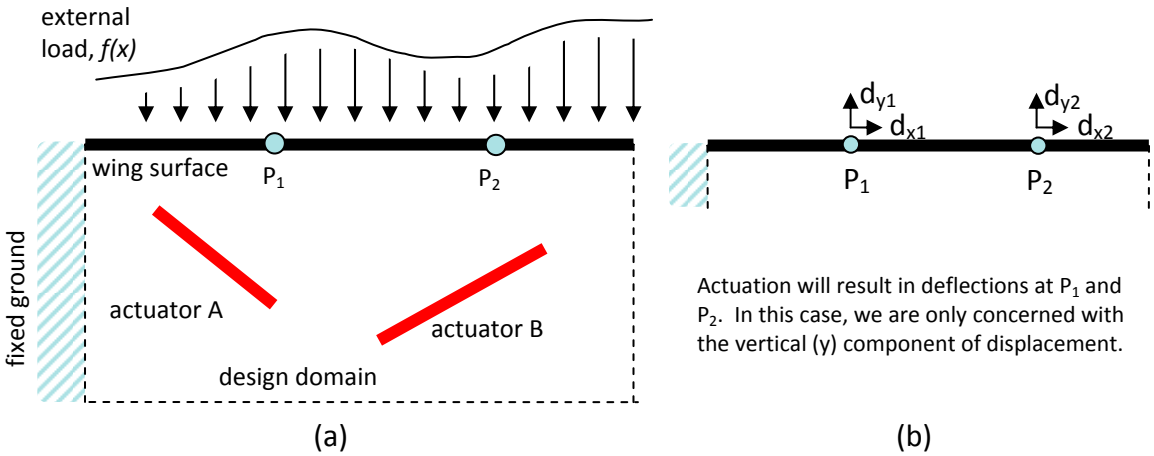

Figure 38: Design Space for the "Design for Control" synthesis problem. Two output ports are indicated as well as two actuators. The location and orientation of the actuators are to be determined via synthesis.

6.1.1.1 Design Space

The design space (Figure 38-a) is nearly the same as that used in the basic embedded-actuation problem (see Figure 31). A network of enumerated beams represents the underlying structure, with each beam's presence determined by a discrete design variable (i.e. zero = off, one = on). The left-side of the design space is fixed to the ground. To guarantee a continuous airfoil, the top edge elements (skin elements) are not included in the optimization, but are pre-specified as known-thickness elements. For actuation, I again use axial force actuators with specified stiffness (including bending) and output blocked force. (Actuator blocked force is the maximum output force, achieved when displacement of the actuator is physically constrained to zero.) The actual output load and deflection depend on the stiffness of the entire compliant system, and are determined by the FEA solution (see §3.3.3). The actuators are not considered as binary (on or off) but as continuously controlled, allowing for flexibility in mixing the independent effect of each actuator on the structure.

6.1.1.2 Loading

When calculating the fitness function within the synthesis procedure, the structures are first loaded by only the internal actuators, one at a time, with no external load. While the goal is to support external loads, those loads are not yet known. Instead, I attempt to optimize the actuator layout within the structure to result in the greatest freedom to control the displacement output points (P_1 and P_2 in Figure 38). Such a structure is believed to best handle *variable* load. To maintain structural integrity, I then add an *additional* external load case with no active actuators. The structural response is then added to the objective function in a minimization term.

6.1.2 Objective function and constraints

To develop a measure of controllability, the effect of each actuator within the structure is first tested via FEA. The output points P_1 and P_2 will have displacements (d_{1x}, d_{1y}) and (d_{2x}, d_{2y}). We are interested in the coupled output of both actuators in the vertical direction, represented by the vector: $\bar{d}_i = \left[d_{1y}, d_{2y}\right]_i$, where i represents the active actuator. Thus, for actuator A, $\bar{d}_A = \left[d_{1y}, d_{2y}\right]_{\mathrm{A}}$. Likewise, a second FEA is run with actuator B activated, resulting in: $\bar{d}_B = \left[d_{1y}, d_{2y}\right]_{\mathrm{B}}$.

6.1.2.1 Linear independence

To increase the controllability of the structure, it is desired that the $\bar{d}_i$ vectors be linearly independent. This condition means that the effect of each actuator will not be redundant, allowing for the controller to be effective. Thus, the combination of the two actuators ($\bar{d}_{combined} = w_A\bar{d}_A + w_B\bar{d}_B$) can be used to cover as broad a range of output

combinations as possible. An example of potentially orthogonal vectors is shown in Figure 39. By the nature of compliant structures, all output points are affected by all actuators, making it impossible to have each output point simply controlled by only one input. That is, a scenario such as $\bar{d}_A$=[1,0] and $\bar{d}_A$=[0,1] is not possible, but other linearly independent combinations should be achievable, such as $\bar{d}_A$=[0.5,0.5] and $\bar{d}_B$=[0.5,-0.5].

6.1.2.2 Controllability

Controllability and observability are well known concepts in control theory, as indicated in §3.5. I use these terms primarily in metaphor, with specific definitions within a structural context. I define **controllability** as the degree of independence between the multiple vectors obtained by creating a matrix of the $\bar{d}_i$ vectors and then dividing its determinant by the product of the magnitudes of the vectors, as shown in the formula below:

$$\eta_c = \left| \frac{det\left[\bar{d}_A\ \bar{d}_B\ \cdots\ \bar{d}_m\right]}{\left|\bar{d}_A\right|\left|\bar{d}_B\right|\ \cdots\ \left|\bar{d}_m\right|} \right| \tag{27}$$

(where m is the number of outpoint points, equal to the number of actuators)

The denominator in Eq. (27) normalizes the metric to have a value between zero and one (100%). Here, a value of zero implies linear dependence, while values closer to one (100%) imply orthogonality of the *m* vectors. For a 3-point case (m=3), we also recognize $\left|\bar{d}_A\right|\left|\bar{d}_B\right|\left|\bar{d}_C\right|\eta_C = det\left[\bar{d}_A\ \bar{d}_B\ \bar{d}_C\right]$ from Cartesian linear algebra as the volume of the parallelepiped formed by the three vectors $\bar{d}_A$, $\bar{d}_B$, and $\bar{d}_C$. (a.k.a. *triple product*.) When the vectors are all orthogonal, the maximum volume is achieved, indicating that

larger values of η_C are desirable for the objective. The controllability, $\eta_{C,}$ serves as the objective function to be maximized during the genetic algorithm.

Note that the matrix inside the determinant, $\bar{d} = [\bar{d}_A\ \bar{d}_B\ \bar{d}_C]$, is also the transformation between input force and output displacements. Its inverse will be used later to drive a structure to specific displacement commands, thus allowing for arbitrary shape control.

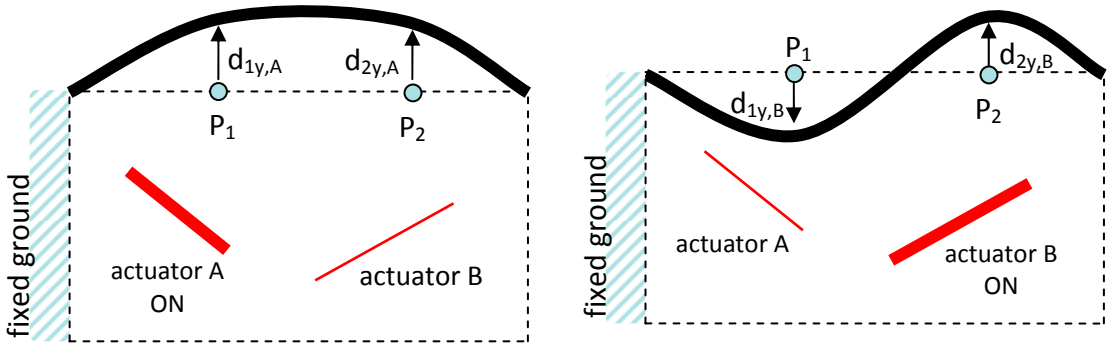

Figure 39: An example of two possibly orthogonal actuation modes. It is seen how the deformations due to each actuator are not only different, but also not redundant.

The determinant formula used is only one of several ways to represent the linear independence of a set of vectors. It works well because it is numerically robust for values not near zero; all of the values we are concerned with are near one. It is also intuitive to see how the independent vectors are orthogonal in n-dimensional space. Other possibilities often used are SVD (singular value decomposition) values and the condition numbers of the matrix. Another possibility is to seek harmonic shape functions that comprise a Fourier series, from which any function can be assembled. While providing an excellent means of shape control, these are numerically expensive. More importantly, they would require a more explicit statement of the objective function. The current measure of controllability works very well precisely because it

does not state the kinds of functions that are required to achieve linear independence. Rather, any set of shapes that work are acceptable and the optimizer is not overly constrained.

6.1.2.3 Other constraints and terms to be optimized

While the primary objective is the orthogonality of the output vectors, it is also required that these vectors surpass a minimum displacement magnitude ($d^{act}_{min,target}$) so that the structure can sufficiently deform. This can be checked by making sure that for every output point at least one vector meets the minimum displacement required of that point. Designs are judged by the maximum displacement of their *lowest*-displacement output point, d^{act}_{min}. At the same time, it is desired to restrain motion caused by *external* loading, d^{ext}_{max}. The external loading is applied at the same output nodes, all at once, opposite the desired direction of motion. Again, a total element length (L_t) constraint is also used, resulting in the final objective function of Eq. (28).

$$maximize \begin{bmatrix} \eta_c - w_1 \times (d^{ext}_{max}) - w_2 \times \left(d^{act}_{min,target} - d^{act}_{min}\right) \dots \\ \dots - w_3 \times \left|L_t - L_{target}\right| \end{bmatrix} \tag{28}$$

6.1.3 Results for Controllability

A sample problem is studied for the optimization of controllable designs. The design space is depicted in Figure 40, with the design parameters and optimization variables listed in Table 8 and Table 9.

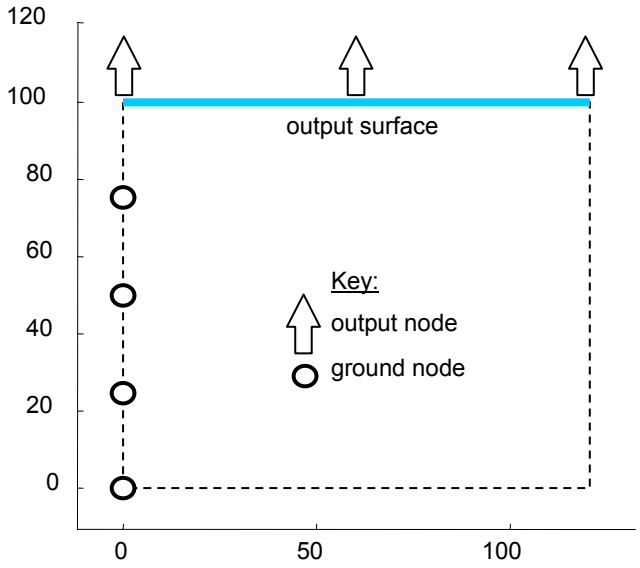

Figure 40: Design Space for Controllability Problem. The shape morphing surface is located at the top of the structure, and is represented by the 3 indicated nodes. Units for the x and y axes are mm.

Design Parameters	
actuator block force	90N
element modulus	2,480MPa
actuator modulus	500MPa
output load magnitude	0 and 0.1N
element out-of-plane thickness	1.5mm
minimum output deflection	5mm
domain footprint	120mm x 100mm
grid size	5 x 5

Table 8: Design and Algorithm Parameters for the Controllability Problem

Number	Variable	Type	Possible Values
1	Beam Thickness	discrete	0, 0.5, 1, 1.5mm
…	…	…	…
168	Beam Thickness	discrete	0, 0.5, 1, 1.5mm
169	Actuator 1	discrete	1-168
170	Actuator 2	discrete	1-168
171	Actuator 3	discrete	1-168

Table 9: Optimization Variables. There are 168 beam variables that determine whether the beam is absent or present with one of three discrete thickness values.

The task for these examples is to control a simple airfoil exposed to unknown and variable pressure loads along its external surface. The design specifications are actuator block force: 90N, actuator modulus: 500MPa, element modulus: 2,480MPa, and minimum output deflection: 5mm. Each problem used the same design domain, similar to that in Figure 38, but with three output nodes.

6.1.3.1 No External Load Case

To demonstrate that capturing all of the conflicting objectives is essential to multifunctional system design, I begin with a counter-example where no external loads are present. This is discovered to not be a properly constrained problem, with results that are often haphazard "spaghetti" structures with no obvious structural integrity. Thus, the load cases are important to result in meaningful structures. Imposing even very small external loads causes a load-bearing skeleton to appear, and a much more desirable result is instantly recognizable.

Figure 41 shows results for the best of a population of 200 over 680 generations. Note the orthogonality of the output curves; the shapes are more complex than any trivial solution (where each actuator primarily affects only one output node): all of the nodes

are moving, yet high orthogonality (99.98%) is still achieved. However, the first and last skin nodes are cantilevered and have questionable integrity if under external loads, leading us to the second example with the additional external load case present.

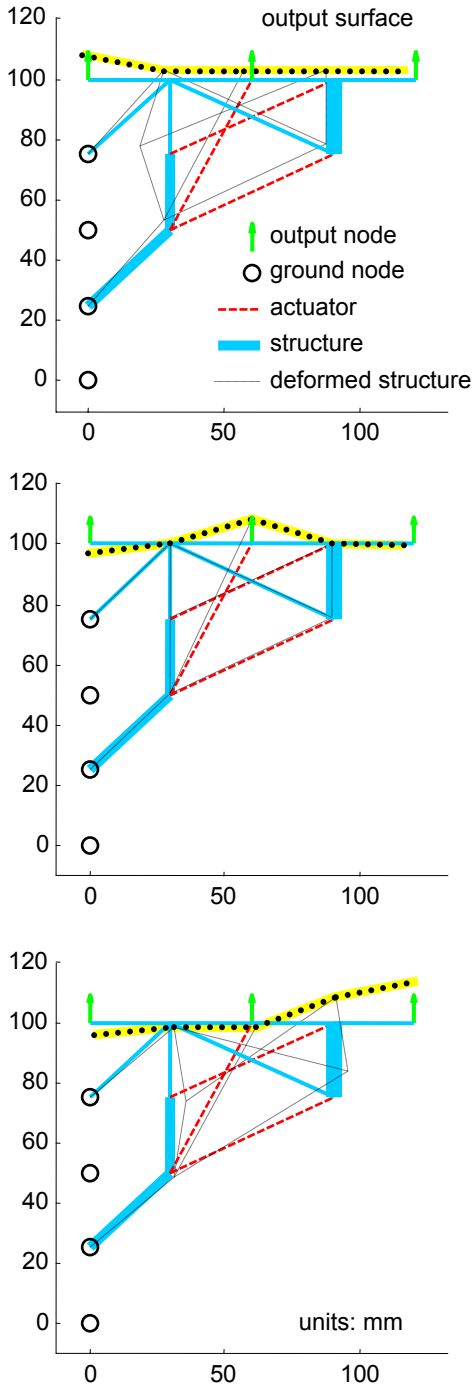

Figure 41: Results of optimization for controllability. No external load-case considered. Each figure shows the response of a different actuator (dashed red line) firing. Dotted black lines indicate deformed structure. Parameters: population=200, generations=680, actuator modulus=500MPa. orthogonality=99.98%

6.1.3.2 With External Load Case

Figure 42 shows the results for the best of a population of 200 over 400 generations. Note the orthogonality of the output curves (dotted lines); the shapes are more complex than any trivial solution (where each actuator would primarily affect only one output node): all of the nodes are moving, yet high orthogonality (99.98%) is still achieved. The maximum vertical deflection for a downward load of 0.1N simultaneously applied at all three output nodes is 0.29mm. Results from nonlinear FEA are also shown to validate the results.

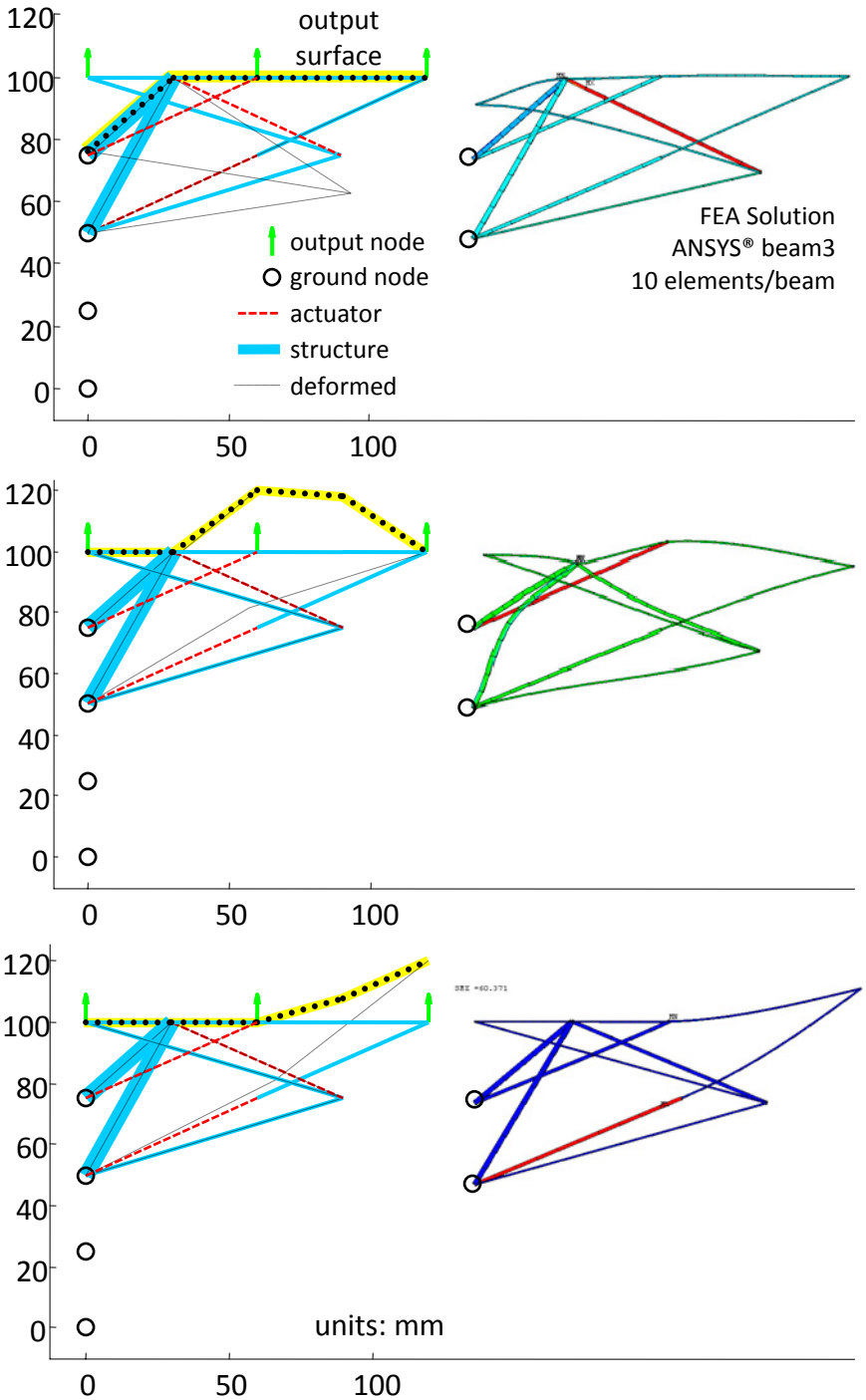

Figure 42: Results of optimization for controllability. Each figure shows the response of a different actuator (dashed red line) firing. Dotted black lines indicate deformed structure. Parameters: population=200, generations=1,500, external load= -0.1N at each output node, actuator modulus=500MPa, skin element thickness=0.5mm, orthogonality=99.99%, max. deflection under load=0.29mm.

6.1.3.3 On Controllability and Degrees of Freedom

In both sets of results provided above for controllability, it is important to highlight the difference between controllability and degrees of freedom. *Controllability* refers to the ease of achieving all the different modes shapes desired for an application. The *degree of freedom* of the shape morphing surface is the *number* of different mode shapes. Thus, the number of degrees of freedom is a design choice made by the application engineer as a design parameter, and is separate from the goal of controllability. Degree of freedom corresponds to the desired complexity of the possible shape responses. This is to say that even for low degree of freedom morphing (e.g. 3 mode shapes), near 100% controllable designs are possible. Any amount of desired complexity can be made controllable, but it is up to the designer to determine how much complexity is needed ahead of time. Fortunately, the previous results and those in following sections all demonstrate that three mode shapes appear to be quite adequate for achieving shape control. It is subjectively observed that since the mode shapes are *smooth* curves, they can be combined in ways that seem to fully span all possible desired shapes. That is, even though only three points on the surface are being *exactly* controlled, the smooth continuity gives partial but reasonable control of *all* points on the curve.

6.1.4 Design Studies

To better understand the problem and design space, I have evaluated many parametric studies with the genetic algorithms. Two parametric trends from one study are presented, which depict the tradeoffs tied to the magnitude of the external load applied to assure structural integrity. The objective function, Eq. (29), includes terms for

controllability, displacement under external load, achievable actuated displacement, and the length constraint. The design parameters and optimization variables for these case studies are listed in Table 10 and Table 11. The design domain is the same as that used in the previous example (see Figure 40), with the dimensions expanded to 250mm by 200mm.

$$maximize \begin{bmatrix} \eta_c - w_1 \times (d_{max}^{ext}) - w_2 \times \left(d_{min,target}^{act} - d_{min}^{act}\right) \dots \\ \dots - w_3 \times \left|L_t - L_{target}\right| \end{bmatrix} \quad (29)$$

Design Parameters	
actuator block force	90N
element modulus	2,480MPa
actuator modulus	500MPa
external load magnitude	0.05, 0.5, and 5N
element out-of-plane thickness	3mm
minimum output deflection	5mm
domain footprint	250mm x 200mm
grid size	5 x 5
Algorithm Parameters	
element mutation rate	8%
actuator mutation rate	10%
cross-over rate	95%

Table 10: Design and Algorithm Parameters for the Controllability Case Studies

Number	Variable	Type	Possible Values
1	Beam Thickness	discrete	0, 1, 2, 3mm
…	…	…	…
168	Beam Thickness	discrete	0, 1, 2, 3mm
169	Actuator 1	discrete	1-168
170	Actuator 2	discrete	1-168
171	Actuator 3	discrete	1-168

Table 11: Optimization Variables. There are 168 beam variables that determine whether the beam is absent or present with one of three discrete thickness values.

In these studies, the penalties were adjusted to keep the controllability at a level above 99.5%, so that the effects on displacement can be isolated. Specifically, we are concerned with the maximum deflection under external load (d_{max}^{ext}) and the achievable displacement under actuation (d_{min}^{act}) for a structure with high controllability. These quantities are tracked in Figure 43 and Figure 44 under varying external load magnitudes (0.05, 0.5, 5N per node) and target length ratios (η_L = 2, 3, 4). Each data point is an average of 10+ optimization runs.

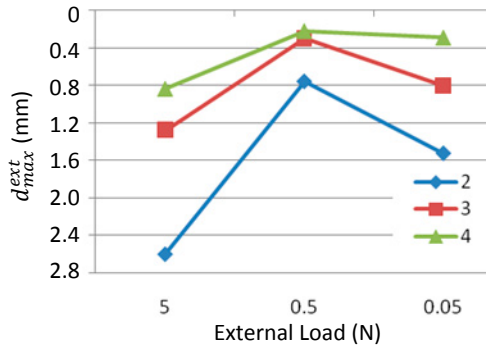

Figure 43: Surface Displacement under External Load, d_{max}^{ext} (mm). Here, the 0.5N load designs are best, providing the least deflection under load.

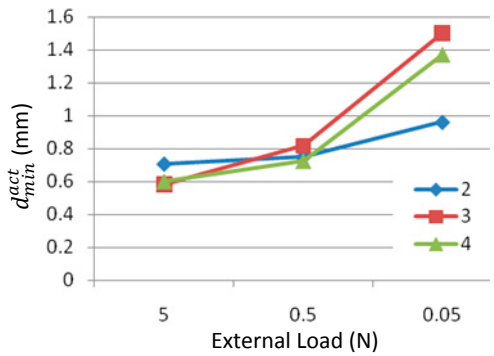

Figure 44: Achievable Displacement of Wing Surface under Actuation Load, d_{min}^{act} (mm). Here, the 0.05N load designs are best, providing the most deflection under actuation.

With the above results, I infer the trends of overall structural stiffness. At higher external loads, there is some stiffening to compensate, but d_{max}^{ext} still increases (see Figure 43). This limited stiffening, however, is capable of decreasing displacement under actuation (see Figure 44). At lower external loads, the structures are less stiff, allowing for greater d_{min}^{act}, which they clearly take advantage of. In fact, the stiffness goes so low as to cause d_{max}^{ext} to *increase* again, but it is still outpaced by the advantages from the increased d_{min}^{act}. That is, as the external load decreases, the stiffness decreases even faster to balance the objective function terms. Future work should investigate Pareto analysis of the conflicting objectives, to observe these trends for *all* combinations of penalty weights. In general it appears that flexibility is favored at low external loads and stiffness is favored under higher loads.

6.1.5 Physical Prototype

Several designs have already been prototyped in ABS plastic (E=2,480MPa) to provide physical demonstration of orthogonality. Figure 45 shows a model designed to be extra compliant to exaggerate deflections for visual inspection. However, a truss-like structure capable of supporting external vertical loads is still evident.

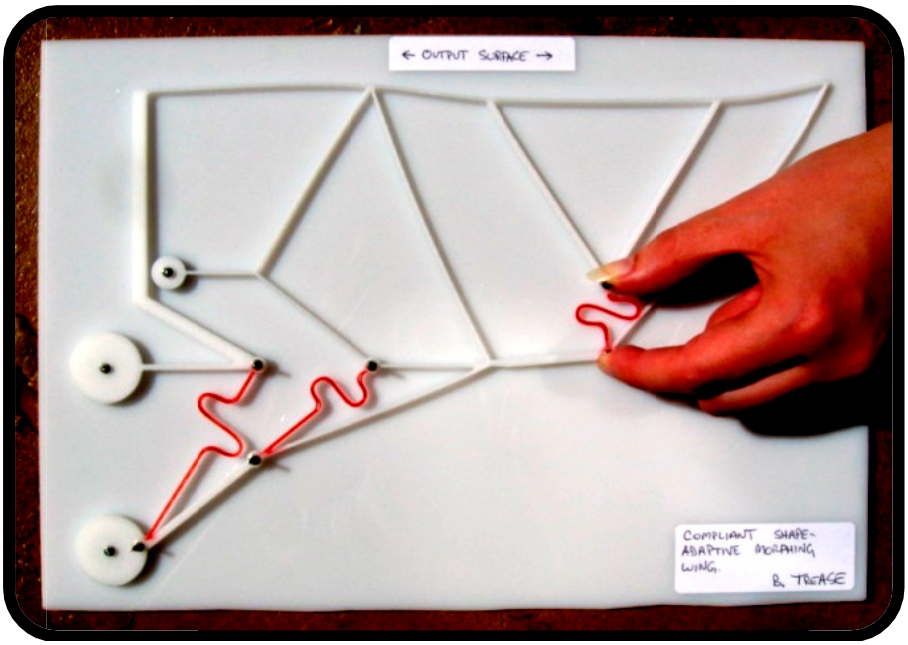

Figure 45: Physical Prototype of 3-Actuator Shape-Morphing Wing. Material is ABS Plastic fabricated via Fused Deposition Modeling. Actuators are simplified as springs to allow for finger actuation. Structure is fixed to ground on left edge.

6.1.6 Discussion

Encouragingly, the results are not trivial designs, i.e. actuators merely connected directly from the output nodes to the ground. It is recognized that the achievement of control is somewhat binary when under extreme constraints; values for orthogonality tend to be below 10% or greater than 90%. This discontinuity makes it difficult for the optimizer to balance the requirements for orthogonality and large displacements (d_{min}^{act}). This is possibly because for a controllable structure with some given geometry (i.e. skin thickness), there is only so much displacement one can achieve before the structure becomes completely uncontrollable.

Often, either orthogonality or large displacements (d_{min}^{act}) dominates the objective function and the other falls far behind. The balance is very sensitive to the values for

skin modulus, actuation modulus, and the magnitude of output load; these all not only affect the design, but specifically affect the displacement/orthogonality conflict. Skin elements that are too compliant or actuator elements that are too stiff make orthogonality overly easy to achieve, resulting in its dominance. Strategically placed stiffness is required to create the different modes shapes, but stiffness in general retards output deflection. These parameters effectively control the coupling between the three output nodes, and thus the possibility of orthogonality.

Note that the relative weighting of all the corresponding objective function terms are also important to these tradeoffs. Not reported here are the numerous iterations taken to find the correct set of weights to find good designs and expose the above mentioned trends. In the future, multi-objective techniques that explore combinations of all penalty weights are clearly motivated.

Regarding grid resolution (described in §4.2.1), one observes that there should be an adequate number of elements along the shape-morphing edge to allow for the different desired mode shapes. In the previous examples, four elements proved to be enough to capture the desired independent mode shapes. In general, it is suggested to use at least twice as many morphing edge elements as there are mode shapes. This offers an ideal amount of freedom in achieving independent shapes.

In the end, these design studies provide some insight into the general properties of controllable structures, but the goal of discovering fundamental design principles of multifunctional structures remains elusive. The results demonstrate the specified objectives in non-intuitive ways because they are satisfying several objectives at once. Every element is linked to each other in different ways for the each conflicting objective, making a building block approach seem out of reach. The final results can be described as emergent properties of the structure, which further validate the use of genetic algorithms as the appropriate design tool.

6.2 Design for Observability

Sensors are also required in any controlled system. In this section I develop a means for measuring *observability* that is very analogous to the method already given for measuring controllability. Through an inversion of inputs and outputs, the framework for embedded actuation can be extended to distributed sensing. While these are analogous, some new issues arise related to measurement resolution. However, of key significance is that this is not the traditional ad hoc design; sensor design will be simultaneous and synergistic, with sensor placement affecting structural topology and vice versa. This new sensing paradigm corresponds to an "*internal* state of stress" that relates to the *external* conditions of the system environment.

6.2.1 Formulation

The goal is now to describe the conditions at the output points described in the previous section, P_1 and P_2. It may be desired to know the pressure load acting on those points

or the shape of the deformed curve. I consider these equivalents as they are related by the structural elasticity. In this example, the ability of the sensors to detect pressure loadings of unknown shape will be investigated.

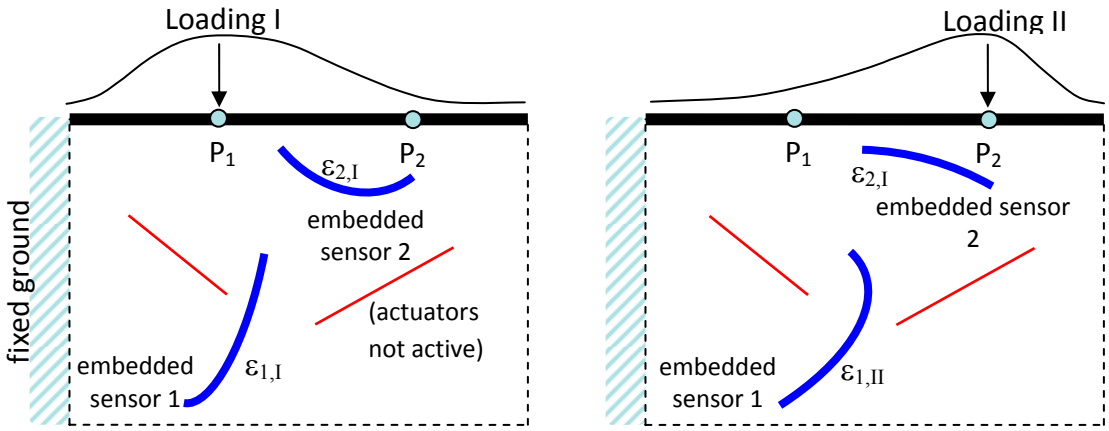

Figure 46: Response of "embedded and distributed sensors" to different applied loads. The loadings are designed to be orthogonal, with the intent that the sensors respond differently and uniquely to each loading case.

The integration of sensor and structure is slightly different now, as there will be no "beam replacement" as there was for the actuators. Rather, the nature of the embedded sensors allows them to be directly added to the beams, without changing the beam properties. Sensor location is determined by variables in the same manner that actuator location was determined in the previous section. That is, sensors are not *added* to a design topology, but are *part of* the topology. Since optimal performance depends on the quality of the sensor layout, the sensor locations determine the overall topology just as much as they are determined by it. Two sensing strategies are identified as applicable: strain gauges placed directly on the beams or embedded mutual inductance sensing (MIS, see Peshkin U.S. Patent (2004) in §2.9).

The formulation for calculating sensor strain is given in Chapter 3, Eq. (1). I choose to locate all sensors in the center of the beam's length. While it is true that placing the sensors anywhere along the beam further opens the design space to find independent strain values, these values vary linearly along the beam. That is, the strains along the beam for a set of load-cases are closely proportional to the strain at the center for the same set of load-cases, thus not giving actuator location (along the beam) a large effect in the value of controllability.

The task of optimal distributed sensing is to find beam deflections that correspond to orthogonal external loading. For example, we consider two orthogonal loads by loading only one output point at a time (Figure 46). Just as two FEA runs were required before for finding the output vectors for each actuator ($\bar{d}_A$ and $\bar{d}_B$), two FEA runs are required to find the sensing vector for each loading condition ($\bar{s}_I$ and $\bar{s}_{II}$). The sensing vector comprises the total signal (ε) found in each of the embedded sensor beams: $\bar{s}_i=[\varepsilon_1,\varepsilon_2]_i$, and observability is defined as:

$$\eta_o = \left| \frac{det[\bar{s}_I\ \bar{s}_{II}\ \cdots\ \bar{s}_m]}{|\bar{s}_I||\bar{s}_{II}|\cdots|\bar{s}_m|} \right| \tag{30}$$

As with controllability, note that the matrix inside the determinant, $\bar{s} = [\bar{s}_I\ \bar{s}_{II}\ \bar{s}_{III}]$, is also a transformation, which in this case transforms external forces into internal strains. Its inverse can be employed to map sensor readings directly to the external load profile.

Now, while it has been argued that location of the sensor along the beam is not critical, which *side* of the beam the sensor is on is very important, reflected by the ± operator in Eq. (1). Thus for each set of three actuators, each having two strain values, there are eight (2^3) unique combinations of strain. In deciding which combination to use in the objective function, one could possibly have extra design variables that determine of which side of the beam each sensor is placed. However, with only eight combinations, the solution space is easily tractable, and the implementation in this dissertation calculates the observability for all eight combinations, recording the highest value for use in the objective function.

A potential problem arising from the above heuristic is that the strains that correspond to the best value of observability may not be the optimal strain values with regard to minimum and maximum allowable strains. A more thorough optimization might pick the combination that has the best weighted combination of observability and strain. However, I feel I am safe in making the assumption that the minimum value of strain does not change much for each of the eight cases, at least remaining in the same order of magnitude.

6.2.2 Implementation

Sensing is to be accomplished with strain gauges measuring ε as the combined bending and axial strain on the surface of the center of a beam. Maximum structural *stresses* are found with a nodal load of 2N. For these studies, designs with overstressed elements are penalized, proportionally to the degree they are overstressed ($\eta_{stress} = \sigma_{max}/\sigma_{yield} - 1$).

To ensure measurement resolution, *strains* are calculated for a load 10 times smaller, 0.2N. A penalty term is added to limit the minimum value of strain ($\min|\varepsilon|$) to that readable by commercial strain gauges (ε_{min}). A visual reference for the operating range of the strain gauges is shown in Figure 47. The complete objective function for the observability is shown in Eq. (31).

$$maximize \begin{bmatrix} \eta_o - w_1 \times (d_{max}^{ext}) - w_2 \times (\eta_{stress}) - \cdots \\ \ldots w_3 \times \left|L_t - L_{target}\right| - w_4(\varepsilon_{min} - \min|\varepsilon|) \end{bmatrix} \quad (31)$$

One additional change is made in the mutation operators for sensors, not used in the algorithm for actuators. When an element is deemed to be a sensor, that element's own thickness variable is turned on if it was zero before. If the sensor variable later crosses over or mutates to a new value, the underlying would remain turned on because its own variable recorded the change. In a sense, this gives the sensor variables a power of element generation. As this element generation may be beneficial or not, it is neither prevented nor encouraged, but limited by randomly turning off any element variable that had been a sensor element in the previous design but is no longer a sensor.

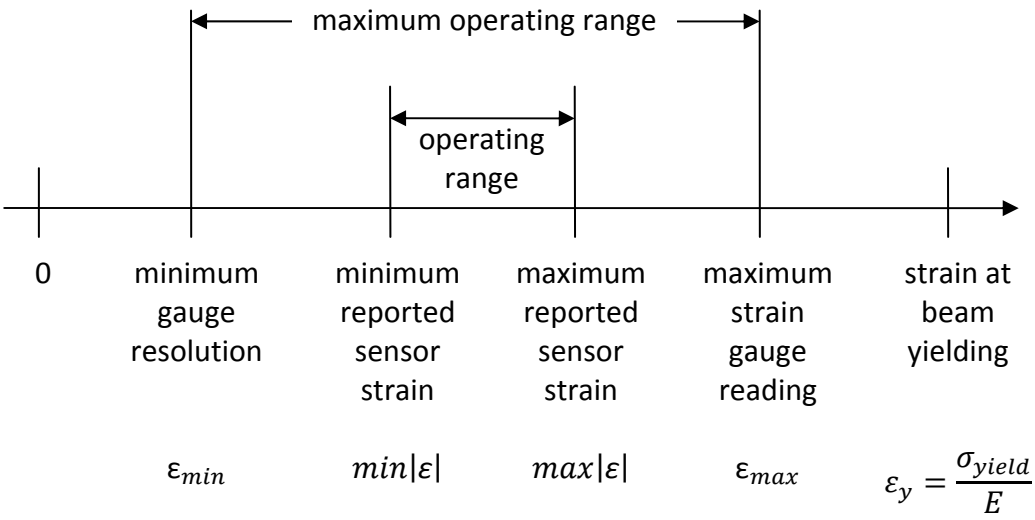

Figure 47: Operating Range of a Strain Gauge

Design Parameters	
element modulus	2,480MPa
element yield stress	37.7MPa
external load magnitude	2N (0.2N for minimum strain check)
element out-of-plane thickness	1.5mm
domain footprint	250mm x 200mm
grid size	5 x 5
Algorithm Parameters	
element mutation rate	8%
sensor mutation rate	10%
cross-over rate	95%

Table 12: Design and Algorithm Parameters for the Observability Problem

Number	Variable	Type	Possible Values
1	Beam Thickness	discrete	0, 0.5, 1, 1.5mm
…	…	…	…
168	Beam Thickness	discrete	0, 0.5, 1, 1.5mm
169	Sensor 1	discrete	1-168
170	Sensor 2	discrete	1-168
171	Sensor 3	discrete	1-168

Table 13: Optimization Variables. There are 168 beam variables that determine whether the beam is absent or present with one of three discrete thickness values.

6.2.3 Results for Observability

Using the same design space and material parameters as for the controllability problem, several sample solutions have been generated for the objective function in Eq. (31), three of which are shown in Figure 48. The design parameters and optimization variables are listed in Table 12 and Table 13. Here, there are no actuators; only sensor placement is considered. The external load is applied to each node in a separate load case. Maximum stresses (under 2N loading) are less than 10MPa and as with controllability, the final observability values approach 100%.

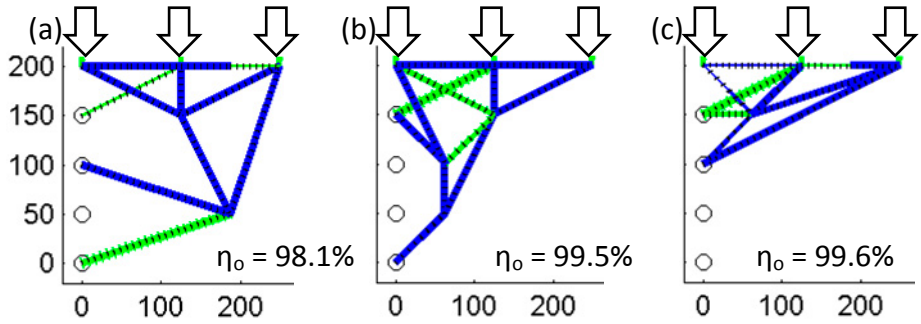

Figure 48: Three Example Solutions that exhibit the property of observability. Length units are mm. Material is ABS Plastic. External load magnitude: 0.2 to 2N. Sensor elements are shown in green (lighter shade).

The data for all optimization runs for all length ratio constraints is reported in Table 14. Each optimization was run 15 times; the average performance and standard deviation

are reported in Table 14 for an external load magnitude of 2N. To better understand the robustness of the algorithm and its ability to search the design space, two solution maps are shown in Figure 49 and Figure 50. Figure 50 replicates the first study, but with the external force increased from 2N to 20N. These two figures also help demonstrate how the multiple objectives are traded off to achieve the optimal objective fitness value.

length ratio	control.	disp. under external load	max. stress
η_L	η_C	d_{max}^{ext}	σ_{max}
	%	mm	MPa
2	97.3 (1.8)	2.0 (1.0)	6.7 (3.2)
3	97.9 (2.3)	1.8 (0.9)	5.7 (2.4)
4	98.8 (1.5)	1.7 (0.6)	6.2 (2.6)
5	99.3 (1.0)	1.2 (0.5)	4.3 (1.4)

Table 14: Summary of Results for Observability. External Force = 2N. Average values and (standard deviation) are provided for each of four different length ratio constraints.

The two solution point figures show the robustness of the algorithm in finding highly observable solutions. The majority of solutions are all above 98% observable, with the worst results being only 92%. There is more variation in d_{max}^{ext}, especially for the problem with the larger external load. Solutions are grouped toward the lower values of 1 and 4mm, but these values can double or triple for some of the individual solutions. For the designer greatly concerned with the amount of deflection under load, this means that either several optimization runs should be performed to guarantee performance, or that a higher weight should be placed on the penalty for d_{max}^{ext}.

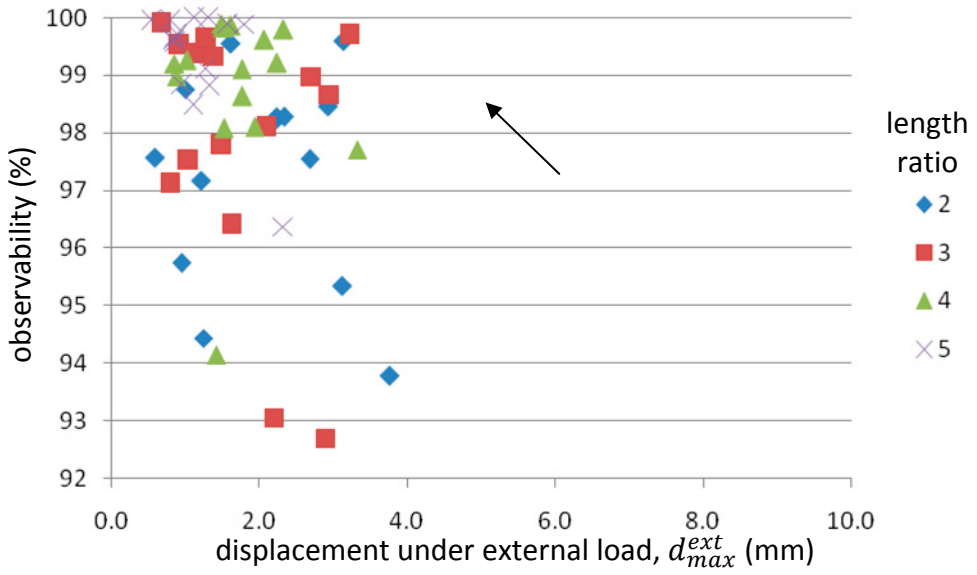

Figure 49: Solution Points for Observability. External Force = 2N.
Each point represents the individual solution attained for each optimization run.
This figure displays the relationship between achievable observability and d_{max}^{ext}. Optimality increases toward the upper-left corner.

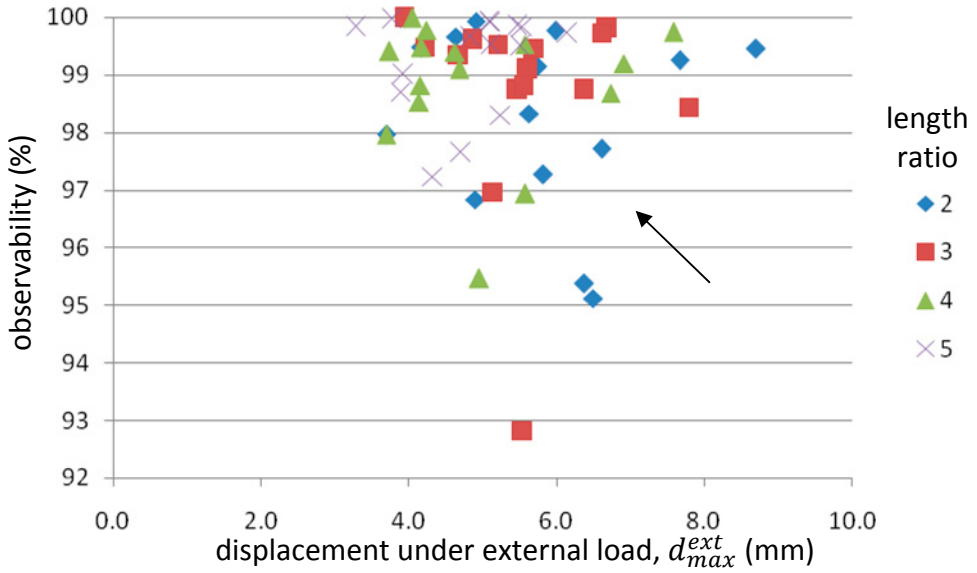

Figure 50: Solution Points for Observability. External Force = 20N.
Each point represents the individual solution attained for each optimization run.
This figure displays the relationship between achievable observability and d_{max}^{ext}. Optimality increases toward the upper- left corner.

Figure 51 depicts the case-by-case results for the structure in Figure 48-b, including the strain values that are found to be linearly independent (i.e. the nine numbers in the

figure comprise a linearly independent matrix). Absolute strain (under 0.2N loading) is in the range of 11 to 84 microstrain. For downward loading (2N) on all three points at once, the maximum combined sensor strain is 889 microstrain. Hence, this would require strain gauges with a sensing range of 11 to 889 microstain. Finally, under 2N loading on all three points at once, the maximum stress *anywhere* in the structure is 6.3MPa. With the yield stress of ABS plastic at 37.7MPa, this indicates a factor of safety of 37.7/6.3 = 6.0.

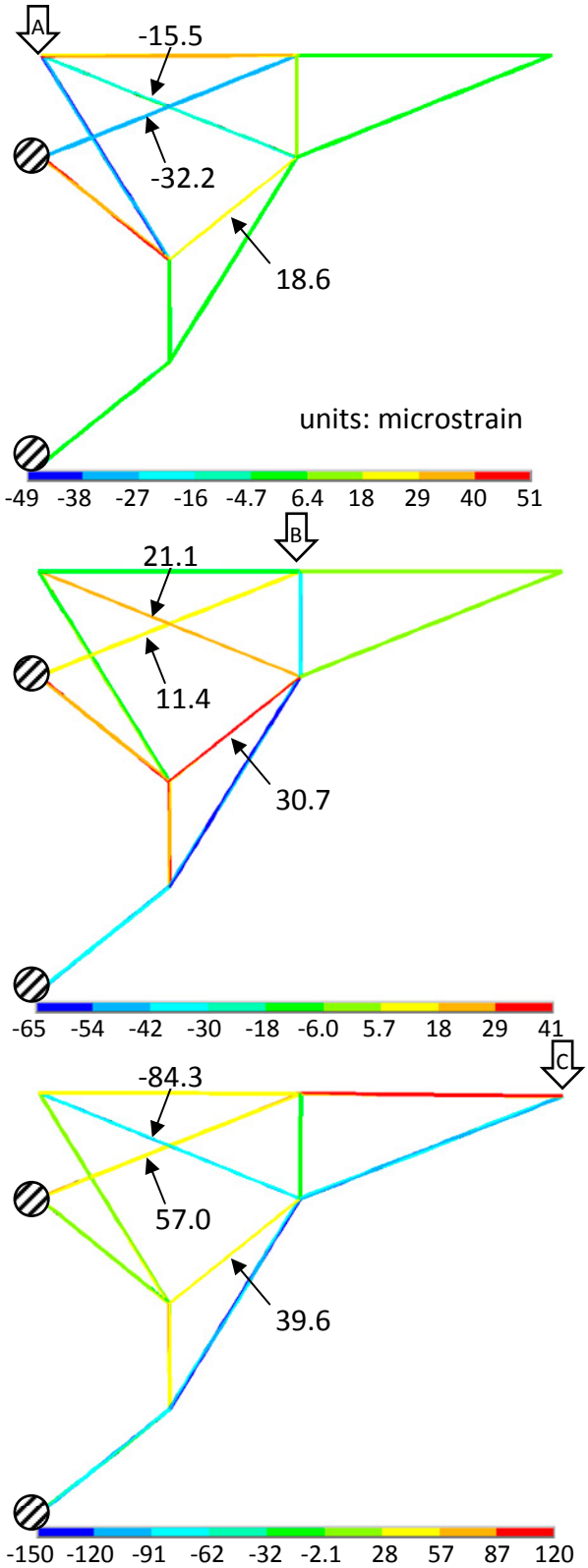

Figure 51: Optimal Sensor Set Response to Orthogonal Load Vectors. The magnitude of the external load is 0.2N. The normal strain components on the beam surfaces are reported. Units are microstrain. Load magnitude is reduced (from 2N) to assess the required strain gauge resolution.

The results for controllability in this section demonstrate that high-performance designs can be created even with the simplifying constraints imposed on the problem. In future work it may be desired to reduce these constraints to explore a larger design space. For example, rather than restricting actuator placement to the center of a beam, a method that allowed its location to vary along the beam length could lead to many more potentially good designs. Going a step further, all three actuators could be located at different locations on the same beam. Exploring this possibility could lead to even further manufacturing simplifications.

6.3 Combined Controllability and Observability

To demonstrate the full power of the formulation and algorithm, the goals of controllability and observability are now combined within a single structure. Note that this is dramatically different than taking the results from both cases alone and combining them together. The essence of this dissertation is that actuator and sensor placement are no longer independent of the final structural topology; here they now both have an impact on the structural layout and even on the placement of each other.

The design example for this section is again the same simple shape-morphing wing approximation of the previous two examples. There is no constraint implemented to prevent sensors from directly laying on the actuator elements. While some might argue for explicit collocation or non-collocation of actuator and sensor, here it is left up to the optimizer to prove out the best solution. An understanding of the difference between the actuators and sensors does allow for the following hypothesis: since the actuator

elements activate the axial modes of the beams, whereas the sensor elements measure the bending modes of the beams, the two types of components are most likely to be non-collocated.

The design parameters and optimization variables for this problem are listed in Table 15 and Table 16.

Design Parameters	
actuator block force	80N
element modulus	2,480MPa
element yield stress	37.7MPa
external load magnitude	5N
element out-of-plane thickness	1.5mm
desired deflection under actuation	4mm
domain footprint	250mm x 200mm
grid size	5 x 5
Algorithm Parameters	
element mutation rate	8%
actuator/sensor mutation rate	10%
cross-over rate	97%

Table 15: Design and Algorithm Parameters for the Combined Problem

Number	Variable	Type	Possible Values
1	Beam Thickness	discrete	0, 0.5, 1, 1.5mm
…	…	…	…
168	Beam Thickness	discrete	0, 0.5, 1, 1.5mm
169	Sensor 1	discrete	1-168
170	Sensor 2	discrete	1-168
171	Sensor 3	discrete	1-168
172	Actuator 1	discrete	1-168
173	Actuator 2	discrete	1-168
174	Actuator 3	discrete	1-168

Table 16: Optimization Variables. There are 168 beam variables that determine whether the beam is absent or present with one of three discrete thickness values.

The combined problem brings together all of the objectives and constraints discussed thus far, as seen in the objective function, Eq. (32).

$$maximize \begin{bmatrix} \eta_o + \eta_c - w_1 \times (d_{max}^{ext}) - w_2 \times \left(d_{min,target}^{act} - d_{min}^{act}\right) \cdots \\ \cdots - w_3 \times (\eta_{stress}) + w_4 \times \left|L_t - L_{target}\right| - w_5(\varepsilon_{min} - \min|\varepsilon|) \end{bmatrix} \quad (32)$$

A set of typical results for the combined actuator and sensor problem is shown in Figure 52. Visual inspection indicates that these are not haphazard conglomerations of elements; the structures have the internal truss networks to support cantilevered loads. Also note that none of the designs features collocated actuators and sensors. While collocation did occur in some of the other designs, it never occurred for more than one actuator and sensor.

Additional inspection of the designs leads to the observation that while the function of the resulting actuator sets is usually intuitive, the sensor sets are not. That is, one can view the structures and discern which portion of the external surface each actuation will

predominantly affect. However, the task of mentally decoupling the independent strain responses of the actuators is very difficult. This may be because the response space of the three actuators consists of the deflections of three points in a single line, while the response space under orthogonal loading consists of many stresses (curvatures) distributed in several non-related places throughout the structure, a much less mentally-tractable concept.

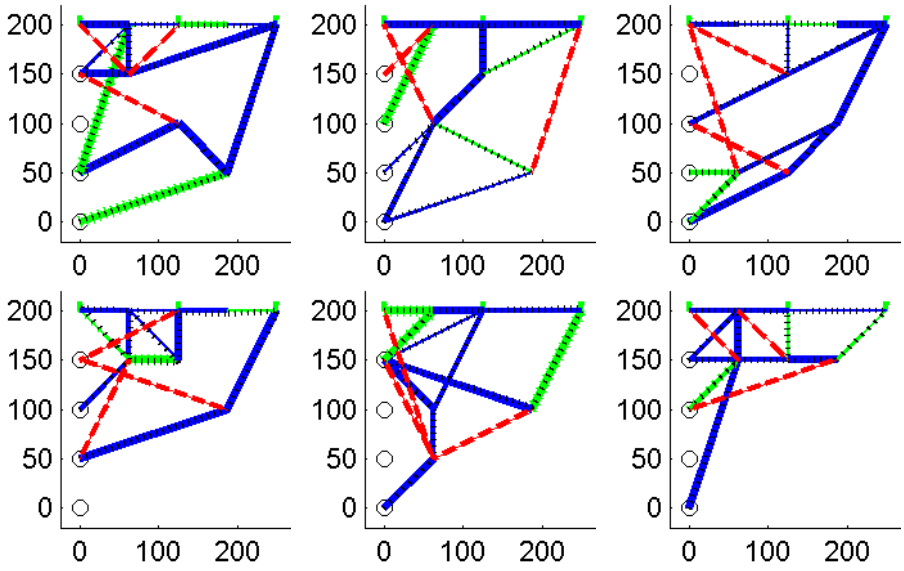

Figure 52: Sample of results for combined synthesis for controllability and observability. Actuators: dashed red lines. Sensors: hashed green lines. Structure: solid blue lines.

A breakdown of the results for the combined problem is provided in Table 17. Each objective and constraint is reported for each target length constraint. The numbers report the average performance and standard deviation for 15 optimization runs. To better understand the robustness of the algorithm and its ability to search the design space, three solution maps are shown in Figures 53-55. These figures also help demonstrate how the multiple objectives are traded off to achieve the optimal objective

fitness value. Figure 53 indicates that the methodology usually results in very high observability values but that the controllability values may have more statistical scattering. At the same time, the majority of the controllability values are still in the 90-100% range. These figures inform the designer that even though several optimization runs might be required to find an optimal solution for controllability, such a solution is very likely to be found.

length ratio	control.	observ.	actuator	external	strain
η_L	η_C	η_o	d_{min}^{act}	d_{max}^{ext}	$\min\|\varepsilon\|$
	%	*%*	*mm*	*mm*	*microstrain*
2	73 (29)	98 (2)	2.3 (1.7)	4.1 (1.8)	11.0 (8.5)
3	88 (15)	98 (3)	1.7 (0.8)	3.6 (1.7)	9.0 (6.9)
4	80 (24)	98 (4)	2.0 (1.3)	3.1 (1.2)	14.3 (8.9)
5	80 (28)	99 (2)	2.3 (1.4)	3.2 (2.1)	15.9 (7.5)

Table 17: Summary of Results for combined Controllability and Observability. Average values and (standard deviation) are provided for each of four different length ratio constraints.

Table 17 shows a solution set where d_{min}^{act} is typically less than d_{max}^{ext}. Although this scenario is still functional in that in can still create small delta mode shapes about the externally deflected shapes, it is less than optimal if the goal is to have a system that completely rejects the deflections caused by external forces. One way to avoid this is to place higher penalty weights on the deflection constraint terms in the objective function. This may, however, lead to an eventual tradeoff resulting in lower controllability and observability. Alternatively, a larger actuator could be used, providing the system with the ability to generate larger displacements when activated. If composite shape-memory-alloy actuators similar to those represented in these studies are used, then the properties of the actuator could be directly parameterized

and included in the optimization. The algorithm could then determine the best blocking force and stiffness for each actuator in a given design.

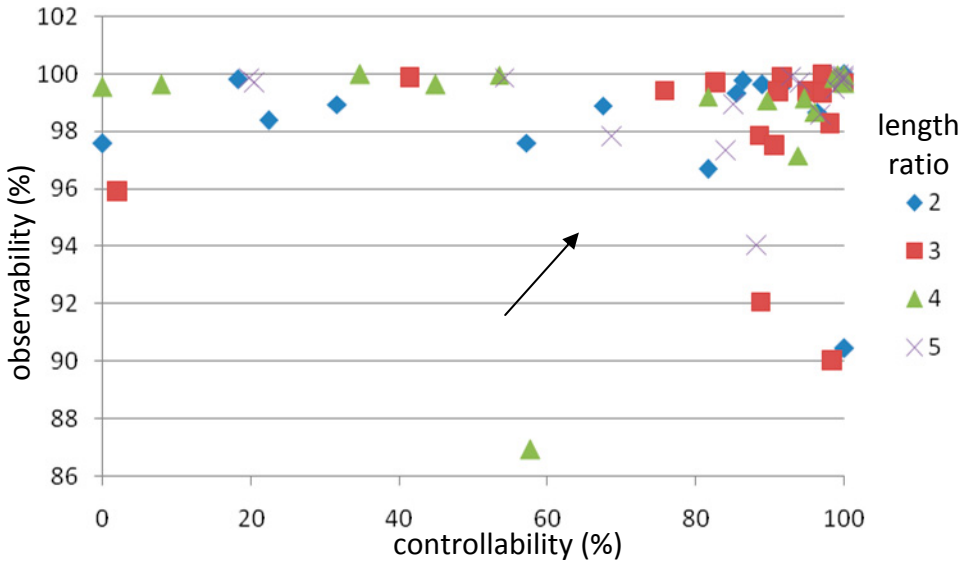

Figure 53: Solution Points for the Combined Actuator and Sensor Problem. Each point represents the individual solution attained for each optimization run. This figure displays the relationship between achievable controllability and observability. Optimality increases toward the upper-right corner.

These figures offer other insight into the problem as well. They report the varying results for an objective function with a fixed set of weights (w_i), and thus are not a true Pareto analysis. However, similar insight is still evident, as seen in Figure 54, where there is an apparent "front" of optimal values as optimality moves toward the upper-right corner. This indicates a tradeoff where designs can achieve much more actuated displacement if they sacrifice some of their controllability. The other solution maps indicate no such front, indicating the displayed objectives are not mutually exclusive.

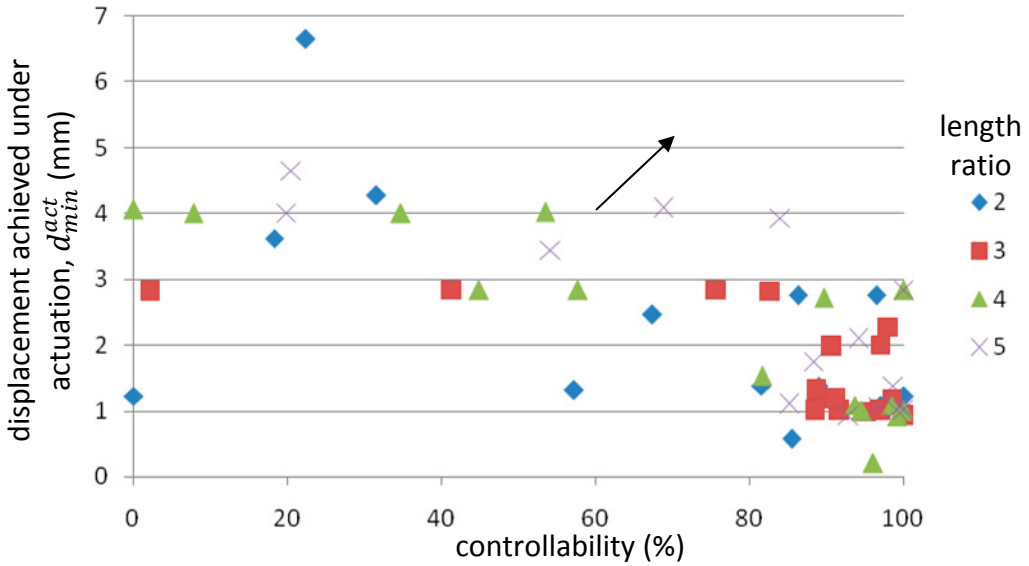

Figure 54: Solution Points for the Combined Actuator and Sensor Problem. Each point represents the individual solution attained for each optimization run. This figure displays the relationship between achievable controllability and d_{min}^{act}. Optimality increases toward the upper-right corner.

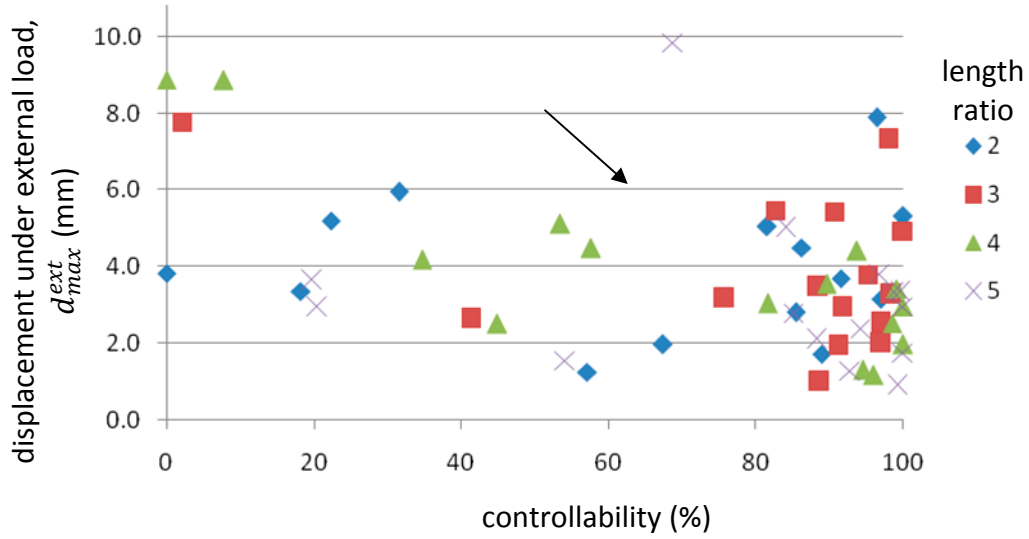

Figure 55: Solution Points for the Combined Actuator and Sensor Problem. Each point represents the individual solution attained for each optimization run. This figure displays the relationship between achievable controllability and d_{max}^{ext}. Optimality increases toward the lower-right corner.

6.3.1 Symmetric Design Space Problem

Since all of the previous problems were for the asymmetric design space of a shape-morphing wing, it is worthwhile to view the results for a symmetric problem. The

parameters and variables are identical to those of the previous section, except that the ground nodes are located along the bottom instead of the left side. Symmetry was not imposed on the resulting structure, to investigate whether the algorithm would generate symmetric structures on its own. While the use of an odd number of actuators (3) imposes an asymmetry on the solution, more often than not the results feature a very recognizable degree of symmetry. Nine of the more symmetric of these designs are shown in Figure 56.

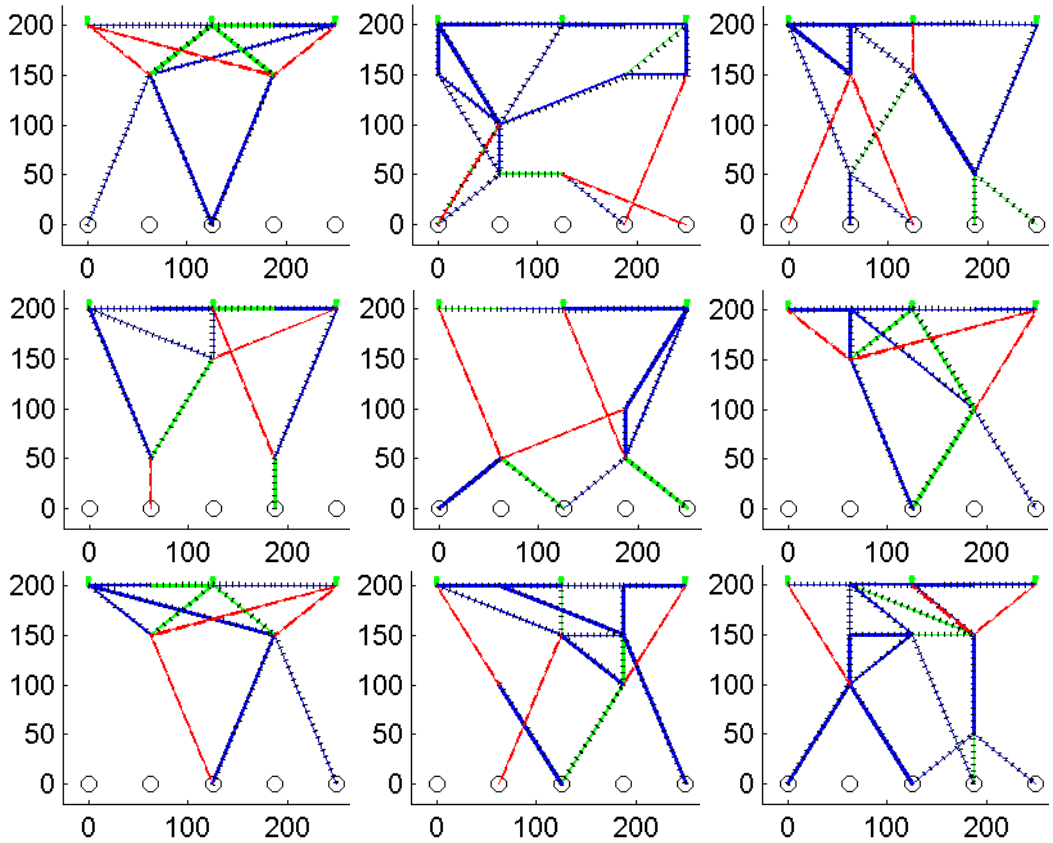

Figure 56: Results of the combined actuator and sensor problem in a symmetric design space. Results tend to favor symmetric solutions even without prescribed constraints for symmetry. The top surface is the controlled shape-morphing edge. Axes indicate x and y coordinates measured in mm. Structure: solid blue lines. Actuators: dashed red lines. Sensors: hashed green lines.

6.4 Sensitivity and Robustness

To validate the practicality of the method, one must inspect the designs for the robustness of their performance. Manufactured artifacts are suspect to many forms of deviation, such as variations in the thickness of machined beams. This section contains a sensitivity study to observe the effects of this variance on performance.

First, the *linear* sensitivity of the controllability, observability, and constraints of one example design (shown in Figure 57) is investigated. As a reminder to the reader, a controllability or observability value of zero implies linear dependence, while values closer to one (100%) imply orthogonality of responses. When reviewing the values of either metric, low values mean it is not easy to activate/sense all the possible modes. That is, if controllability is only 10%, then one of the actuators will need to activate at very high forces to reach certain desired mode shapes. These forces will far exceed what the actuator is capable of, making the device impractical. Therefore, high values of controllability are preferred, as they indicate each actuator can effectively be used in generating a wide variety of mode shapes.

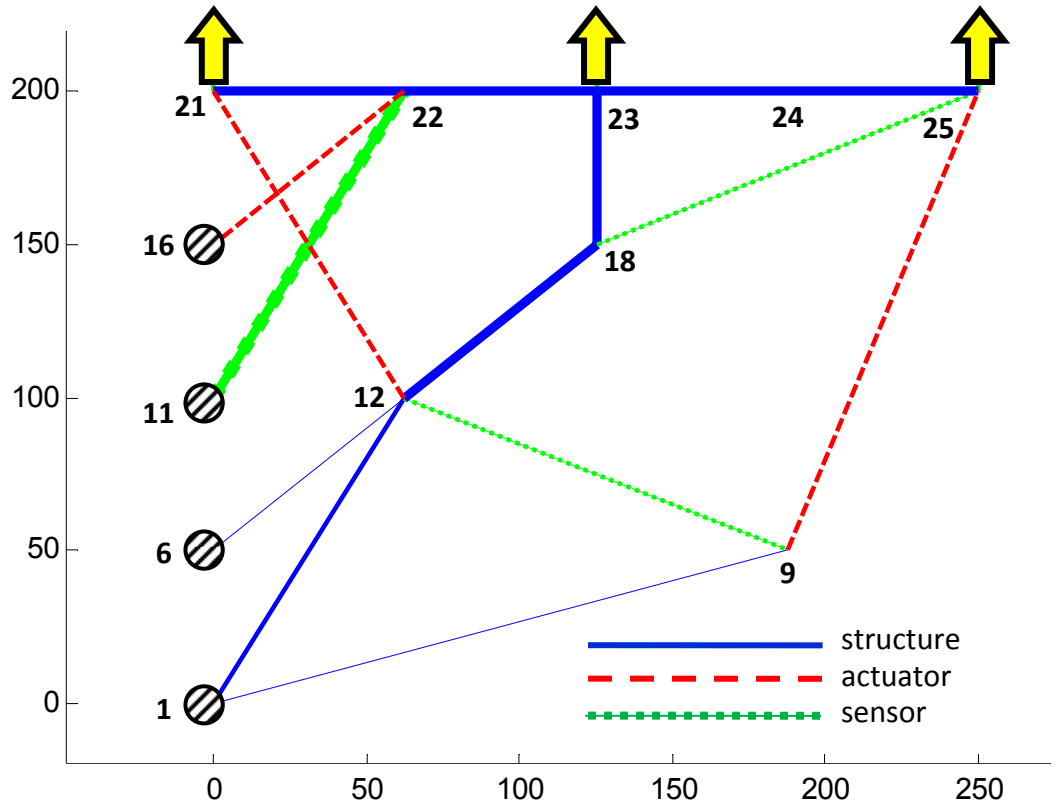

Figure 57: Controllable and Observable Design selected for sensitivity analysis. Sensitivity with respect to node location and beam thickness is tabulated in Table 18. Top surface is the shape-morphing edge, represented by 3 output nodes as indicated. Units are mm.

While high values of controllability or observability are important, the precise values are not critical. Controllability is not the *function* of the device, but a description of it. Thus, in reviewing the variability of these metrics the reader should keep in mind that small changes are acceptable. Once the actuators and sensors are physically calibrated, the force and displacement function of the device will not change.

		control.	observ.	actuator	external	strain
		η_C	η_o	d_{min}^{act}	d_{max}^{ext}	$\min\|\varepsilon\|$
Nominal Value		91.54%	99.55%	1.09	3.70	364
		Values below are in units / mm				
Node		*%/mm*	*%/mm*	*mm/mm*	*mm/mm*	*microstrain / mm*
1	x	0.146%	0.075%	0.00013	0.15	12.5
	y	0.137%	0.028%	0.00001	0.10	12.5
6	x	0.189%	0.090%	0.00000	0.08	11.5
	y	0.303%	0.142%	0.00002	0.11	17.5
9	x	0.035%	0.001%	0.00004	0.01	5.9
	y	0.018%	0.009%	0.00003	0.01	1.5
11	x	0.003%	0.006%	0.00001	0.08	0.4
	y	0.006%	0.006%	0.00003	0.04	0.3
12	**x**	**0.046%**	**0.063%**	**0.00923**	**0.73**	**16.9**
	y	**0.037%**	**0.230%**	**0.00435**	**0.71**	**29.5**
16	x	0.019%	0.009%	0.00004	0.10	0.8
	y	0.037%	0.011%	0.00000	0.14	0.9
18	**x**	**0.480%**	**0.086%**	**0.00050**	**1.02**	**29.4**
	y	**0.442%**	**0.120%**	**0.00058**	**1.23**	**39.2**
21	x	0.128%	0.004%	0.01002	0.04	2.4
	y	0.082%	0.008%	0.01562	0.04	1.4
22	x	0.070%	0.038%	0.00048	0.04	5.2
	y	0.367%	0.161%	0.01101	0.47	18.6
23	x	0.112%	0.045%	0.00023	0.21	9.1
	y	0.486%	0.208%	0.00026	1.04	34.2
24	x	0.000%	0.000%	0.00000	0.00	0.0
	y	0.089%	0.115%	0.00023	0.11	6.4
25	x	0.187%	0.022%	0.00012	0.17	11.5
	y	0.001%	0.055%	0.00007	0.05	6.3
average		0.14%	0.06%	0.00221	0.28	11.4
maximum		0.49%	0.23%	0.01562	1.23	39.2

Table 18: Sensitivity of Node Location. Note: Node spacing is 62.5mm in the x-direction and 50mm in the y-direction. The overall design footprint is 250mm x 200mm.

The functional sensitivity to x and y location of each node in Figure 57 is summarized above in Table 18. The maximum sensitivities for controllability and observability are 0.49%/mm and 0.23%/mm. As the nodes are spaced apart 62.5mm in the x-direction

and 50mm in the y-direction, this indicates relatively high robustness. It is noted that nodes 12 and 18 exhibit the highest sensitivity for all the reported metrics. These nodes are located in the center of the structure with many elements connected to them, and thus have the greatest influence on variations in performance. Table 19 summarizes the performance sensitivity of the same compliant system for variations in beam thickness.

			control.	observ.	actuator	external	strain
			η_C	η_o	d_{min}^{act}	d_{max}^{ext}	$\min\|\varepsilon\|$
Nominal Value			91.54%	99.55%	1.09	3.70	364
			Values below are in units / mm				
Beam	Thickness	Nodes	*%/mm*	*%/mm*	*mm/mm*	*mm/mm*	*microstrain / mm*
3	1	1-9	0.90%	0.91%	0.0006	0.10	6
6	2	1-12	0.07%	0.80%	0.0030	1.28	32
34	1	6-12	6.47%	3.04%	0.0014	0.64	287
71	**3**	**11-22**	**0.19%**	**0.40%**	**0.0046**	**0.82**	**21**
74	**1**	**9-12**	**0.13%**	**11.77%**	**0.0004**	**0.03**	**973**
80	3	12-18	3.51%	1.43%	0.0003	0.68	54
117	3	18-23	2.66%	0.07%	0.0010	0.33	77
118	**1**	**18-25**	**1.07%**	**8.71%**	**0.0008**	**3.31**	**33**
137	3	21-22	0.20%	0.11%	0.0011	0.05	14
143	3	22-23	3.48%	1.41%	0.0056	0.57	231
148	3	23-24	0.21%	0.14%	0.0006	0.13	32
152	3	24-25	0.04%	0.16%	0.0000	0.13	30
Act1	1	12-21	1.52%	1.17%	1.0990	0.89	239
Act2	1	9-25	0.41%	1.09%	0.0083	0.79	59
Act3	1	16-22	0.00%	0.49%	0.0085	0.78	38
average			1.6%	2.4%	0.0016	0.67	149
maximum			6.5%	11.8%	1.0990	3.31	973

Table 19: Sensitivity of In-plane Beam Thickness. Sensors are located on elements 71, 74, 118.

Here, the sensitivity is found to be greater than in Table 18, yet still reasonable. Beam thickness has a stronger effect on performance than beam length, as the former has a

cubic impact on stiffness and the latter a linear impact. Sensitivity is reported in deviation per millimeter of fabrication error. Since the nominal beam thicknesses are between 1 and 3mm, the performance is relatively safe from degradation. It is also noted that elements 71, 74, 118 are the location of the sensors and therefore have the largest performance sensitivities.

If one assumes a manufacturing process capable of 0.1mm tolerance for the beam thickness machining, then the worst case scenario for the performance reported in Figure 19 is $\Delta\eta_C$ = 0.65%, $\Delta\eta_o$ = 1.2%, Δd_{min}^{act} = 0.1mm, Δd_{max}^{ext} = 0.3mm, and $\Delta\min|\varepsilon|$ = 97μstain. These worst case values all correspond to beams with a nominal thickness of 1mm. Thus, a 10% manufacturing variation usually results in much less than a 10% performance variation. The exception is $\min|\varepsilon|$, which relates to the required resolution of the strain gauges. Variation should be acceptable though, as the devices already require calibration when physically constructed. Provided that the minimum strain, $\min|\varepsilon|$, does not drop below the resolution of the strain gauge, operation will be as normal.

The previous tables examined the sensitivities of the compliant system within the small range of *linear* operation. However, it is also noted that there are many factors that cause the variation to be nonlinear in reality, even when assuming small, linear displacements. For example, linear stiffness is a cubic function of beam thickness and linear controllability is a nonlinear function of the different mode shapes. To be clear,

this nonlinear variation is not related to the nonlinear performance of a given structure. In fact, all of the following results are attained with multiple linear analyses of the given structure. The combined overall nonlinear variation for 4 of the design variables in the structure (Figure 57) are shown in Figure 58 through Figure 66.

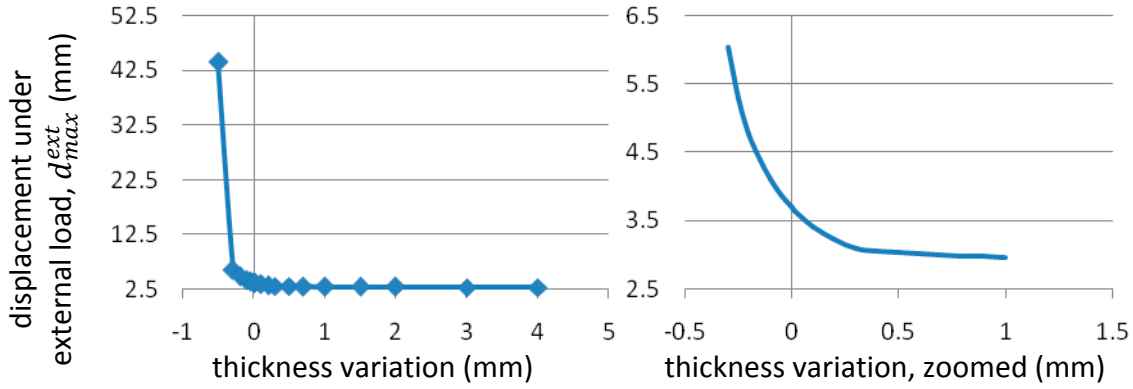

Figure 58: Nonlinear variation of d_{max}^{ext} with respect to changes in the thickness of beam 118. Nominal thickness of beam 118 is 1mm.

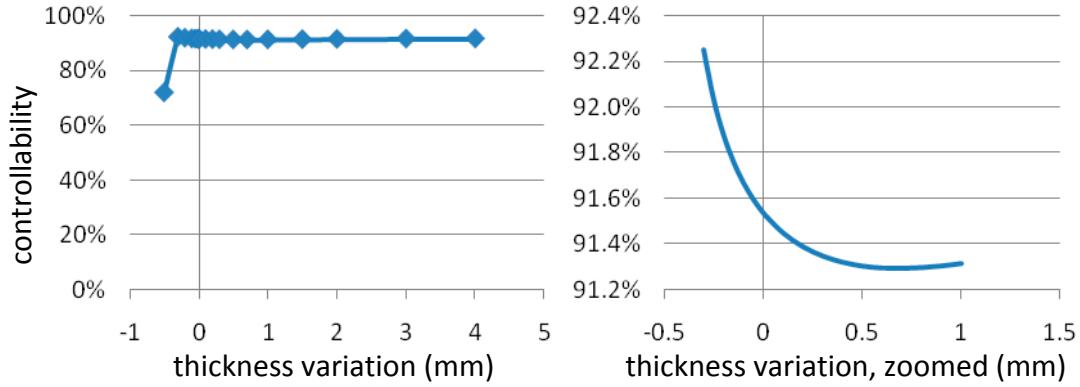

Figure 59: Nonlinear variation of controllability with respect to changes in the thickness of beam 118. Nominal thickness of beam 118 is 1mm.

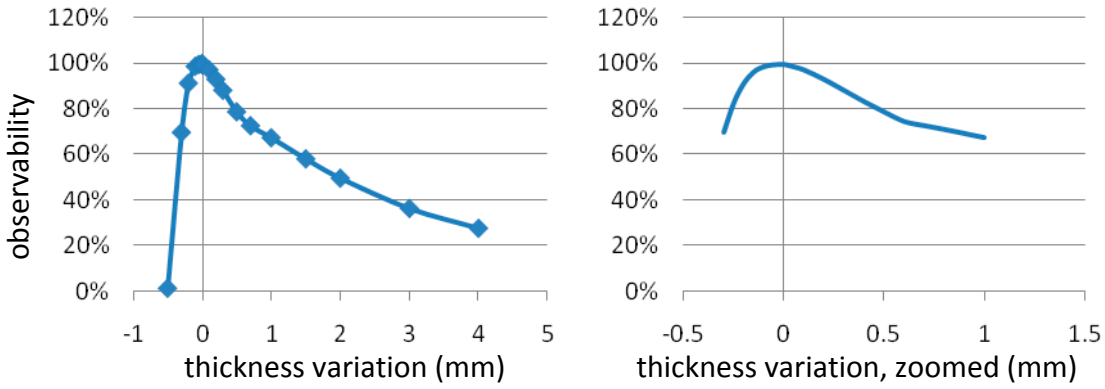

Figure 60: Nonlinear variation of observability with respect to changes in the thickness of beam 118. Nominal thickness of beam 118 is 1mm.

Figure 58 through Figure 60 show the impact of varying the thickness of beam 118 (connecting nodes 18 and 25). Observe that decreases in thickness have a greater effect than increases. Similar results are found for the thickness of beam 6, shown in Figure 61 through Figure 63.

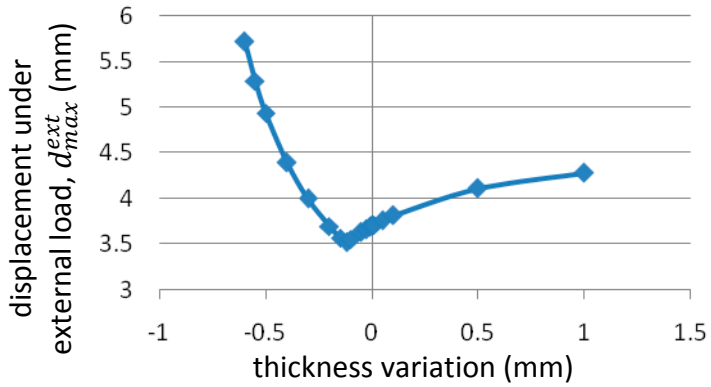

Figure 61: Nonlinear variation of d_{max}^{ext} with respect to changes in the thickness of beam 6. Nominal thickness of beam 6 is 2mm.

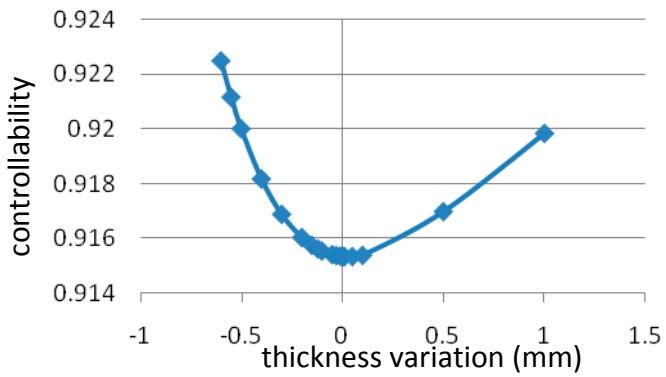

Figure 62: Nonlinear variation of controllability with respect to changes in the thickness of beam 6. Nominal thickness of beam 6 is 2mm.

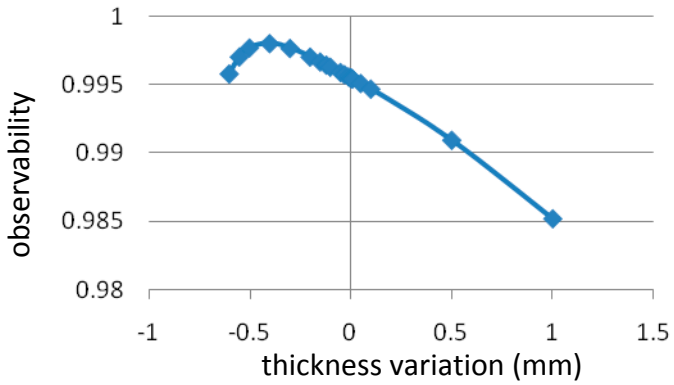

Figure 63: Nonlinear variation of observability with respect to changes in the thickness of beam 6. Nominal thickness of beam 6 is 2mm.

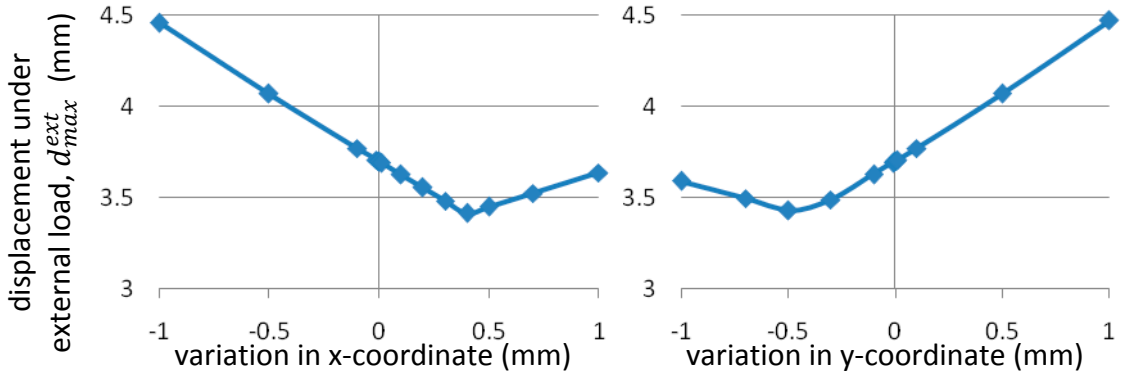

Figure 64: Nonlinear variation of d_{max}^{ext} with respect to changes in the coordinates of node 12.

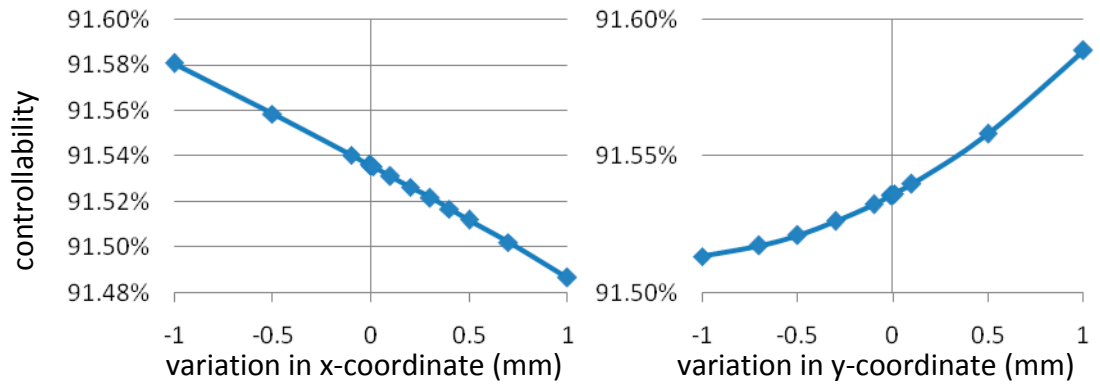

Figure 65: Nonlinear variation of controllability with respect to changes in the coordinates of node 12.

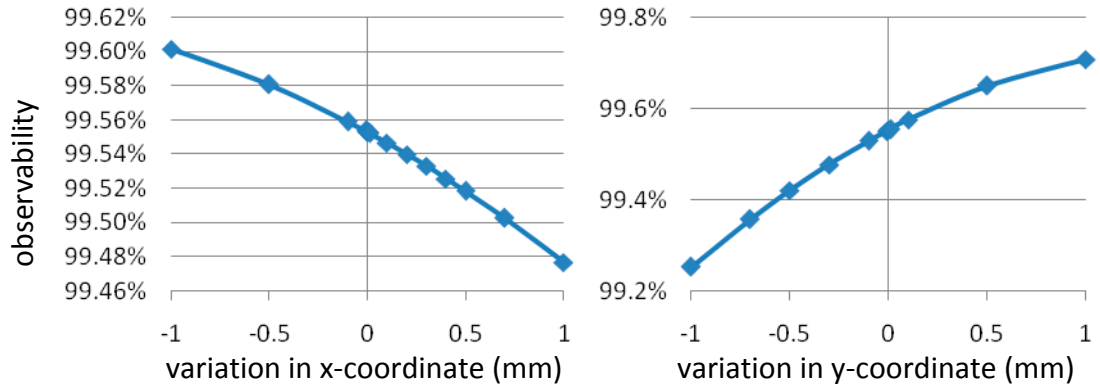

Figure 66: Nonlinear variation of observability with respect to changes in the coordinates of node 12.

Figure 64 through Figure 66 show the effect of varying the coordinate location of node 12. Controllability and observability are nearly unaffected by these changes. Displacement under external force experiences more variation that is also discontinuous. The kinks in Figure 64 result because d_{max}^{ext} is a maximum value equation. The abrupt change indicates a change in which node is experiencing the largest deflection.

6.5 Nonlinear Deviation of Performance

The usefulness of a controllable and observable compliant system is predicated on it having a linear response. This linear response is required so that superposition can be

used to control and sense shape modes in a predictable way. However, it is the nature of compliant mechanisms to have large, geometrically nonlinear deflections before material yielding. Hence, it is necessary to investigate how far the linear range of operation extends for these devices. There are a number of ways to look at and quantify the nonlinear behavior. Presented first are the nonlinear deflections as a function of the actuator input force. As structures are also subject to external forces, the effect of such forces on the metric of controllability is also investigated. Figure 67 shows the structure to be used in both studies and is from the same set of results as those shown in Figure 52.

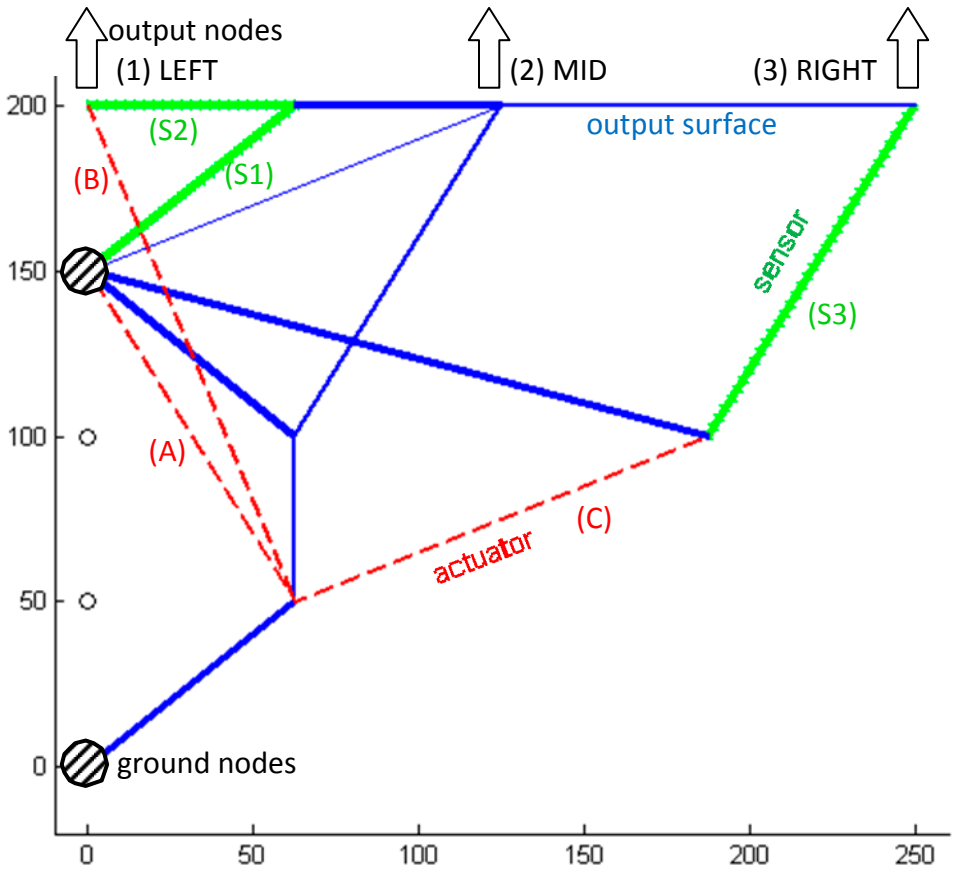

Figure 67: Controllable and Observable Compliant System used for Nonlinear Performance Studies. The top edge is the shape-morphing surface, with the three control nodes indicated. Axes are x and y coordinates in mm. Output nodes 1, 2, and 3 are labeled, as well as actuators A, B, and C and sensors S1, S2, and S3.

6.5.1 Implications for Actuation

The range of linear behavior for test structure is shown in Figure 68 through Figure 70.

The intended actuator block force to be applied to this structure is 80N. The range of block force shown in the figures is from zero up to 800N, ten times the normal input.

However, this range is truncated for the examples where the structure buckles.

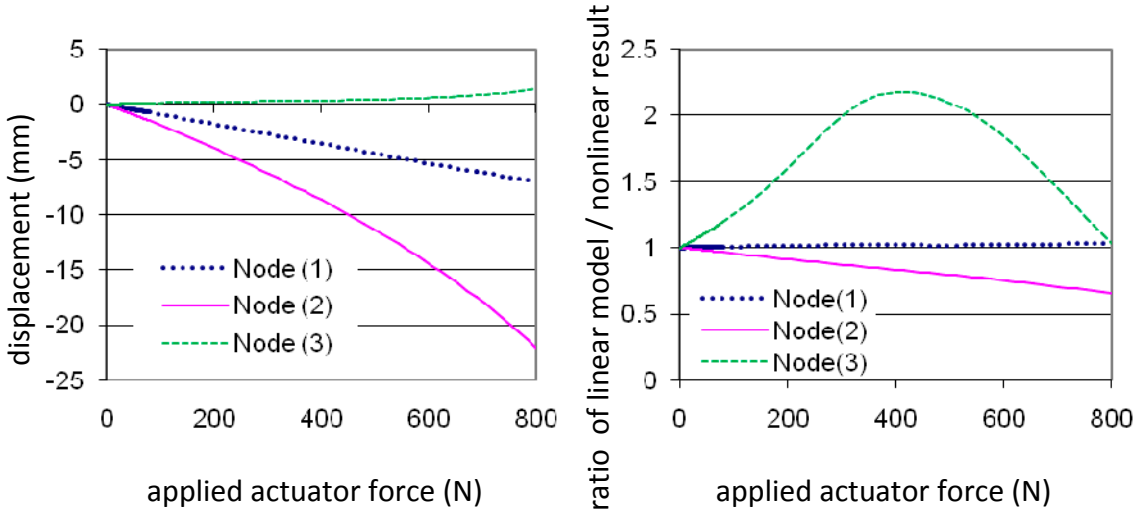

Figure 68: Nonlinear Response of test structure to the input force of actuator (A).
Left: Displacement of the 3 output nodes
Right: Ratio of Linear Prediction to Nonlinear Response for the 3 output nodes

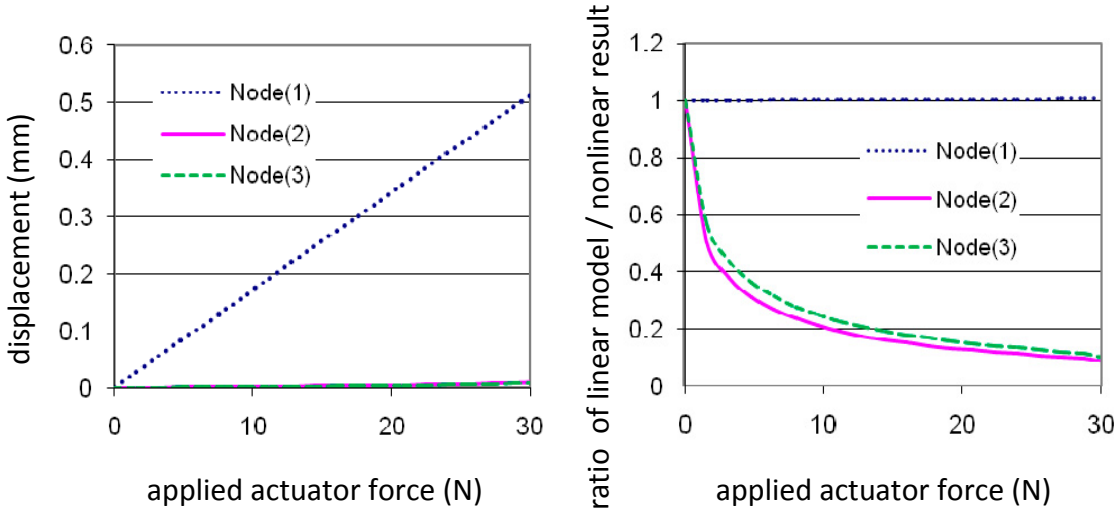

Figure 69: Nonlinear Response of test structure to the input force of actuator (B).
Left: Displacement of the 3 output nodes
Right: Ratio of Linear Prediction to Nonlinear Response for the 3 output nodes

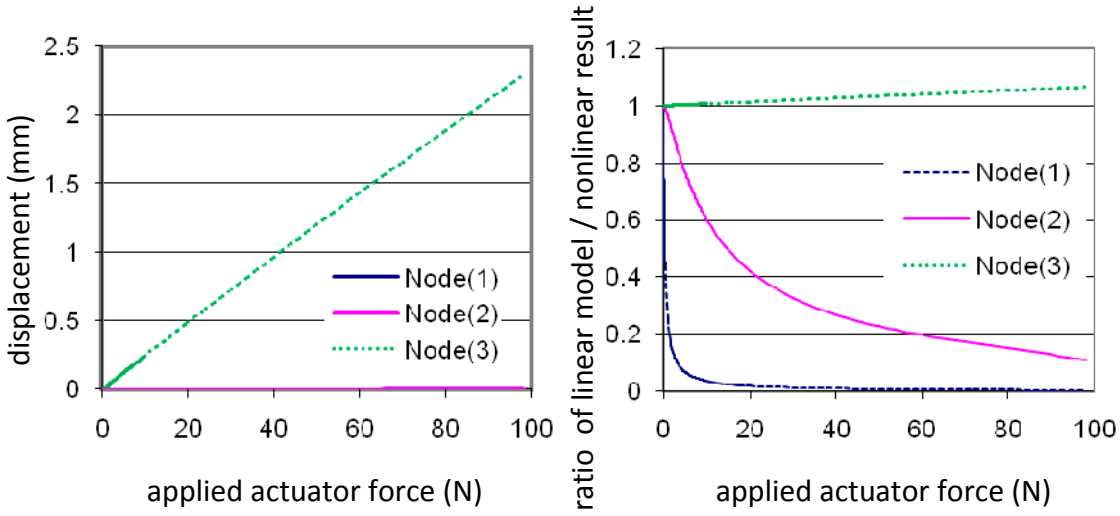

Figure 70: Nonlinear Response of test structure to the input force of actuator (C).
Left: Displacement of the 3 output nodes
Right: Ratio of Linear Prediction to Nonlinear Response for the 3 output nodes

The linear response is evident in the previous figures. In each case, the nodes that have the largest deformation also tend to have the most linear response. The nodes that have almost no motion suffer the most nonlinearity. This should be acceptable in operation, as the nonlinear components will be negligible when superimposed with the linear components.

6.5.2 Error in Actuator Command

The previous subsection studied the displacement results for the activation of each actuator, one at a time. However, it is also possible to coordinate the actuators to achieve *any* desired output response; this is the intent of having a controllable structure. To do so requires using a transformation matrix that maps a desired response to the required actuator inputs. The next example looks at the nonlinear error in commanding a specific output shape. The shape to be commanded is one where only the right-most node moves.

As described in §6.1.2.2, $\bar{d} = [\bar{d}_A\ \bar{d}_B\ \bar{d}_C]$ is the transformation from actuator forces to nodal displacements. When $\bar{d}$ is created using unit actuator forces, its inverse can be used to specify the actuator forces ($\bar{F}$) required to achieve a specified displacement vector ($\bar{u}$), as demonstrated in Eq. (33).

$$\bar{F} = \bar{d}^{-1}\,\bar{u} \tag{33}$$

For the device being considered in this section, the transformation matrix is:

$$\bar{d} = \begin{bmatrix} 6.29339\text{E-}07 & 0.017233 & -0.009087 \\ 1.14359\text{E-}05 & 2.73\text{E-}05 & -0.018088 \\ 0.024866497 & 2.78\text{E-}05 & 0.001828 \end{bmatrix} \text{ mm/N} \tag{34}$$

For this example, the inverse of $\bar{d}$ in Eq. (34) is substituted into Eq. (33) to calculate the forces required to generate a displacement vector of $\bar{u} = [0\ 0\ 1]^T$mm.

$$\bar{F} = \bar{d}^{-1}\,[0\ 0\ 1]^T = [0.0254\ \ 0.0119\ \ 40.2]^T\ N \tag{35}$$

The next figure shows the nonlinear response as the actuator goes from zero to 4 × $\bar{F}$.

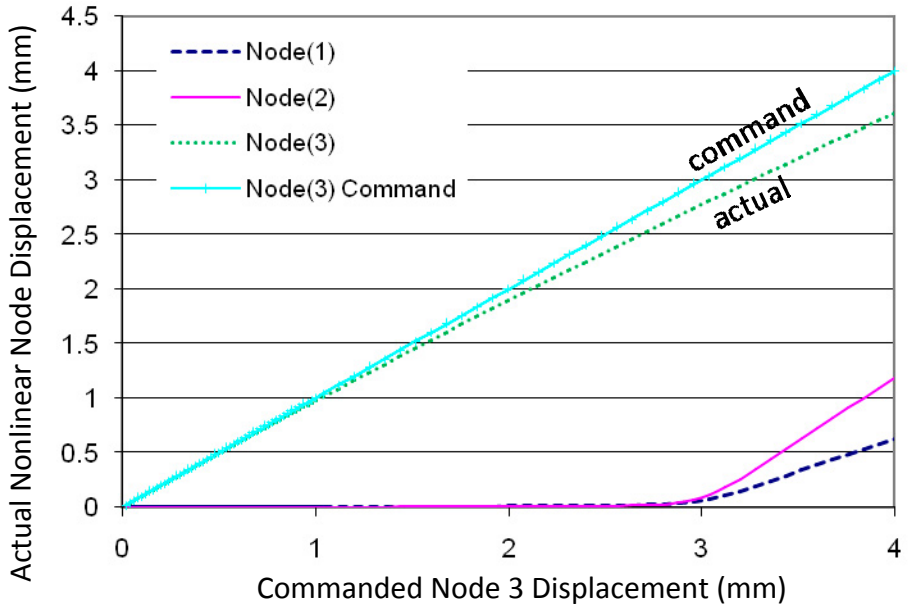

Figure 71: Nonlinear Response as a [0, 0, 1] mode shape is commanded. The solid line indicates the intended linear response.

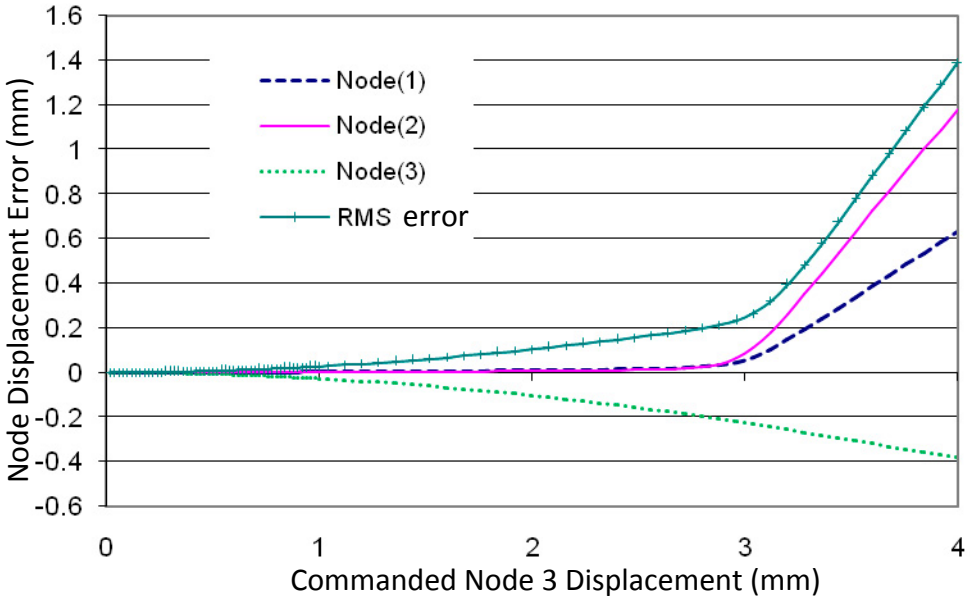

Figure 72: Displacement error for command of a [0, 0, 1] shape mode. The error is close to zero for displacement command up to 1mm. The RMS error for the three nodes combined is shown by the hashed line.

6.5.3 Implications for Sensing

For sensing, the transformation matrix from §6.2.1, $\bar{s} = [\bar{s}_I\ \bar{s}_{II}\ \bar{s}_{III}]$, is required to evaluate the sensor measurements. When $\bar{s}$ is created using unit external forces, its

inverse can be used to determine the external forces ($\bar{F}_e$) that map to the strain readings ($\bar{e}$), as demonstrated in Eq. (36).

$$\bar{F}_e = \bar{s}^{-1}\,\bar{e} \tag{36}$$

Using this equation, the nonlinear performance of the sensors is investigated in the following examples. In each example, one of the three output nodes is gradually loaded with a vertical external force. The surface strain values ($\bar{e}$) at the location of the sensors is then calculated with nonlinear FEA. The calculated forces, $\bar{F}_e$, are then compared to the actual applied forces to see where the linearity breaks down and how much error is caused by the nonlinearities.

The selected structure exhibits buckling during loading of each of the output nodes, at less than 1N of force. Results for the left and middle node are shown for an extended range to depict the buckling, and also zoomed in upon to show the linear range. The left-side plot in each figure shows the strain ($\bar{e}$) in each sensor. The right-side plot shows the corresponding force reading, as transformed by Eq. (36). Thus, the right-side plots show the erroneous readings that will result once displacement is beyond the range of linearity.

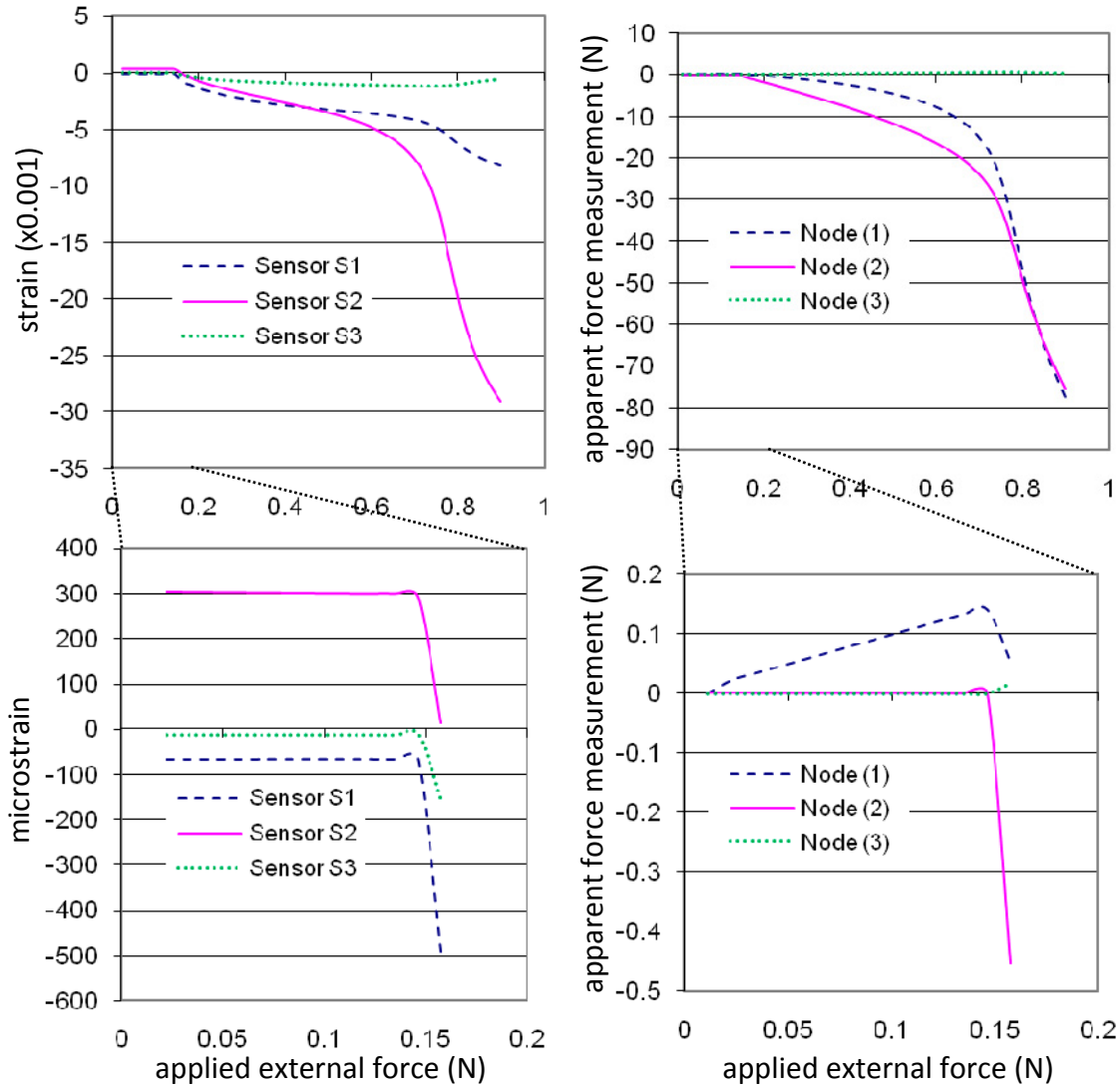

Figure 73: Sensing of a force applied to the left-most node on the surface of the test structure in Figure 67. The top two figures show the nonlinear buckling behavior. The bottom two figures zoom in on the range of linear behavior. Left: Sensor strain from nonlinear FEA for increasing load applied to Node (1) Right: Transformed force measurement based on reported sensor strain, using Eq. (36).

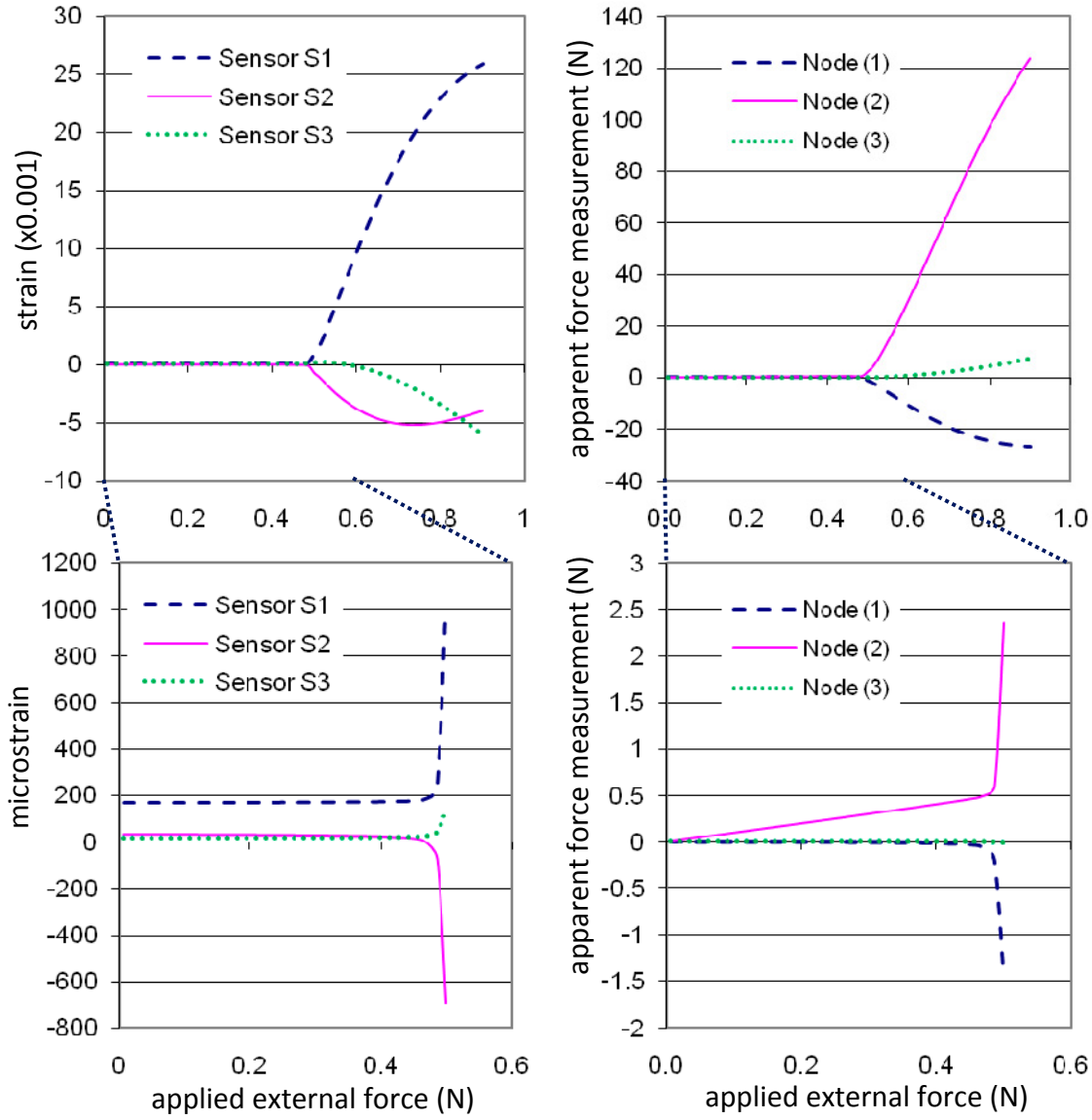

Figure 74: Sensing of a force applied to the middle node on the surface of the test structure in Figure 67. The top two figures show the nonlinear buckling behavior. The bottom two figures zoom in on the range of linear behavior. Left: Sensor strain from nonlinear FEA for increasing load applied to Node (2) Right: Transformed force measurement based on reported sensor strain, using Eq. (36).

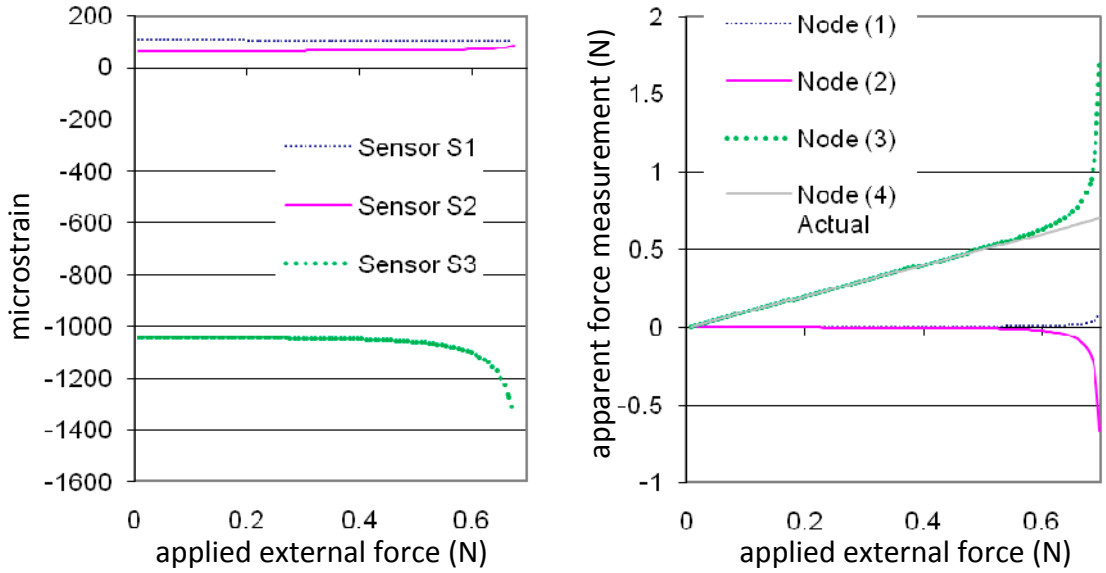

Figure 75: Sensing of a force applied to the right node on the surface of the test structure in Figure 67.
Left: Sensor stress from nonlinear FEA as the applied load increases to 0.7N
Right: Transformed force measurement based on reported sensor strain, using Eq. (36).

The results reported in the section have indicated that nonlinearity arises in most of the systems very early, at least well within the desired range of operation. As linearity is the cornerstone for the utility of controllable and observable structures, suggestions to overcome this problem are proposed in §6.8 and a strategic plan for future work is offered in the conclusions of §8.3.1.

6.6 Effect of External Loading on Controllability

Another way of viewing the effect of nonlinearity on the desired system performance is to see how controllability changes as a function of external load. For a linear system, it would remain constant, and regardless of the deformation caused by the external load, the actuators would still be able to achieve the original mode shape displacements. The actuated mode shapes would be superimposed on the deformed shape caused by the external forces. However, Figure 82 indicates that the nonlinear response causes the

controllability to drop off as the external load increases. Thus, while the actuators would still remain functional under larger external forces, they would not be nearly as capable of achieving a wide variety of new mode shapes.

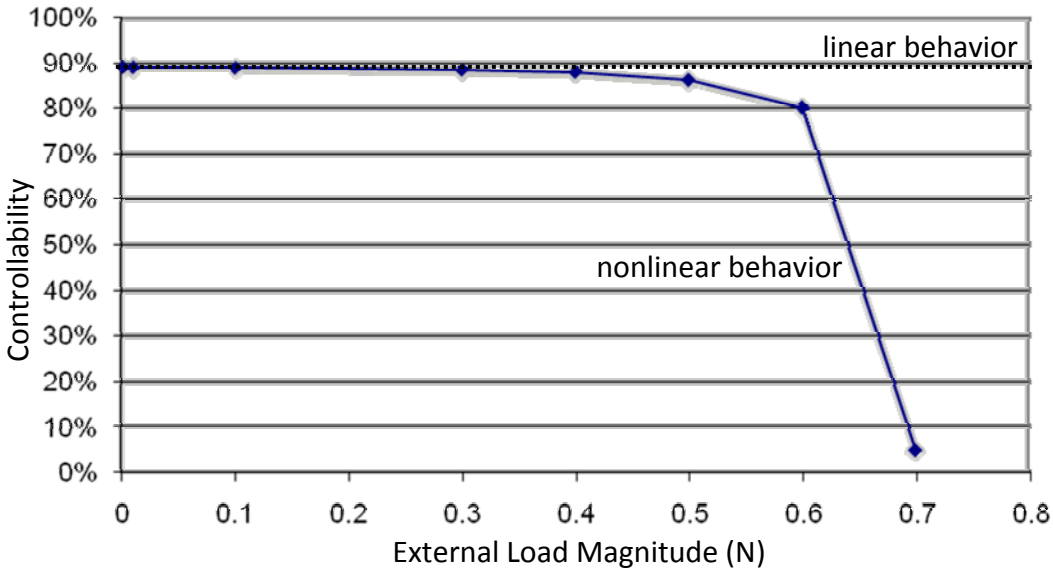

Figure 76: The nonlinear effect of External Loads on Controllability. Linear analysis predicts constant controllability. The external load is applied to all three output nodes at the same time. The compliant system is that seen in Figure 57.

6.7 Case Studies

To demonstrate the utility of the methodology beyond the simple test problems used in the previous sections, two case studies are presented. The first example is an adaptive-fit compliant socket for prosthetic devices. The second example is an adaptive shape-morphing wing for an unmanned air vehicle (UAV). The UAV problem is therefore similar to the test problems from earlier in this chapter, now applied with a more realistic parameter set and load conditions.

6.7.1 Alternative Stress Constraint Method

During initial runs of these case studies, it was observed that the very large actuation force often caused the structures to be over-stressed. Accordingly, I applied a different strategy to contain the stresses, first described in §4.4.1. Rather than always assuming the entire actuation force must be applied, this method scales down the actuation force to avoid material yielding. First, the maximum structural stress resulting from the activation of a given actuator is measured. If this is greater than the yield stress, then the force is scaled down by the ratio: yield stress / measured stress. Since the structural response is assumed to be linear, a second analysis is not required. Rather, the output vector of the mode shape nodes is also multiplied by the above ratio. Thus, large stresses can result in very small displacements, which will not be favored by the algorithm. In this fashion, stress constraints are handled implicitly and do not need to be part of the objective function.

6.7.2 Adaptive Prosthetic Device

The first case study is the design of an adaptive prosthetic device. Many current devices must be custom fit to every individual and then cannot be changed during use. A self-adjusting device would resolve both of these issues. A person's limb will swell and change shape during use, creating discomfort for the user. With a system capable of sensing the external pressure load and changing the shape to minimize any stress concentrations, discomfort can be alleviated. Such devices could also be used for functional changes in different scenarios. For example, an orthosis could adjust to increase stiffness during running and before jumping.

The design parameters for this problem are listed in Table 20. The chosen actuator is based on a composite shape-memory-alloy material. Prosthetic sockets are often made from glass fiber composites, which are chosen here as the structural material.

Design Parameters	
actuator type	SMA Composite
actuator modulus	68,000MPa
actuator block force	1600N
element material	Glass Fiber Composite
element modulus	5,000MPa
element yield stress	150MPa
external load magnitude	2N
element out-of-plane thickness	10mm
desired deflection under actuation	2mm
domain footprint	175mm x 75mm
symmetry	about y-axis
grid size	8 x 7
Algorithm Parameters	
element mutation rate	8%
actuator/sensor mutation rate	10%
cross-over rate	97%

Table 20: Design and Algorithm Parameters for the Adaptive Compliant Socket Problem

The full design space and 8x7 grid is not used, as shown in Figure 77. In total, there are 185 edge variables. The optimization variables are listed in Table 21.

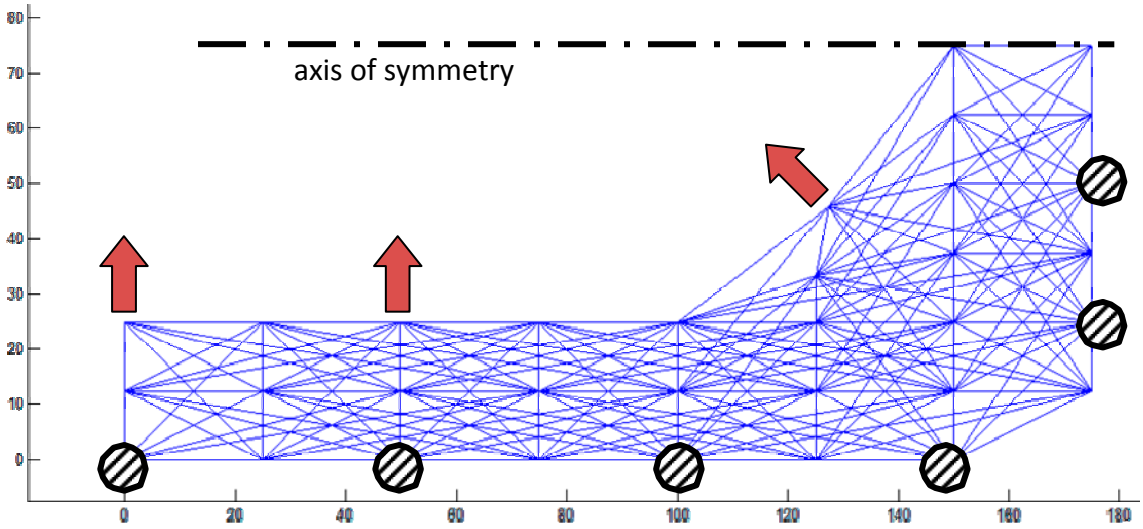

Figure 77: Design Space for the Adaptive Socket Problem. The resulting planar structure would be repeated axisymmetrically several times around the limb. The axes represent the x and y coordinates measure in mm.

Number	Variable	Type	Possible Values
1	Beam Thickness	discrete	0, 0.5, 1, 1.5mm
…	…	…	…
185	Beam Thickness	discrete	0, 0.5, 1, 1.5mm
186	Sensor 1	discrete	1-185
187	Sensor 2	discrete	1-185
188	Sensor 3	discrete	1-185
189	Actuator 1	discrete	1-185
190	Actuator 2	discrete	1-185
191	Actuator 3	discrete	1-185

Table 21: Optimization Variables. There are 185 beam variables that determine whether the beam is absent or present with one of three discrete thickness values.

The objective function for this problem (see Eq. (37)) contains controllability and observability, as well as the constraints for minimum achievable deflection (d_{min}^{act}), maximum deflection under external load (d_{max}^{ext}), total element length (L_t), and the minimum strain resolution ($\min|\varepsilon|$).

$$maximize \begin{bmatrix} \eta_o + \eta_c - w_1 \times (d_{max}^{ext}) - w_2 \times (d_{min}^{act}) \\ -w_3 \times \left|L_t - L_{target}\right| - w_4(\varepsilon_{min} - \min|\varepsilon|) \end{bmatrix} \quad (37)$$

A sample of the typical results for this case study are displayed in Figure 78. An artistic sketch to show how the results would be implemented into an axisymmetric physical structure is given in Figure 79.

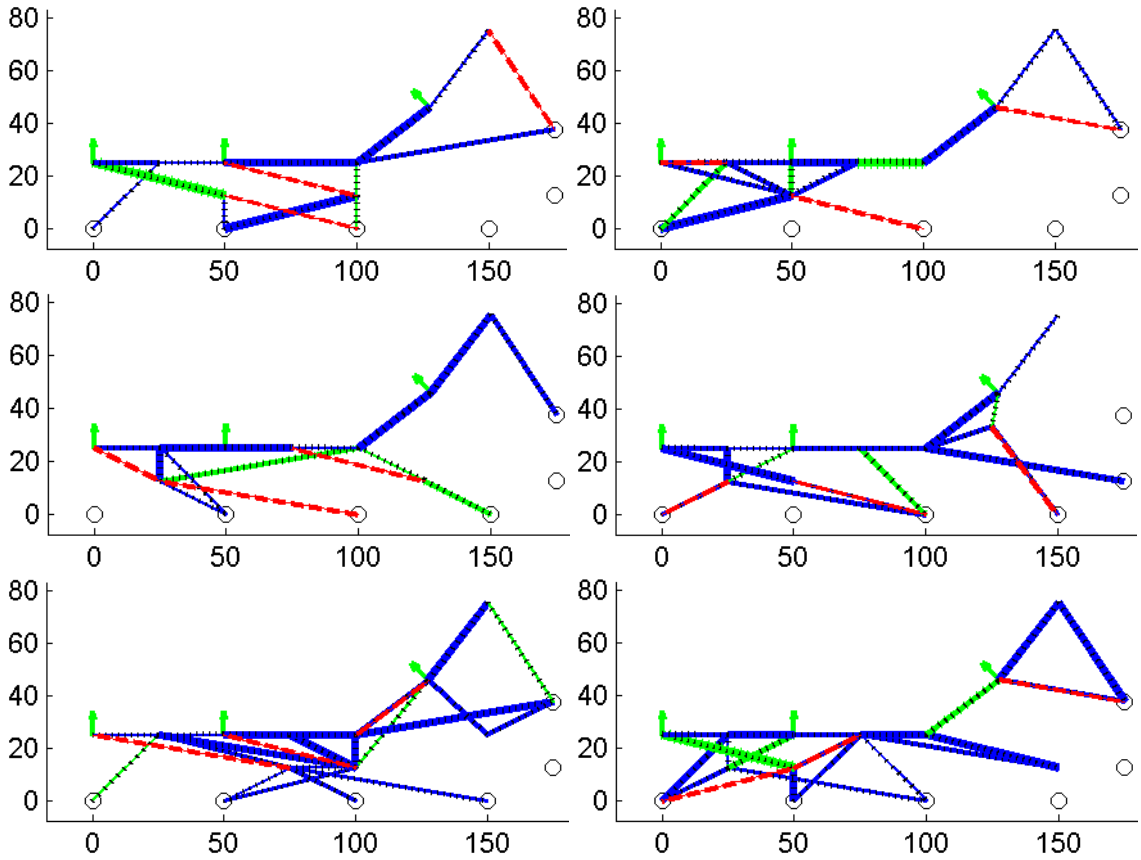

Figure 78: Six sample solutions for the Adaptive Prosthetic Problem. Figure 79 depicts how these results would be incorporated in an axisymmetric socket design. Actuators: dashed red lines. Sensors: hashed green lines. Structure: solid blue lines.

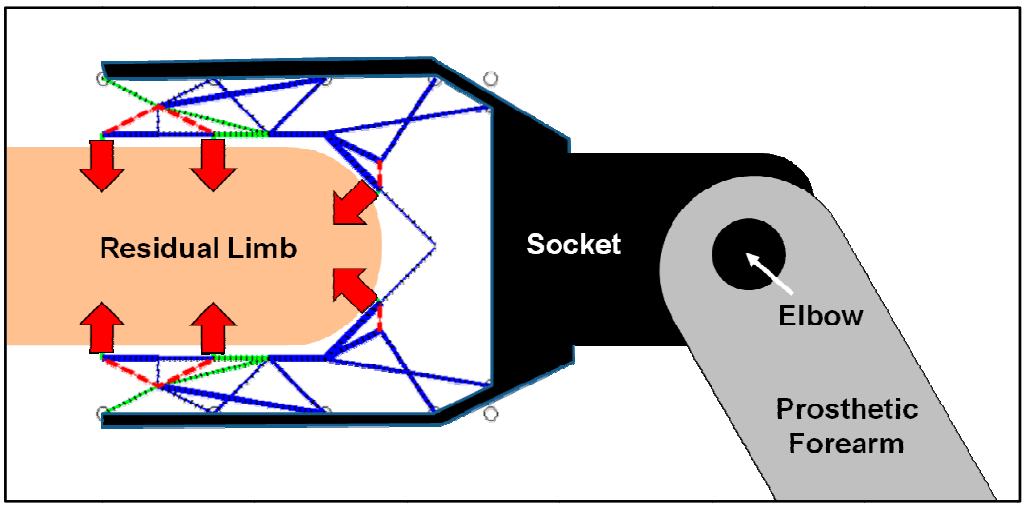

Figure 79: Artistic depiction of an Adaptive Socket Compliant System. The planar results from Figure 78 are to be repeated several times around the axis of the limb. This system will be able to monitor varying pressure distributions along and around the limb. High stresses can be avoided and snug fit maintained by the adaptive shapes achievable with the actuators.

6.7.3 Shape-changing Wings and Fins

The second case study is a continuation of a standard compliant mechanism problem, the shape-changing aircraft wing or aqua-craft fin. In this study, however, the goal would be to create as system that could sense a variety of external pressure load profiles and respond with a variety of shape changes. Such sense-and-control variable geometry wings could adjust to the most appropriate and efficient configuration for both predicted and unpredicted flight conditions. These benefits would also apply to loading-dependent shape-changing aqua-craft fins.

The design parameters for this problem are listed in Table 22. The chosen actuator is a McKibben Muscle (Shulte, 1961), which is a compliant pneumatic actuator with human-muscle-like stiffness properties. Their compliant nature of these actuators suits this dissertation and the benefits of stiffness matching in system design. Furthermore, the

large force output of these actuators is needed to deform the chosen structural material, carbon-fiber composite.

Design Parameters	
actuator type	McKibben Pneumatic Muscle
actuator block force	1,200N
actuator stiffness	28.6N/mm
element material	Carbon Fiber Composite
element modulus	34,500MPa
element yield stress	250MPa
external load magnitude	varies along the edge, from 0 to 2.78N
element out-of-plane thickness	10mm
desired deflection under actuation	5mm
domain footprint	300mm x 100mm
symmetry	none
grid size	8 x 4
Algorithm Parameters	
element mutation rate	8%
actuator/sensor mutation rate	10%
cross-over rate	97%

Table 22: Design and Algorithm Parameters for the Shape-Adaptive UAV Problem

The full design space and 8x4 grid is not used, as shown in Figure 77. In total, there are 150 edge variables. The optimization variables are listed in Table 23.

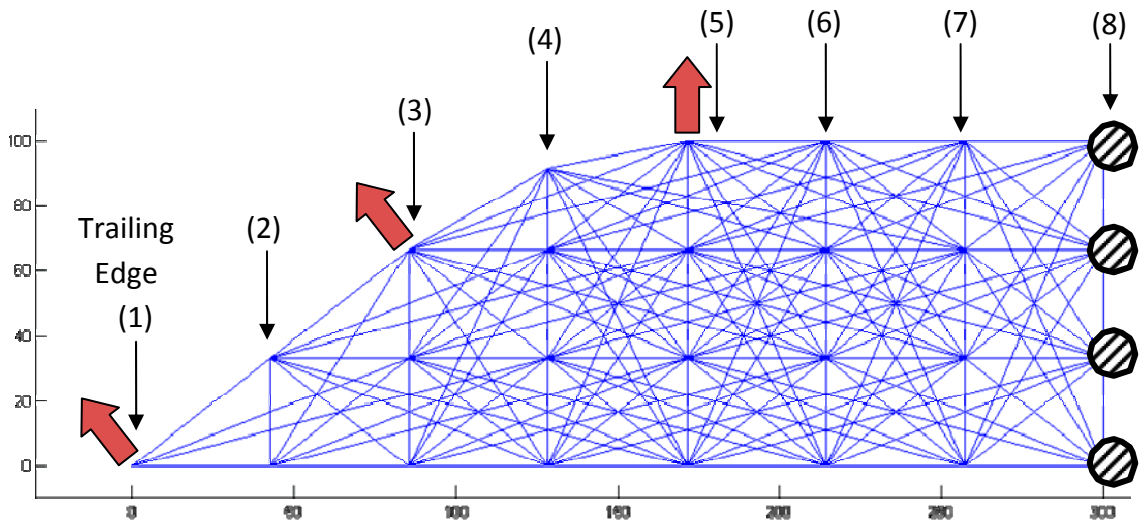

Figure 80: The red block arrows indicate the three nodes representing the surface to be controlled and sensed. The black lines arrows indicate the external air load on the wing. The load magnitude varies along the chord as listed in Table 24. The summed external force is 11.1N.

Number	Variable	Type	Possible Values
1	Beam Thickness	discrete	0, 1, 2, 3mm
…	…	…	…
150	Beam Thickness	discrete	0, 1, 2, 3mm
151	Sensor 1	discrete	1-150
152	Sensor 2	discrete	1-150
153	Sensor 3	discrete	1-150
154	Actuator 1	discrete	1-150
155	Actuator 2	discrete	1-150
156	Actuator 3	discrete	1-150

Table 23: Optimization Variables. There are 168 beam variables that determine whether the beam is absent or present with one of three discrete thickness values.

The objective function for this case study is the same as used in the previous prosthetic problem, Eq. (37).

6.7.3.1 Wing Load Estimation

For the small unmanned air vehicle (UAV) with a ten-foot wingspan, a reasonable wing loading would be 1.2 lbs/ft^2 for a 30 ft/sec speed, which is typical for a model sailplane

of this size. If the chord length is 2 ft, then the wing area is approximately 20 ft^2, giving an aerodynamic loading of 24 pounds. For each wing semi-span the loading is 12 lbs. Using four ribs per semi-span, each rib will carry 3 lbs in 1 "g" flight. Because of maneuver/gust loads the "g" requirement should be 2.5, giving a load per rib of 3 x 2.5 = 7.5 lbs. This load is distributed over the chord with a constant load from the leading edge to 50% (12") chord. The loading then decreases from this level in a straight line to zero at the wing trailing edge. This means the structure will carry half the load (2.5lbs) from the 50% chord point to the TE as it does on the first 50% chord (5lbs).

In this example, I am designing a compliant system for the aft half of the chord. Thus, the load varies linearly along this section. Using eight nodes along the chord requires the following load distribution, depicted in Figure 80, which sums to 11.1N (2.5lbs).

Node (1)	(2)	(3)	(4)	(5)	(6)	(7)	(8)
0 N	0.397N	0.794N	1.19N	1.59N	1.99N	2.38N	2.78N

Table 24: External Air Load Distribution along the UAV Trailing Edge

A sample of the typical results for this case study are displayed in Figure 81. An artistic sketch to show how the results would be implemented into the rib of a physical structure is shown in Figure 82.

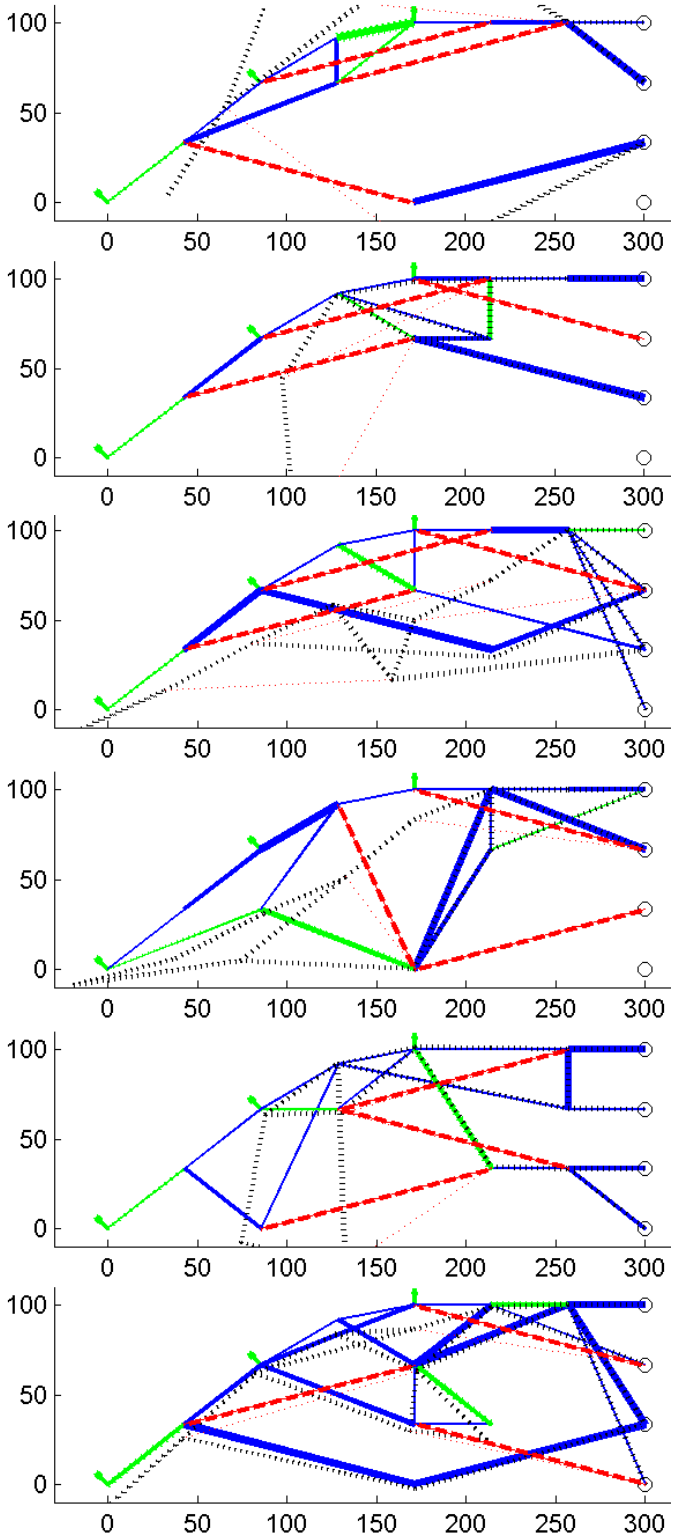

Figure 81: Six sample solutions for the Adaptive Morphing UAV Problem. Figure 82 depicts how these results would be incorporated into a physical design. The axes represent the x and y coordinates, measured in mm.

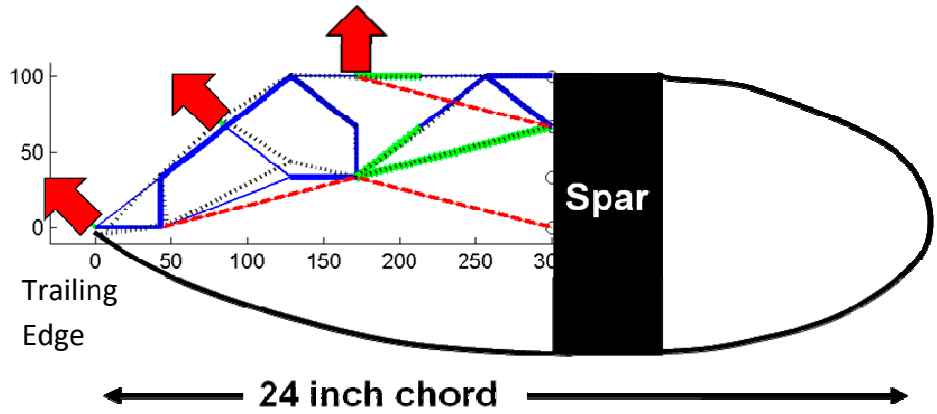

Figure 82: Artistic sketch of the integration of the resulting compliant system into the rib of an aircraft wing. See Figure 81 for other typical results.

6.8 Buckling and Range of Linearity

To attain robust results that perform as predicted, the designs generated in this chapter should have a large range of linear operation and should not buckle. However, the issue of nonlinearity is unavoidable in large displacement compliant mechanisms, and requires a strategic plan that is described in §8.3.1 of Future Research. First, though, it is worthwhile to push further within the linear range of operation. In fact, nonlinear analysis of many of the devices reported in this chapter indicates buckling well within the desired range of motion. Even when designs do not buckle, they have highly nonlinear response beyond a small percentage of the actuator displacement magnitude. Thus, future work should include a buckling constraint within the optimization routine to avoid this problem. Further, the range of linearity could be added as another weighted term to the objective function. Even though this would be costly to calculate, it could possible greatly extend the range of utility for the metrics of controllability and observability.

6.9 Chapter Summary

This chapter introduced and formulated the concept of component independence, new for the field of compliant mechanisms and unique to this dissertation. This concept was first explored as the logical step to incorporate controls with shape-morphing structures for a high degree of control and manipulability. The metric of controllability derives from the basic algebra of linear independence. After results are given and validated for the actuator problem, the concept is applied to sensing of the system, resulting in the second new metric for compliant systems: observability. Results were shown for the design of an observable truss structure with internal strain sensors. Finally, the sensor and actuator problems were combined to generate single devices that are both highly controllable and observable, allowing for the ready application of standard control methods. The next chapter takes these same concepts and reapplies them to single-point manipulation, further demonstrating the usefulness of the metrics in creating a wide variety of coupled, multifunctional systems.

Chapter 7

Point Control and Sensing

The concepts of component independence were shown to be valuable for shape-changing applications in the previous chapter. One of the strengths of the component independence metrics is that they are also useful for other mechanical design problems. In this chapter, rather than looking at several points that define a surface, I look at the multiple degrees-of-freedom of a *single* point. When the concept of controllability is applied to a single point, one finds a correspondence to the concept of *manipulability* of end-effectors in the field of robotics. This provides a new venue for compliant mechanisms to perform as efficient, monolithic manipulators while also supporting various external load cases.

Potential applications include precision control of optics and switches in MEMS devices. The ability to control x and y displacement along with rotation allows for robust control of sensitive devices, which may find application in semiconductor manufacturing and assembly. Tip manipulators for probing cells can also benefit from the three degree-of-freedom control, while being able to support possible loads from microfluidic flow. Position changing fluid vane structures would allow for redirection and control of flows while remaining strong and adaptable against fluid-structural loading.

7.1 Formulation and Implementation

In practice, even though the task is very different than that of the previous chapter, the design algorithms are nearly the same. The key issues are the presence of rotations and that the three target degrees-of-freedom are now much more coupled. (Recall from Section 6.1.6 that coupling of the three output nodes via skin stiffness has an inherent effect on the capability for controllability.)

The presence of both displacements and rotations in the displacement vectors present a problem of units that is easily handled. The rotation values are converted to displacement by multiplying them by a characteristic length chosen by the designer. This may change from application to application, where the value of a degree of rotation may be worth much more or less than a millimeter of deflection. In the cases presented here, the logic for choosing a characteristic length (L_c) is to infer it from the desired ranges of motion. For example, if it is desired to have x and y displacement of 5mm and rotation of 5 degrees, then for the conversion of "length = L_c × rotation",

$$L_c = \frac{length}{rotation} = \frac{5\ mm}{5\ degrees} = 1\frac{mm}{degree} = 57.3\frac{mm}{rad} \tag{38}$$

Another more fundamental issue regarding rotation results from the use of linear analysis in calculating structural response. Linear analysis has been favorable for most of the small *displacements* covered thus far in the design examples of this dissertation. But linear analysis is constrained to relatively small *rotations*, and severely limits the

achievable range of motion. My efforts have shown that larger targets such as 30 degrees are not possible, but that smaller goals less than a few degrees are achievable.

7.2 Results for Single Point Manipulation

Two sets of boundary conditions are studied for this problem, to account for the likely extra difficulty in decoupling the degrees of freedom at a single point. The first example has potential ground points available around the border of the design space, with the node to be controlled in the middle. This is to allow for the potential isolation of actuator load paths in controlling the output point. In the second example, the output point is far removed from the ground points, requiring the more complex coordination of essentially a multifunctional cantilever. The parameters for both examples are listed in Table 25.

Design Parameters	
actuator type	SMA Composite
actuator block force	80N
actuator modulus	6,800MPa
element material	Carbon Fiber Composite
element modulus	34,500MPa
element yield stress	37.7MPa
external load magnitude	3N
element out-of-plane thickness	1.5mm
desired deflection under actuation	3mm and 0.052rad
characteristic length, L_c	57.3mm/rad
domain footprint	250mm x 200mm
symmetry	none
grid size	5 x 5
Algorithm Parameters	
element mutation rate	8%
actuator/sensor mutation rate	10%
cross-over rate	97%

Table 25: Design and Algorithm Parameters for the Single Point Manipulation Problem

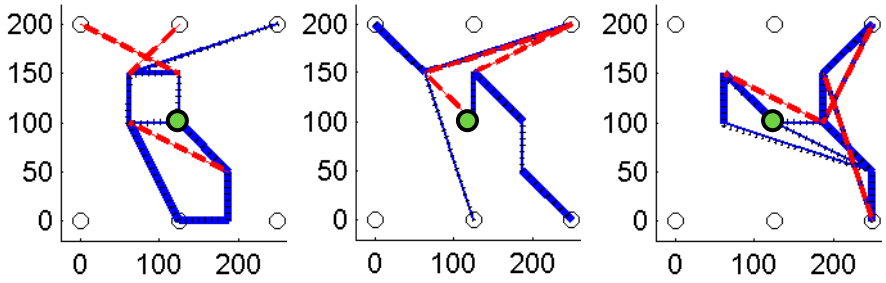

Figure 83: Sample results for manipulability of a node located in the center.

A set of typical results for the center node problem is shown in Figure 83. No clear topology ever resulted for the 60+ separate optimization runs, and the amount of displacement remained limited. Better results followed from the remote node problem, shown in Figure 84 and Figure 85. The problem is limited to only three available ground nodes in Figure 84 and five nodes in Figure 85.

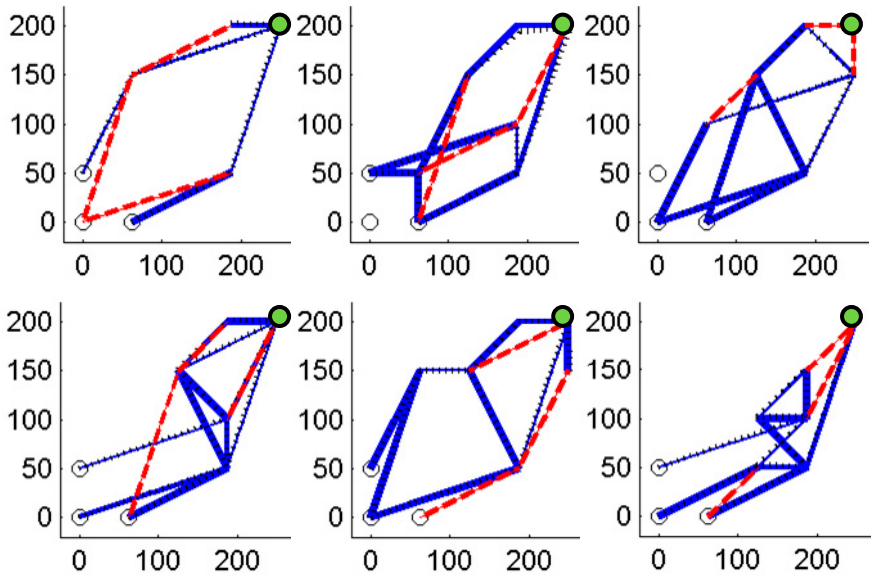

Figure 84: Sample results for Manipulability of a point located remotely from the ground, in the upper-right corner. 3 ground nodes.

Several of the designs in both of the remote node sets reappeared in similar form during multiple optimization runs, and similarities can be seen between the sets. The two sets of ground nodes were targeted because it was believed the set with only three nodes would have more difficulty in finding controllable solutions. The final results indicated a robustness of the algorithm to find highly controllable solutions regardless of the number of ground nodes available.

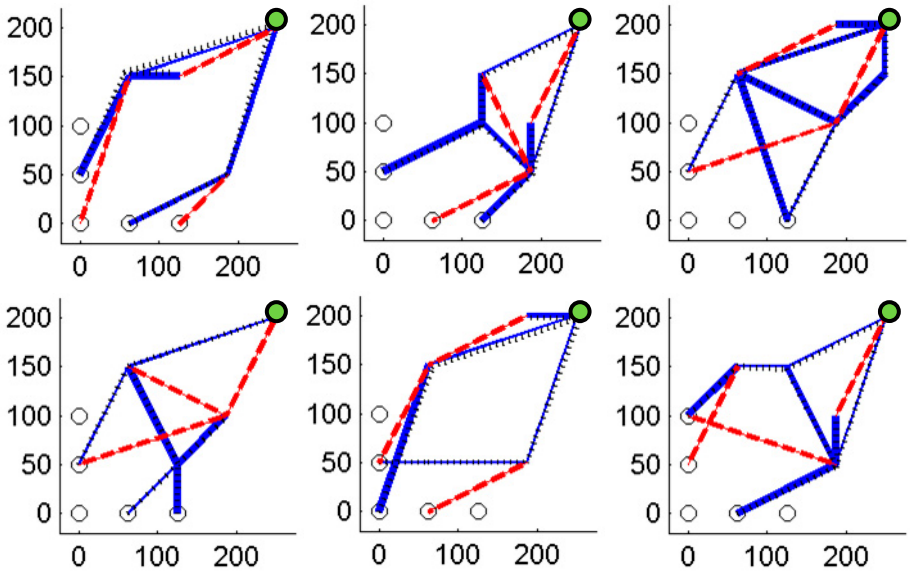

Figure 85: Sample results for Manipulability of a point located remotely from the ground. 5 ground nodes.

A breakdown of the results for the 5-node problem is provided in Table 26. To better understand the robustness of the algorithm and its ability to search the design space, two solution maps are shown in Figure 86 and Figure 87. These two figures also help demonstrate how the multiple objectives are traded off to achieve the optimal objective fitness value.

length ratio	control.	actuator	external	stress
η_L	η_C	d_{min}^{act}	d_{max}^{ext}	σ_{max}
	%	*mm*	*mm*	MPa
2	86 (11)	1.9 (0.9)	1.7 (1.6)	11 (6.9)
3	92 (6)	2.2 (1.0)	3.5 (3.6)	8 (6.2)
4	96 (7)	1.7 (0.8)	1.4 (1.5)	15 (8.4)
5	97 (5)	1.2 (0.7)	0.7 (0.5)	12 (6.1)

Table 26: Summary of Results for Single Point Manipulation. These report the averages and (standard deviations) for the results of the 5-ground-node problem, seen in Figure 85.

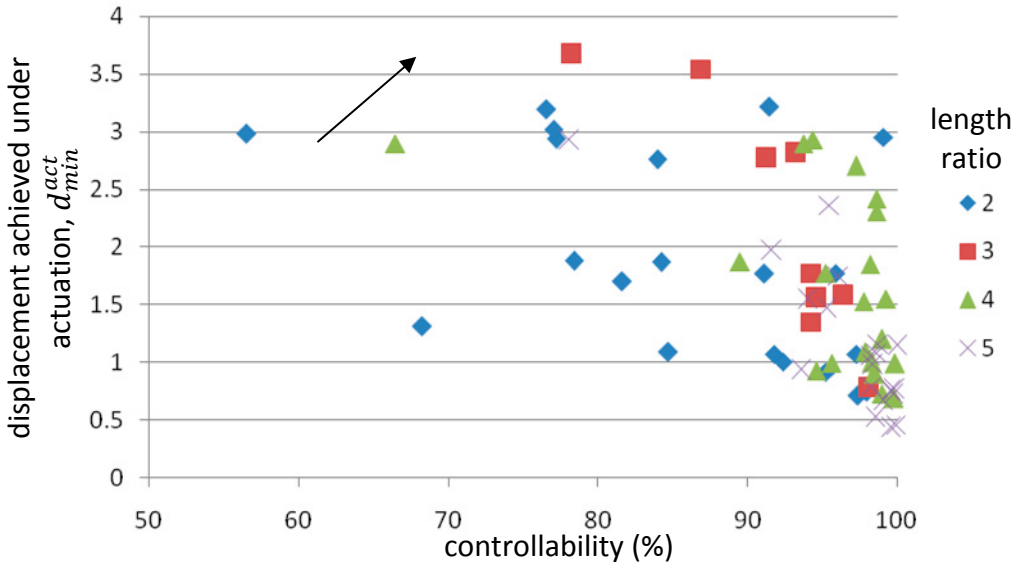

Figure 86: Solution Points for Single Point Manipulability. 5-ground-node problem. Each point represents the individual solution attained for each optimization run. This figure displays the relationship between achievable controllability and d_{min}^{act}. Optimality increases toward the upper-right corner.

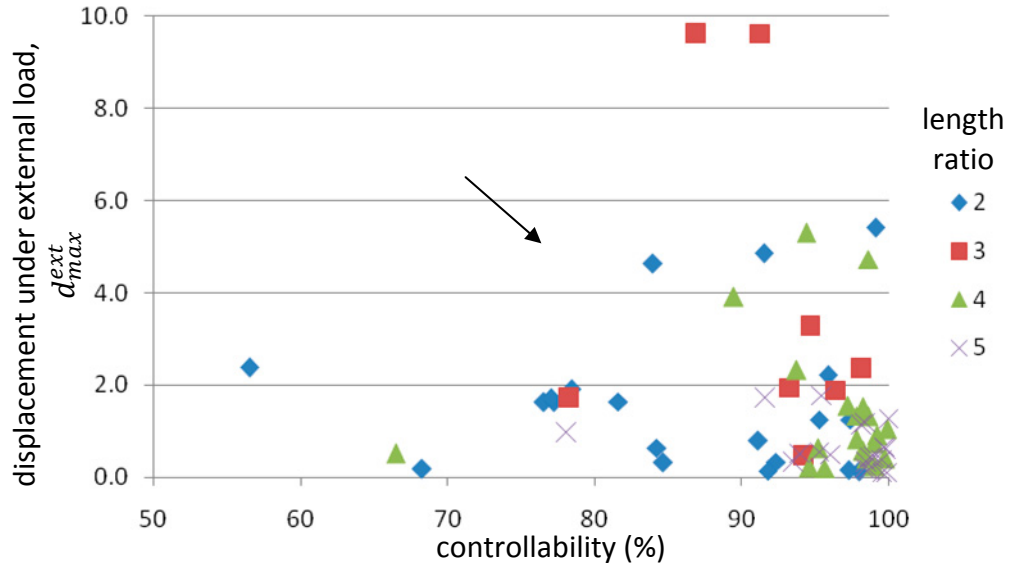

Figure 87: Solution Points for Single Point Manipulability. 5-ground-node problem. Each point represents the individual solution attained for each optimization run. This figure displays the relationship between achievable controllability and d_{max}^{ext}. Optimality increases toward the lower-right corner.

Figures 88-90 depict the nonlinear analysis of the structural deformation caused by each of the three actuators for one of the resulting structures. Displacement is multiplied by 5 to allow easy observation of the different directions achieved by each actuator.

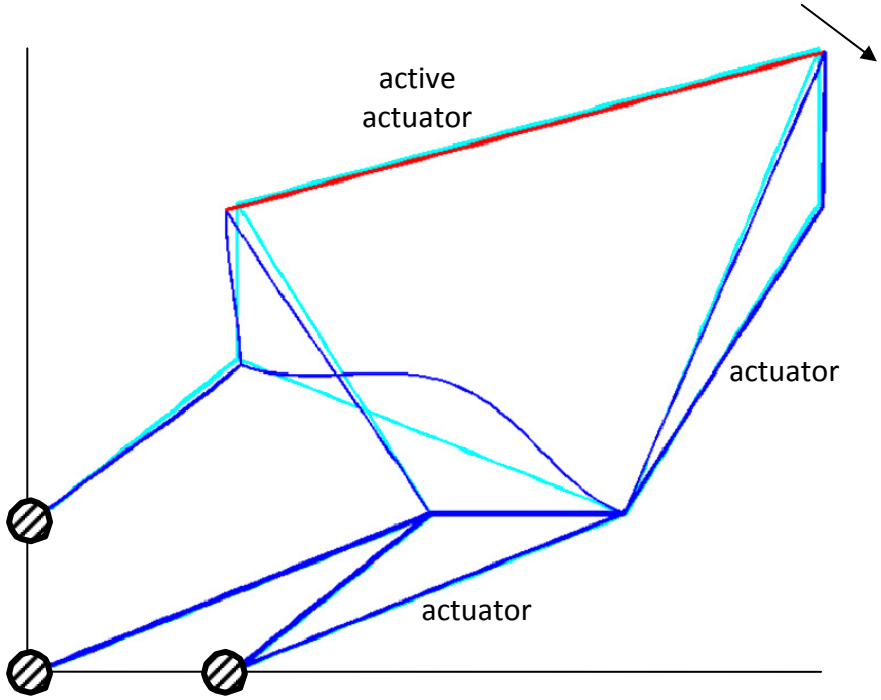

Figure 88: Nonlinear FEA results for Manipulability. The output node in the upper-right corner is deflected due to the activation of the indicated actuator. Design footprint is 250mm x 200mm.

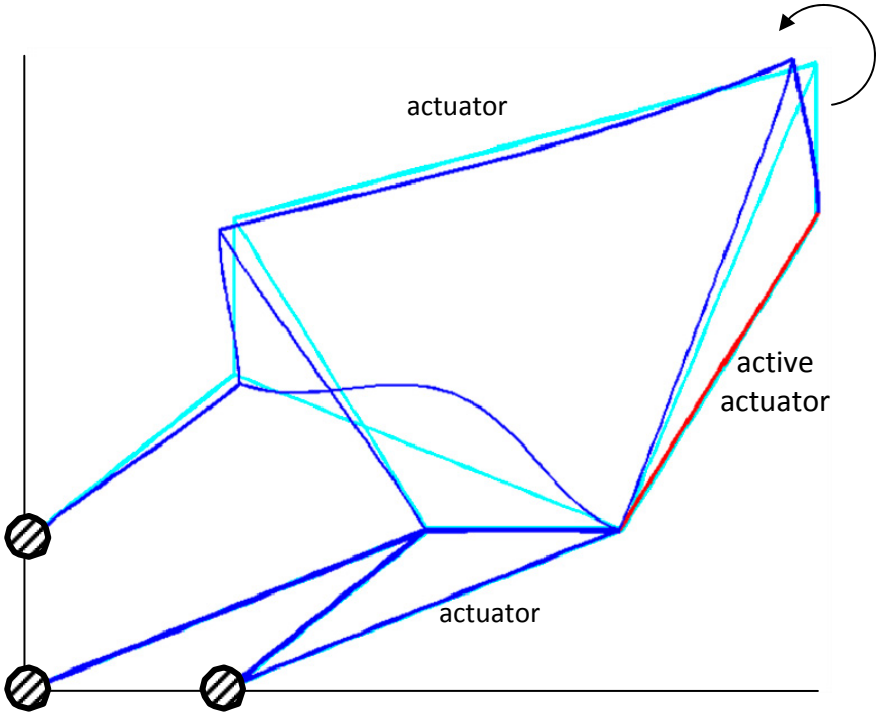

Figure 89: Nonlinear FEA results for Manipulability. The output node in the upper-right corner is deflected due to the activation of the indicated actuator. Design footprint is 250mm x 200mm.

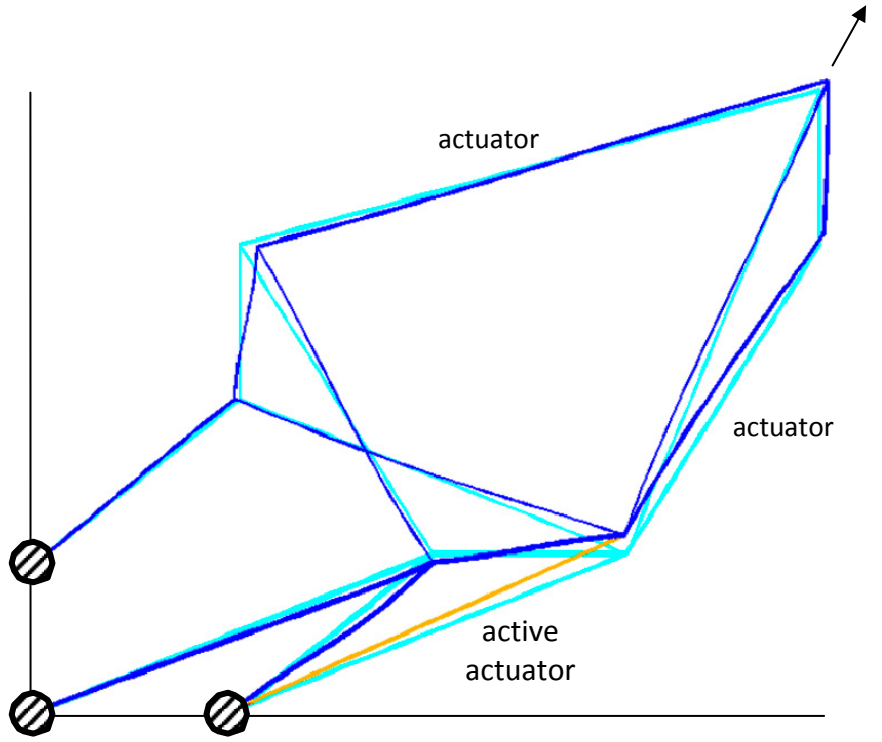

Figure 90: Nonlinear FEA results for Manipulability. The output node in the upper-right corner is deflected due to the activation of the indicated actuator. Design footprint is 250mm x 200mm.

7.3 Chapter Summary

This chapter extended the concepts of component orthogonality from the previous chapter to the task of single-point manipulation. As with the shape-morphing results, designs were able to achieve linear independence of control at levels near 100%. However, the desire to control rotation introduced a new limitation on the methodology, as large rotations are beyond the scope of linear analysis and thus the metrics of linear independence. Even with several different arrangements of fixed points in the design domain (to encourage leverage in different directions), large rotations were still infeasible. This finding is addressed in the next chapter, in terms of how to handle the large (and desirable) nonlinear deflections commonly exploited in compliant mechanisms. But first, the next chapter summarizes all of the work thus far, highlighting the major contributions and findings. Then, in addition to the issue of nonlinearity, other future work is proposed in the areas of controls and dynamics.

Chapter 8

Conclusions

8.1 Conclusions

I have demonstrated the ability to design flexible structures (i.e. compliant mechanisms) possessing the qualities of controllability and observability. Even with low-fidelity linear modeling, the attained results demonstrate all of the design requirements, indicating strong algorithm performance. The addition of nonlinear analysis and additional analysis elements for each beam will allow greater flexibility in any given structure and increase the likelihood of more and better multifunctional solutions. These studies also pointed out other basic research issues, particularly in parameterization and forming objective functions. Convergence required complex, nonstandard "genetic engineering" of the design population members during the genetic algorithm: trimming of superfluous substructures, computationally expensive graph searches, and identification of ineffective rigid-body segments. The unbalanced tradeoff between controllability and large actuated deflection has also been identified, along with a family of parameters to balance the struggle.

While genetic algorithms are often criticized for their slow speed, many of the simplifying assumptions allow for large optimization runs to be completed with appreciable speed. A given design study typically requires 60 optimization runs (15 runs

for 4 different length constraints) each with 200 members in the population, running for 300+ generations, and yet finishes in a few hours. With the ground node structure, the elemental stiffness matrices and the connectivity data structures are calculated only once. Further time savings come from the linear analysis.

Further, the actual utility of the genetic algorithms exceeds that reported in this work. While it is useful in looking at *average* performance when designing the best design algorithm, in actual practice it is the *maximum* values that matter. That is, when solving a particular problem one might run the algorithm 10 or 20 times and choose the *best* of all the resulting solutions.

8.2 Contributions

This dissertation advances the current state of the art in electromechanical systems design in several fundamental ways. Traditionally, structures, mechanisms, actuators, and sensor design is the focus of different people paying marginal attention to one another, resulting in suboptimal systems. This research paves a way for a scientific approach to true multifunctional, mechatronic system design.

- Essential metrics for the inclusion of embedded components in a multifunctional compliant system have been developed and investigated.

- A design parameterization capable of representing both structural topology and actuator/sensor placement simultaneously has been implemented and tested.

- The essential framework for the integration of controls with compliant mechanisms has been established. Specifically, the concepts of controllability and observability, as defined for compliant systems, have been proven as a successful starting point for the design of controllable systems.

- Through examples and design studies, the metrics and the methodology have demonstrated that multiple, optimally-placed components indeed offer performance benefits for mechanical systems, both in terms of efficiency and multifunctional execution.

One final intended contribution is the exposure of readers to the creative extension of the new metrics and methodology beyond their intended purpose. That controllability works as well for point manipulation as it does for shape-morphing should suggest these tasks are only the beginning and that much more is likely capable of compliant systems.

8.3 Future Research

Further work may enable new applications in the compliant paradigm, such as medical implants (low back pain/disk replacement), exoskeletons, adaptive-fit prosthetics, artificial organs, flapping-wing micro-air-vehicles, and reconfigurable surfaces for a wide range of applications. Specific methods to explore include alternative parameterizations, such as Load Path (connectivity-based discretization), and nonlinear FEA analysis within synthesis. The combination of both controllability and observability terms within the same objective function has closed the loop for adaptive shape-

morphing structures. A future example is a wing that can perform large (nonlinear) changes between different trailing edge configurations and yet be (linearly) adaptable to variable loading conditions while in any one of those configurations.

8.3.1 Issues of Nonlinearity

Extending the range of motion of these systems to the larger, nonlinear displacements is of immediate interest. One of the inherent benefits of compliant mechanism is their ability to undergo large deformations and rotations within the linear yield stress limits of their constitutive materials. It is likely that another broad range of applications will become evident after large-deformation, controllable devices are feasible.

One of the key issues to be investigated is the development of metrics of controllability/observability for nonlinear mechanisms. The guiding principle of this dissertation, superposition via linear independence, is no longer definable for nonlinear structures. That is, (a) a new definition is required and (b) the metric will require explicit calculation. The task of quantifying such a new concept of controllability requires explicitly looking at all the possible shapes a given set of actuators can achieve, and the work becomes more similar to the calculation of workspace size in robotics. Accordingly, the metric is not achievable by any simple one-time calculation. Rather, the range of achievable shapes is only found by doing a complete search of all combinations of each degree of motion being actuated through their ranges of motion. New optimization techniques may be required to handle the corresponding explosion in computation costs.

8.3.1.1 Possible Solutions

As an alternative to all the developmental work and computation required for the thorough design metric described above for nonlinear performance, there are several more readily handled options. First, for many applications it may turn out that linear may be good enough for topology synthesis. Further fine tuning can be done on finished topologies, where the cost of the aforementioned workspace analyses will not be so significant.

Even without doing the workspace analysis, it may be found acceptable to use the linear results if the limits of linear motion are acceptable. If this is not the case, then one requires a method of easily estimating the amount of error for when the linearly designed device is used in the real nonlinear world.

A final possibility is to seek local, linear controllability about several shape configurations that are separated by large, nonlinear displacements. For example, one might design a shape-morphing aircraft structure that uses nonlinear deformation to move between two specific target shapes, but has small-displacement controllability in both of those configurations so as to reject disturbance and fine-tune the performance.

Ultimately, I suggest considering the shape-change problem where the airfoil has an initial curve and a *target deflected curve* to achieve a prescribed function. The system will need to be adaptable and robust to unknown external loading in *both* configurations.

8.3.2 Nonlinear Actuators

The previous section addressed nonlinearities of the structural performance. However, there is the issue of the actuators themselves, which often have nonlinear force-displacement relationships. It should be possible to find the structural response under nonlinear actuation, which may have very little effect on the nonlinearity of the overall structure. That is, the actuators act only locally, and their effect throughout the structure may be quite constant, allowing for the principle of superposition.

8.3.3 Controls

I have succeeded in developing controllable and observable structures without regarding the controller design itself. In essence, I have made the systems as controllable as possible so that any desired controller can be applied in the quasi-static regime. That is, for any given deformed shape that is sensed, the control designer can design a lookup map ahead of time with the appropriate actuation response. Another option would be simple disturbance rejection, where a PID controller tries to maintain structural shape under changing loads. Some applications may favor an adaptive controller that takes into account the structural response along with another exterior metric such as measured air speed, drag, or turbulence, and modifies the actuated response until the exterior metric is satisfied.

One issue of immediate importance is determining the closed-loop performance of systems with the properties of controllability (or observability). For these systems, controllability is defined in the case of zero external structural load. The effect of

external loads on controllability must also be explored, as these structures are intended to always be interacting with the environment. See Figure 76 in §6.6 for an initial examination of this problem. It is currently assumed that the combination of actuator and external loading can be superimposed. Thus, when under external load, application of the actuators will not result in the shapes calculated above, but in *relative* displacements of the same magnitude. The data acquired from the sensors will therefore consist of components from both the actuator loading and external loading. However, a system model within the controller should be able to separate these components and provide the desired closed-loop effect. In the end though, the absolute range of controllable surface motion is not a constant, but will change with changing external loads.

8.3.4 Dynamics

This work has solely focused on static and quasi-static applications of compliant systems. The next step to dynamic operation is a considerable one. Here, the solutions will be tightly coupled with the controller design, which will no longer be able to reside outside of the optimization loop. Some tasks such as vibration isolation have already been addressed in the literature, as described in Chapter 2. However, the combination of these tasks with mechanical shape-change tasks is yet to be explored. Further, it may be possible to design the natural vibration modes of a structure to be precisely the required independent shape modes required for controllability. On the other hand, just the opposite would be required in some applications: the desired shape-change modes

should be as far from the vibration modes as possible, to decouple the system and prevent undesirable shape-change in vibratory situations.

8.4 Chapter Summary and Final Word

There are many applications to be explored that can benefit from highly multifunctional and controllable systems with embedded actuation and sensing. While there are still many issues to be addressed, the methodology and findings of this dissertation open the door for a much broader approach to creating highly multifunctional systems. Addressing the issue of nonlinearity will extend the benefits to many more applications, as devices will become more adaptive and "life-like" in their function and performance. Likewise for the consideration of dynamics and controls algorithms, these will all enable tighter integration of a device with its environment and an eventual sense of "self" that will drive its internal model of interaction.

Many of the systems in nature have clearly solved the problem of using a limited number and supply of materials to perform many conflicting objectives, effectively *and* all at once. As research in the field of compliant systems grows, it will continue to benefit from the study and inspiration of biology, and will eventually aid in understanding the underlying design principles of nature herself.

References

Anathasuresh, G.K., 1994, "A New Design Paradigm for Micro-Electro-Mechanical Systems & Investigations on the Compliant Mechanism Synthesis", Ph.D. Dissertation, Department of Mechanical Engineering, The University of Michigan, Ann Arbor, MI.

Ananthasuresh, G. K. and Kota, S., 1995, "Designing compliant mechanisms," Mechanical Engineering Magazine, **117**:93–96, November 1995.

Anusonti-Inthra, P., Gandhi, F., and Frecker, M., 2003, M., "Design of a Conformable Rotor Airfoil Using Distributed Piezoelectric Actuation," Proceedings ASME Int. Mechanical Engineering Congress and Exposition, Adaptive Structures Symposium, Washington, DC, IMECE2003-42659.

Begg, D.W. and Liu, X., 2000, "On simultaneous optimization of smart structures - Part II: Algorithms and examples," Computer Methods in Applied Mechanics and Engineering, **184**(1):25-37.

Bendsoe, M.P. and Kikuchi, N., 1988, "Generating Optimal Topologies in Structural Design Using a Homogenization Method," Computer Methods in Applied Mechanics and Engineering, **71**:197-224.

Bendsoe, M.P., 1989, "Optimal Shape Design as a Material Distribution Problem," Structural Optimization, **1**:193-202.

Bernardoni, P., Bidaud, P., Bidard, C., and Gosselin, F., 2004, "A new compliant mechanism design methodology based on flexible building blocks," Proceedings of SPIE, **5383**:244-254.

Bharti, S. and Frecker, M., 2003, "Compliant Mechanical Amplifier Design Using Multiple Optimally Placed Actuators," Proceedings ASME Int. Mechanical Engineering Congress and Exposition, Adaptive Structures Symposium, Washington, DC, IMECE2003-42658.

Bharti, S., Frecker, M., Lesieutre, G., and Ramrakhyani, D., 2005, "Optimal design of tendon-actuated morphing structures: nonlinear analysis and parallel algorithm," Proc. SPIE Smart Structures and Materials, **5757**:132-143.

Bruant, I., Coffignal, G., Lene, F., and Verge, M., 2001, "A Methodology for Determination of Piezoelectric Actuator and Sensor Location on Beam Structures," Journal of Sound and Vibration," **243**(5):861-882.

Canfield, S.L., Chlarson, D.L., Shibakov, A., and Hull, P.V., 2006, "Towards Uniformly Distributed Compliance in Compliant Mechanisms: A Multi-Objective Approach," 2006 ASME Design Engineering Technical Conferences , Philadelphia, PA, September 10-13, 2006.

Cham, J.G., Bailey, S.A., Clark, J.E., Full, R.J. and Cutkosky, M.R., 2002, "Fast and Robust: Hexapedal Robots via Shape Deposition Manufacturing," The International Journal of Robotics Research, **21**(10), October 2002.

Eiben, A. and Smith, J., 2003, "Introduction to Evolutionary Computing," Springer, New York, NY.

Frecker, M.I., Ananthasuresh, G.K., Nishiwaki, S., Kikuchi, N., and Kota, S., 1997, "Topological Synthesis of Compliant Mechanisms Using Multi-Criteria Optimization," ASME Journal of Mechanical Design, **119**(2):238-245.

Frecker, M., 2003, "Recent Advances in Optimization of Smart Structures and Actuators," Journal of Intelligent Material Systems and Structures, **14**(4-5):207-216.

Goldberg, D.E., 1989, "Genetic Algorithm in Search, Optimization, and Machine Learning," Addison Wesley, Reading, MA.

Hać, A. and Liu, L., 1993, "Sensor and Actuator Location in Motion Control of Flexible Structures," Journal of Sound and Vibration, **167**(2):239-261.

Hetrick, J. and Kota, S., 1999, "An Energy Formulation for Parametric Size and Shape Optimization of Compliant Mechanisms," ASME Journal of Mechanical Design, **121**:229-234.

Hetrick, J.A., 1999, "An Energy Efficiency Approach for Unified Topological and Dimensional Synthesis of Compliant Mechanisms," Ph.D. Dissertation, Department of Mechanical Engineering, The University of Michigan, Ann Arbor, MI.

Hetrick, J. and Kota, S., 2003, "Displacement Amplification Structure and Device," United States Patent No. 6,557,436.

Huber, J.E., Fleck, N.A., and Ashby, M.F., 1997, "The selection of mechanical actuators based on performance indices," Proc R. Soc., **453**:2185-2205.

Johnson, T. and Frecker, M., 2004, "Optimal Placement of Active Material Actuators Using Genetic Algorithm," Proc. of SPIE, Smart Structures and Materials, **5383**(1):221-231.

Joo, J., Kota, S., and Kikuchi, N., 2001, "Large Deformation Behavior of Compliant Mechanisms," ASME 2001 Design Engineering Technical Conference, Pittsburg, PA, DETC2001:DAC-21084.

Jutte, C.V., and Kota, S., 2007, "Design of Planar Nonlinear Springs for Prescribed Load-Displacement Functions," ASME 2007 DETC, Las Vegas, NV, DETC2007-35535.

Kim, C.J., Kota, S., and Moon, Y.M., 2006, "An Instant Center Approach Towards the Conceptual Synthesis of Compliant Mechanisms", ASME Journal of Mechanical Design, **128**(3):542-550.

Kota, S., 1999, "System for Varying a Surface Contour," United States Patent No. 5,971,328.

Kota, S., 2002, "System for Varying a Surface Contour," United States Patent No. 6,491,262.

Kota, S., Hetrick, J., Rodgers, S., and Li, Z., 2001, "Compliant Displacement Amplification Apparatus for Micro Electro Mechanical Systems," U.S. Patent No. 6,175,170.

Kota, S., Hetrick, J., Li, Z., and Saggere, L., 1999, "Tailoring Unconventional Actuators Using Compliant Transmissions: Design Methods and Applications," IEEE/ASME Transactions on Mechatronics, **4**(4):396-408.

Langelaar, M. and Van Keulen, F., 2004, "Design Optimization of Shape Memory Alloy Structures," 10th AIAA/ISSMO Multidisciplinary Analysis and Optimization Conference, Albany, New York, Aug. 30-1, 2004, AIAA-2004-4414.

Liu, X., Begg, D.W., and Matravers, D.R., 1997, "Optimal Topology/Actuator Placement Design of Structures Using SA," J. Aerosp. Engrg., **10**(3):119-125.

Lipson, H., 2005, "Homemade: The future of Functional Rapid Prototyping," IEEE Spectrum, May 2005, pp. 24-31.

Loomis, J.M., 1992, "Distal attribution and presence," Presence: Teleoperators and Virtual Environments, **1**:113-119.

Lu, K.J. and Kota, S., 2003, "Design of Compliant Mechanisms for Morphing Structural Shapes," Journal of Intelligent Material Systems and Structures, **14**(6):379-391.

Lu, K.J., 2004, "Synthesis of Shape Morphing Compliant Mechanisms," Ph.D. Dissertation, The University of Michigan, Ann Arbor, MI.

Luo, Z., Tong, L., and Wang, M.Y., 2007, "Design of distributed compliant micromechanisms with an implicit free boundary representation," Structural and Multidisciplinary Optimization, Online First™, Published Online Dec 11, 2007.

Malone E., Lipson H., 2006, "Freeform Fabrication of Complete Devices: Compact Manufacturing for Human and Robotic Exploration", AIAA Space 2006, San Jose, CA, 19-21 Sept 2006, AIAA 2006-7406.

Nelli Silva, E.C., Nishiwaki, S., and Kikuchi, N., 2000, "Topology Optimization Design of Flextensional Actuators," IEEE Transactions and Ultrasonics Ferroelectrics, and Frequency Control, **47**(3):657–671.

Ogata, K., 1990, "Modern Control Engineering," Englewood Cliffs, NJ: Prentice Hall.

Padula, S. and Kincaid, R., 1999, "Optimization Strategies for Sensor and Actuator Placement," NASA Technical Memorandum/TM-1999-209126.

Paros, J.M. and Weisbord, L., 1965, "How to Design Flexure Hinges," Machine Design, pp. 151-156.

Parsons, and Canfield, S.L., "Developing genetic programming techniques for the design of compliant mechanisms," Structural and Multidisciplinary Optimization, **24**(1):78:86.

Peshkin, M., 2004, "Force Sensors," U.S. Patent No. 20,040,261,544.

Sadri, A.M., Wright, J.R., and Wynne, R.J., 1999, "Modelling and optimal placement of piezoelectric actuators in isotropic plates using genetic algorithms," Smart Mater. Struct., **8**:490-498.

Saggere, L., 1997, "Static Shape Control of Smart Structures: A New Approach Utilizing Compliant Mechanisms," Ph.D. Dissertation, Department of Mechanical Engineering, The University of Michigan, Ann Arbor, MI.

Saggere, L. and Kota S., 1999, "Static Shape Control of Smart Structures Using Compliant Mechanisms," AIAA Journal, **37**(5):572-578.

Saxena, A. and Ananthasuresh, G.K., 2001, "Topology Optimization of Compliant Mechanisms with Strength Considerations," Mechanics of Structures and Machines, **29**(2):199-221.

Schulte, H. F., 1961, "The characteristics of the McKibben artificial muscle," The Application of External Power in Prosthetics and Orthotics, Publication 874, National Academy of Sciences - National Research Council, Washington DC, Appendix H, pp. 94-115.

Skelton, R.E., Helton, J.W., Adhikari, R., Pinaud, J.P., and Chan, W., 2001, "An Introduction to the Mechanics of Tensegrity Structures," The Mechanical Systems Design Hand-book: Modeling, Measurement, and Control, CRC Press.

Trease, B. and Kota, S., 2006, "Synthesis of Adaptive and Controllable Compliant Systems With Embedded Actuators and Sensors," Proceedings of IDETC/CIE 2006, September 10-13, Philadelphia, Pennsylvania, USA.

Trease, B. and Kota, S., 2007, "Adaptive and controllable compliant systems with embedded actuators and sensors," Proceedings of SPIE, **6525**.

Yin, L. and Ananthasuresh, G.K., 2003, "Design of Distributed Compliant Mechanisms," Mechanics of Structures and Machines, **31**(2):151-179.